ROLES AND INTERPLAY OF ION TRANSPORT PROTEINS IN PLASTID PHYSIOLOGY

By

CARSTEN VOELKNER

A dissertation submitted in partial fulfillment of
the requirements for the degree of

DOCTOR OF PHILOSOPHY

WASHINGTON STATE UNIVERSITY
School of Biological Sciences

DECEMBER 2021

To the Faculty of Washington State University:

The members of the Committee appointed to examine the dissertation of CARSTEN VOELKNER find it satisfactory and recommend that it be accepted.

_____

Michael Knoblauch, Ph.D., Chair

_____

Hans-Henning Kunz, Ph.D.

_____

Asaph B. Cousins, Ph.D.

_____

Helmut Kirchhoff, Ph.D.

ACKNOWLEDGMENT

During my time as a Ph.D. student, I was fortunate to form many new friendships and connections that played a significant role in making me the person I am today and in developing skills beyond those that a dissertation can describe.

First and foremost, I want to thank my advisor, Henning Kunz. Over the years, Henning has become much more than just an advisor. He introduced me to the world of science and professionalism and taught me even more about music. It fills me with pride to become one of the first of many Doctors in his tree. I will always gladly look back on my very first weekend in the USA, countless nights listening to music on the porch, our eventful road trips to Portland, Friday Harbor, and Northern California, and a couple of snowy Christmas holidays in Pullman where Henning and Katrin invited me into their family.

I also want to express my gratitude to my committee members Michael Knoblauch, Asaph Cousins, and Helmut Kirchhoff for their support whenever I had questions and for giving me perspective when I was thinking too small. In particular, I want to thank Dr. Knoblauch, who took over the role of Chair when bureaucracy forced our hand. I am grateful for all the collaborators, teachers, and colleagues that supported me along the way: Drs. Varnum, Dowd, Tanaka, and Jewell at WSU, Dr. Piñeros at Cornell University, and Dr. Bölter at LMU Munich.

Next, I want to thank everybody who became my friend in the sometimes-stressful environment of the laboratory. Thank you, Rachael, for your love for details, your sense of adventure, and writing protocols when I did not. Thank you, Laurita, for many laughs and being such a sunshine in the lab without windows! Thank you, Ben and Mo, for being a constant source of balance and banter. Thank you to Chance & Chase, Katinka, Dunia, and Maria for excellent assistance in the lab and for becoming my go-to vent.

I also want to express my gratitude to family in the US on Orchard and Derby. Living with you has seriously meant everything to me. Thank you, Alli and Jordan, for giving a stranger a place to live and in your life on your biggest day above Lake Tahoe. Thank you, Nolan, for giving me confidence when I did not know that I needed it and for being there whenever I needed somebody to talk to! And thanks so much to Alex for all the road trips where you showed me the best parts of the USA, thanks for your knowledge when we went to Salmon River where you had to do most of the heavy lifting missing a finger, and thanks for picking me up when I was down (and Rob).

Thank you as well to my friends back in Germany, who made coming back feel different every time but treated me as if I had never left. Many thanks to JD for creating experiences that will stay with us forever. Thank you to Flixe for teaching strength in so many aspects. Many thanks to Felix for the training sessions and all the help in writing since 2014! Also, I am very thankful for Lara and Jonas for making the south of Germany feel like yet another home.

Finally, I want to thank and credit my family in my mother tongue, without whom I could not have dreamed of doing any of this. Danke Wiebke, Sven, und Timon. Auch wenn ihr es vielleicht nicht absichtlich gemacht habt, hat mich euer Stolz motiviert wie nichts anderes. Danke auch dir Mama, dass du dich immer um mich gesorgt, und gekümmert hast, wenn ich aus dem nichts aus den USA aufgetaucht bin. Zuletzt danke ich meinem Vater, dem ich meine Dissertation widme. Auch wenn du es nie verlangt hättest, hast du mir immer das Gefühl gegeben, als könnte ich alles schaffen was ich nur wollen würde. Ich bin dir unendlich dankbar für all die Opfer, die du gebracht hast, damit ich mich sicher, glücklich, und geschätzt fühlen kann.

ROLES AND INTERPLAY OF ION TRANSPORT PROTEINS IN PLASTID PHYSIOLOGY

Abstract

by Carsten Voelkner, Ph.D.
Washington State University
December 2021

Chair: Michael Knoblauch

Ion channels and transporters are present in membranes of all living cells. As integral membrane proteins, they can sense and transduce the chemical environment to other cells and cell compartments. Additionally, ion transport proteins affect membrane voltage, balance substrate and water flux, are involved in signaling processes, and help protect cells from damage. In the chloroplast, the plant organelle harboring the photosynthetic apparatus, knowledge about the physiological role of many ion transport proteins is limited. Due to the importance of photosynthesis, it is necessary to uncover the full potential of chloroplast transport proteins, particularly those that use the ion potassium (K^+) as substrate. K^+ is highly abundant in cells and fulfills many roles in plant and plastid physiology. This dissertation describes the roles of transport proteins inside chloroplasts of *Arabidopsis thaliana*. We characterized novel proteins, adding to the chloroplast transportome, discovered unidentified connections between protein families, and revisited the localization and function of another previously described transporter. First, we investigated putative K^+-permeable ion channels in the chloroplast envelope membrane. Even though the mechanism has been described before, the molecular identity of these proteins

was unknown. Candidate proteins PLASTID ENVELOPE ION CHANNEL1/2 (PEC1/2) are localized to the plastid envelope and exhibit K^+-permeability but are most likely not required for K^+ homeostasis since *pec1pec2* mutants displayed no apparent phenotypic abnormalities. However, we found that PEC1/2 play a crucial role in chloroplast Ca^{2+} signaling. Secondly, we examined the interplay of two different ion transport proteins implicated in osmoregulation of plastids, K^+-EFFLUX ANTIPORTER1 (KEA1) and MscS-LIKE2 (MSL2). The simultaneous lack of both proteins in *kea1msl2* mutants resulted in novel phenotypic anomalies, pointing to a concerted function of both proteins. Finally, we studied the localization and role of putative envelope Na^+:H^+ ANTIPORTER NHD1 and found evidence for a thylakoid membrane localization in different approaches. In addition, investigations of *nhd1* mutants revealed the importance of the carrier NHD1 in acclimation to fluctuating light conditions. Overall, this dissertation advanced our understanding of chloroplast ion transport proteins, subcellular Ca^{2+} signaling, and chloroplast homeostasis.

TABLE OF CONTENTS

Page

LIST OF TABLES

Page

LIST OF FIGURES

Page

Dedication

For my father,

who always wanted me to be greater

than him, the greatest man I've ever known.

CHAPTER ONE: INTRODUCTION

This dissertation revolves around the impact and interplay of ion transport proteins in the chloroplast, a highly important organelle in plants. In order to provide context for the reader, this introduction is divided into four major parts: (1.1) Introduction to the green revolution and plant nutrition, (1.2) the impact of climate change on soil conditions, (1.3) membrane proteins in nutrition and physiology, and (1.4) plastid signaling and ion transport.

1.1 Introduction to the green revolution and plant nutrition.

Agriculture and civilization.

Life on planet earth as we know it has always depended on plants. However, the relationship between humans and plants has changed immensely. Even after the emergence of *Homo sapiens* approximately 200,000 years ago, it took many hundreds of generations until the earliest civilizations developed (Stringer and Andrews, 1988; Bar-Yosef, 1998; Boyden, 2004). Agriculture was an essential precondition that supported a sedentary lifestyle and gave rise to human civilizations (Boyden, 2004; Bocquet-Appel, 2011). Due to technological and agricultural improvements, the population working on fields and farms is steadily decreasing. In the late 19th century, half of the United States population worked in the agricultural sector (Lebergott, 1966), compared to 1.4% in 2020 (https://www.ers.usda.gov, accessed Oct 18, 2021). Indeed, the impact of machines during this period was immense, spanning the industrial revolution as well as two World Wars (Ayres et al., 2003). Nevertheless, the agricultural progress following World War II was also tremendous. The 'green revolution' beginning in the 1960s was highlighted by the breeding of high-yielding varieties and the development and application of pesticides and fertilizers (Evenson and Gollin, 2003).

Elements fuel plant growth.

First applied in the middle of the 19th century, fertilizers revolutionized agriculture when scientists discovered the primary limiting nutrients of crops (Van Zanden, 1991). Nowadays, these complete fertilizers are called NPK, named after the three main ingredients – the elements nitrogen (N), phosphorus (P), and potassium (K, for *kalium* in Latin). Together with sulfur (S), calcium (Ca), and magnesium (Mg), they belong to the group of macronutrients. In plants, these elements occur in relatively large amounts of up to 15,000 parts per million (ppm, or 1.5%) of their dry weight, showcasing the physiological importance of macronutrients in all tissues and life stages (Maathuis, 2009). Additional elements essential to plants occurring at smaller concentrations of less than 100 ppm are grouped as micronutrients. Those include iron (Fe), manganese (Mn), copper (Cu), zinc (Zn), nickel (Ni), molybdenum (Mo), boron (B), and chlorine (Cl) (Marschner and Marschner, 2012). Even though plants assimilate micronutrients less abundantly than macronutrients, their presence is critical for overall plant health. Micronutrients are necessary for adequate growth due to their action as cofactors and activators in enzymatic reactions and roles in cell wall synthesis or detoxification (Maathuis, 2009; Marschner and Marschner, 2012).

Nevertheless, humans thrived long before the invention of fertilizers or the discovery of plant nutrients. However, the sharp increase in the global population from 1.6 billion in 1900 to 6.1 billion in 2000 would not have been possible without the application of fixed inorganic N (Smil, 2001).

1.2 The impact of climate change on soil conditions.

Global consequences of large-scale agriculture.

In the early 20th century, the Nobel-prize-winning Haber-Bosch process was invented. In this highly energy-consuming process, atmospheric N_2 is fixed into ammonia (NH_3), generating a source of nitrogen that can be taken up by plants (Smil, 2001). Thus, while fertilizers made large-scale agriculture possible in the first place, the downstream effects of N fertilization on ecological systems are considerable due to the increased demand for N fixation (Smil, 2001; Galloway et al., 2003). N fertilization results in substantial amounts of greenhouse gases (GHGs), specifically the potent GHG nitrous oxide (N_2O) (Millar et al., 2010). N_2O is a GHG 298 times more potent than CO_2. N_2O makes up 7% of total US GHG emissions, 75% of that stemming from agricultural soil management practices (EPA, 2019).

Consequences of GHG mass production, partially attributable to agriculture, confront the humanity of the 21st century with the biggest challenge to date – climate change. Climate change appears in different facets, contingent on the part of the world. For example, in coastal states in the US, rising sea levels will force residents to relocate and governments to spend taxpayer money on raising streets or building seawalls. In Washington State, the cost of keeping up with climate change is estimated at $24 billion by 2040, according to some prognoses (https://www.climatecosts2040.org/, accessed May 11, 2021). In developing countries such as Bangladesh, with its low elevation, high population density, and inadequate infrastructure, it is estimated that 18 million inhabitants will be displaced due to sea-level rise alone (https://ejfoundation.org/reports/climate-displacement-in-bangladesh, accessed May 20, 2021). Another effect of the rising sea levels is the salinization of coastal drinking water and once-

fertile soil (Bhuiyan and Dutta, 2012). However, not only coastal regions are affected by climate change.

Upcoming arid climates and drought will make farmers even more dependent on irrigation water for their crops. Artificial watering systems are considered wasteful, detrimental to soil health, and thereby plant growth (Organisation for Economic Co-operation and Development, 2017). Poor irrigation management results in excess water in the soil, leaving behind ions such as Na^+ and Ca^{2+} once it evaporates (Eynard et al., 2005). Ions will accumulate in the soil and cause soil salinization, diminishing crop growth (Hanin et al., 2016). The majority of conventional crops are so-called glycophytes. By definition, glycophytes cannot tolerate more than 5 g/L total dissolved solids (TDS, 85 mM as sodium chloride (NaCl)). For reference, seawater contains approximately 40 g/L TDS, equivalent to 500 mM NaCl (Glenn et al., 1999). Beans and rice are staple crops least adapted to saline soils and are impacted by as little as 20 mM external NaCl (H Greenway and Munns, 1980; Glenn et al., 1999).

Climate change will have drastic effects on agriculture, and scientists are working on engineering crops productive under adverse conditions.

Salt and drought stress in plants.

Adverse ionic and osmotic conditions result in stress and trigger ionic or osmotic signaling, respectively. These signaling pathways affect cell division and expansion regulation in the plant, as well as detoxification signaling. The pathways themselves are triggered by injuries inflicted by salt and drought. Ion and osmotic homeostasis, inhibition of growth, osmotic control of the damaged areas of the plant, and repair mechanisms ultimately are all needed for plants to adapt to salt stress and develop tolerance (Zhu, 2002). Under continuous salt stress, as can be expected for many crops, detrimental effects can be observed at all growth stages. While

signaling and growth inhibition can take place on a timescale of minutes to hours, the accumulation of salt, especially in older tissues, leads to yellowing or death of the oldest leaves and a severe inhibition of growth of younger leaves over weeks to months. If the plant is still alive, so-called emergency shoots will start to appear, resulting in diminished seed production in the final life stage of annual plants (Kronzucker et al., 2013). This is the most economically devastating consequence as both humans and their livestock are dependent on calories from seeds and the surrounding tissue (Glover and Reganold, 2010). Therefore, designing crops that can withstand high salinity and drought will be critical in feeding the growing population, which will surpass 9 billion by 2050 and require 60-110% more food (Ray et al., 2013).

An intriguing gene modification target for improving plant growth under hostile conditions are membrane proteins such as transporters and ion channels (Kim et al., 2012; Schroeder et al., 2013; Bailey-Serres et al., 2019). Transporters of the HIGH-AFFINITY K^+ TRANSPORTERS (HKT) family, which will be alluded to in more detail later, have proven successful in this approach. When crossing a susceptible wheat strain with a salt-tolerant relative, yields on saline soil could be improved by up to 25%. The salt-tolerance trait was linked to the action of HKT1;5. This transport protein removes Na^+ from the plant vascular tissue, reducing Na^+ transport to leaves and systemic salt stress, leading to improved growth on saline soils (Munns et al., 2012). Amongst others, HKT proteins showcase the significance of membrane transport to plant physiology and productivity.

1.3 Membrane proteins in nutrition and physiology.

Semi-permeable membranes and integral proteins.

Membranes are prerequisites of life and are ubiquitously present in all living organisms. Biological membranes constitute lipid bilayers with hydrophilic heads connected to hydrophobic

fatty acid tails pointing toward each other, creating a ~5 nm thick barrier between the inside of the cell and the environment or other parts of the cell (van Meer et al., 2008). Membranes are semi-permeable, meaning that only water or small, uncharged molecules like some gases can pass through the membrane unassisted. In order to sense environmental cues or facilitate the exchange of charged molecules, *i.e.*, most nutrients, organisms have developed a variety of integral membrane proteins (IMPs). The variety and the abundance of IMPs are immense, which can comprise more than half of the mass of a membrane (Alberts, 2015). IMPs consist, like other proteins, of amino acids (AAs) with distinct properties. For example, hydrophobic AA stretches can insert into or pass the membrane creating transmembrane domains (TMs), connected by hydrophilic loops on either side of the membrane. Furthermore, the hydrophilic loops can also interact with external substrates leading to responses inside the organism, like some receptor proteins (Diallinas, 2014). However, uptake of charged molecules needs to be facilitated by transport proteins such as ion transporters or ion channels (Gouaux and Mackinnon, 2005; von Heijne, 2006).

Transporters and ion channels are grouped as transport proteins.

On a structural level, channels and transporters are distinct. Channels usually occur in multimers, in which several copies of identical or homologous proteins associate and form a functional unit. Ion channels can have 2-4 subunits with 2-10 TM stretches, with some exceptions (Diallinas, 2014). Channels can be activated (gated) by three main mechanisms: Voltage differential across the membrane, binding of ligands such as Ca^{2+}, or by membrane tension in the case of mechanosensitive channels. After gating of the channel and opening of the pore, selectivity of the pore region will determine flux of substrate molecules that will passively cross the membrane (Hedrich, 2012). Some pore regions are more selective than others. For

instance, plant K^+-selective channels carry a hallmark motif in the pore region, comprising the specific amino acid sequence TXGYGD/E (Aiyar et al., 1996; Lebaudy et al., 2007). At the same time, some channel proteins have evolved to be more broadly permeable to a group of molecules like cations and show selectivity for a variety of substrates *in vitro* (Charpentier et al., 2008). Ion channels facilitate ion movement by utilizing the concentration gradient or electrical potential differences ($\Delta\Psi$) of the substrate of interest. It is estimated that ion channels permit the flow of up to 10^8 ions/second. This large flux of charges can itself impact $\Delta\Psi$, leading to the gating of other channel proteins (Diallinas, 2014).

Unlike channels that mostly facilitate ion or small solute flux, transporter substrates can vary. Substrates can range from small molecules like protons to bigger molecules like lipids and even proteins. Transporters can have 10-14 TM domains, may function in a monomeric state, and work at a much slower rate of 10^2-10^5 ions/s (Diallinas, 2014; Milo and Phillips, 2016). While uniporters permit flow down the concentration or electrochemical gradient and are classified as facilitated diffusion mechanisms, other transporters represent active flux carriers. In active transport, energy input is required to transport substrates across the membrane. Active flux carriers can make use of ATP (adenosine triphosphate, primary active) or the pH difference on either side of the membrane (secondary active), working in concert with Hydrogen (H^+)-ATPases which create the pH gradient at the cost of ATP (Gouaux and Mackinnon, 2005).

As mentioned earlier, transport proteins represent prime targets for gene modifications to improve crop productivity. It is estimated that ~10% of the genome of the model organism *Arabidopsis thaliana* encodes transport proteins (Ward, 2001; Schwacke et al., 2003). The sheer amount of putative transport protein-encoding genes illustrates the significance of these proteins in plant physiology. However, the molecular identity and function of many such proteins *in*

planta remains unknown. This dissertation aimed to extend the knowledge about plant ion transport proteins.

K^+ transport proteins and root uptake.

The macronutrient K^+ is the most abundant cation in plants with up to 10% of the plants' dry weight (Leigh and Jones, 1984). Therefore, it is of significant importance in all tissues and throughout all stages of plant development. K^+ plays major roles in ion and pH homeostasis, balancing charges and membrane polarization, as an enzymatic cofactor, and in controlling water content and gas composition through the opening and closing of stomata (Marschner and Marschner, 2012).

Even though K^+ is highly abundant in the earth's crust, most of it is not readily available to plants due to its dehydrated state (Maathuis, 2009). Concentrations in the rhizosphere are estimated to be in the micromolar range, while cytoplasmatic concentrations in healthy plants are usually kept around 100-200 mM (Chou et al., 2003; Maathuis, 2009). Since K^+ carries a positive charge in the hydrated state and cannot pass membranes freely, plants have evolved various transport proteins that facilitate K^+ uptake and homeostasis throughout the plant. In *A. thaliana*, identified K^+ transport mechanisms have been grouped into two channel families and three transporter families (Sharma et al., 2013). The K^+ channel proteins belong to the voltage-gated *Shaker*, or the non-voltage gated TANDEM-PORE K^+ (TPK) channel families, the latter of which include K_{ir} (K inward-rectifier) channels only recently grouped with TPK proteins based on sequence similarity (Marcel et al., 2010; Voelker et al., 2010). Plant transporters are grouped into HAK/KUP/KT (K^+ UPTAKE/HIGH AFFINITY K^+/K^+ TRANSPORTER), HKT-type proteins, and cation:H^+ antiporter (CPA) families featuring the prominent Na^+:H^+ EXCHANGER (NHX), Na^+:H^+ ANTIPORTER (NHAD), and K^+-EFFLUX ANTIPORTER (KEA) members

(Maser et al., 2001; Brett et al., 2005; Gierth and Maser, 2007; Aranda-Sicilia et al., 2012; Gomez-Porras et al., 2012).

The uptake of K^+ at root membranes is realized by H^+:K^+-cotransporter HAK5 and *Shaker*-like channel AKT1 that work in concert to import K^+ against its concentration gradient into the cytoplasm (Fig. 1.1). The concept of high- and low-affinity K^+ uptake was first presented by Epstein and colleagues almost 60 years ago (Epstein et al., 1963) and by now has been substantiated on a molecular level (Hirsch et al., 1998; Gierth et al., 2005; Gierth and Maser, 2007; Rubio et al., 2008). While HAK5 is primarily responsible for K^+ uptake at soil concentrations below 0.05 mM, both HAK5 and AKT1 are active between 0.01 mM and 0.05 mM (Fig. 1.1). The channel, as a facilitated diffusion mechanism, is dependent on membrane polarization. It follows that uptake of positively charged K^+ is only possible if the cytoplasmatic side is more negative than the outside of the cell, *i.e.*, the apoplast, as is the case at K^+ levels below 10 mM. Once soil K^+ concentrations surpass 10 mM, an unidentified uptake mechanism contributes to AKT-mediated K^+ uptake (Kronzucker et al., 2013).

K^+ homeostasis is vital to plant health.

One of the many examples of the effect of K^+ on plant physiology is its role in primary growth and water movement. Due to the absence of an endoskeleton, plants rely on cell walls and turgor pressure for mechanical support. Turgor pressure depends on the accumulation of solutes in the vacuole, first and foremost K^+, and is a driving force for cell growth (Mengel and Arneke, 1982). In addition, also stoma opening and concomitant gas and H_2O exchange with the atmosphere relies on K^+ level and dynamic changes in cell turgor. The opening of stomata results from a cascade of signals within the plant, stemming from various factors, including blue light, lowered CO_2 concentration within the leaf, or high humidity (Kim et al., 2010). It is partially

triggered by an influx of K^+ ions into the vacuole of guard cells, a specialized cell type that constitutes the stoma pore. The shift in osmotic potential is balanced by H_2O influx, causing guard cells to swell. This process opens the pore, allowing for H_2O and CO_2 exchange of the intercellular space with ambient air to maintain appropriate photosynthetic CO_2 levels in the mesophyll (Kim et al., 2010).

Additionally, several enzymes rely on K^+ exclusively as their cofactor, and using Na^+ would not be feasible in those cases. A striking example are cytosol- and plastid-localized pyruvate kinases which are involved in the glycolytic pathway present in nearly all life forms (Duggleby and Dennis, 1973). While the structural differences of cytosolic pyruvate kinase are subtle between Na^+- and K^+-bound forms (Larsen et al., 1998), the impact on enzyme function is tremendous, with only 7-8% activity in the presence of Na^+ instead of K^+ (Kayne, 1971; Guerrero-Mendiola et al., 2017).

Finally, K^+ is an effective charge balancer across the plasma and subcellular membranes due to its small size. For instance, this is critical in plant species engaging in beneficial root symbioses with fungi and bacteria. During the early steps of the formation of these symbiotic relationships, Ca^{2+} transients appear in the nucleus of root cells. These transients initiate downstream signaling processes and thereby allow for the symbiosis to take place. Forward genetics for *Medicago truncatula* mutants defective in establishing bacterial root symbioses resulted in the mapping of the *DOES NOT MAKE INFECTIONS1 (DMI1)* locus, encoding for a nuclear envelope cation channel (Ane et al., 2004). Homologs of *Mt*DMI1 were identified in *Lotus japonicus*, which engages in root symbiosis with fungi, and were termed CASTOR and POLLUX (Charpentier et al., 2008). Plants lacking proteins of the CASTOR/POLLUX/DMI family cannot engage in the symbiotic relationship because they are unable to generate nuclear

Ca^{2+} spikes (Charpentier et al., 2008). By now, these channel proteins have been studied both *in vivo* and *in vitro* with the consensus that they are permeable to K^+, Na^+, and Ca^{2+}, with highest conductivity for K^+ (Charpentier et al., 2008; Kim et al., 2019). A few years later, another channel from the CYCLIC-NUCLEOTIDE-GATED CHANNEL (CNGC) family, *Mt*CNGC15, was found to colocalize with *Mt*DMI1 in the nuclear envelope membrane. It was proposed that CNGC15 is the Ca^{2+}-permeable channel directly responsible for eliciting the Ca^{2+} transients (Charpentier et al., 2016). Comparable modes of action also exist in organelles like the chloroplast. The connection between subcellular K^+ fluxes and Ca^{2+} transients is the focus of Chapter Two.

These examples give a glimpse at the importance of K^+ in plants. Disturbing K^+ homeostasis, and thereby the processes mentioned above, is detrimental to plant health.

Open questions on Na^+ uptake and K^+ exchange at root plasma membranes.

Even though many detrimental effects of disturbed K^+ homeostasis have been determined, researchers are still investigating concentrations at which Na^+ becomes toxic (Kronzucker et al., 2013; Flowers et al., 2015). Similarly, molecular uptake mechanisms of Na^+ into plants are still under debate. Proteins of different families have been identified as candidates for at least partial roles in the influx of Na^+ into the root endodermis cytoplasm: HKT, LCT1 (LOW-AFFINITY CATION TRANSPORTER1) (Schachtman et al., 1997; Amtmann et al., 2001), KUP/HAK/KT (Santa-Maria et al., 1997; Amtmann and Sanders, 1999; Blumwald et al., 2000; Golldack et al., 2003) and AKT (K^+ TRANSPORTER) families, and in addition proteins of the family of non-selective cation channels (NSCCs) (Essah et al., 2003; Malagoli et al., 2008; Moller et al., 2009; Wang et al., 2009; Wetson and Flowers, 2010; Kronzucker et al., 2013). However, the similarity of physicochemical properties, such as ionic radius and hydration state,

and 'loose' binding sites within the pockets of transporters make discrimination between Na^+ and K^+ difficult. This lack of specificity can lead to the transport of either cation (Cotsaftis et al., 2012; Benito et al., 2014) and may explain the presence of many K^+ transport mechanisms in this list.

The influx of Na^+ can lead to depolarization of the membrane, resulting in the activation of K^+ efflux proteins (Shabala et al., 2006). Extracellular Na^+ can inhibit K^+ uptake mechanisms, aggravating the disturbed K^+ homeostasis in the cell, which can be observed in all parts of the plant (Fig. 1.1). The surplus of Na^+ does not remain in root tissues but will be translocated to aerial tissues, where Na^+ will accumulate in leaf apoplasts and vacuoles (Flowers et al., 1991). According to the Oertli hypothesis, osmotic stress, rather than ionic, is responsible for the salt-induced damage of leaves in *Oryza sativa* (rice) (Oertli, 1968). The accumulation of Na^+ in the apoplast causes water to drain out of the cells, disrupting the osmotic balance of cells and leading to drought stress responses.

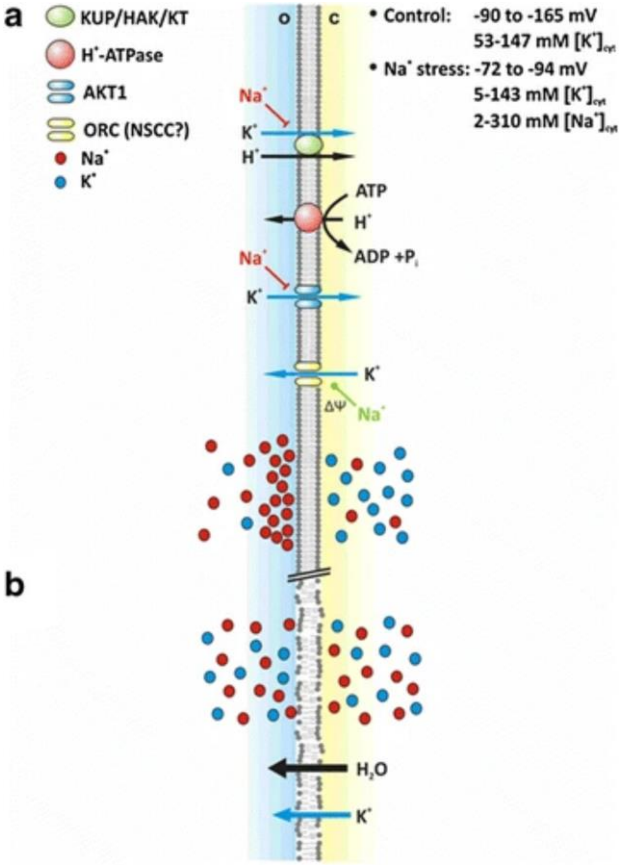

Figure 1.1 Model of K^+ and Na^+ exchange at the plasma membrane of roots (from Kronzucker et al., 2013). A) Under normal, non-stress conditions , KUP/HKT/KT transporters facilitate the transport from the outside (o) into the cell (c) at low K^+, and AKT1 at high K^+ concentrations, inhibited by Na^+. At the same time, electrical potential $\Delta\Psi$ forces outward flux of K^+ by an NSCC, stimulated by Na^+. B) Sudden salinity stress causes accumulation of Na^+ in the apoplast, resulting in efflux of H_2O and K^+ out of cells.

Na^+ is used in cellular processes.

Even though Na^+ can have detrimental effects on plant growth in glycophytes, it can be accumulated by halophytes, and in some other plants is a substrate in cellular processes. C_4 plants in particular benefit from low internal Na^+ concentration (Brownell and Crossland, 1972; Subbarao et al., 2003; Marschner and Marschner, 2012). In some C_4 species, Na^+ is involved in a cotransport reaction that supplies pyruvate to the chloroplast (Ohnishi et al., 1990). In others, like the C_3 plant *A. thaliana*, pyruvate uptake is H^+-dependent (Ohnishi and Kanai, 1990; Furumoto et al., 2011). Nevertheless, pyruvate is an essential substrate for different enzymatic reactions in primary and secondary metabolism in the chloroplast and is also taken up from the cytosol (Schwender et al., 2004). For example, in *Flaveria trinervia*, BILE ACID:SODIUM SYMPORTER FAMILY PROTEIN2 (BASS2) facilitates the co-transport of pyruvate and Na^+ into the stroma at the inner envelope membrane. Na^+ homeostasis was suggested to be balanced by NHAD-type Na^+:H^+ antiporter NHD1 to avoid the accumulation of Na^+ in the stroma (Furumoto et al., 2011). However, at least in the C_3 glycophyte *A. thaliana*, the exact localization of NHD1 within chloroplast membranes remains controversial. Localization of *At*NHD1 and characterization of *nhd1* loss-of-function mutants are the focus of Chapter Four.

Ca^{2+} signals as a response to salt stress.

The majority of crop plants are C_3 glycophytes and therefore need to balance cellular Na^+ content. In response to osmotic challenges, glycophytes try to control cell function and integrity by sensing salt and osmotic stress and employing signaling pathways to prime detoxification and aid plant survival (Hanin et al., 2016). For example, salt exposure causes a rapid spike in cytosolic Ca^{2+} levels ($[Ca]_{cyt}$), which can be observed in many cell types, different compartments, and organelles throughout the entire plant (Knight et al., 1997; Nomura et al.,

2012; Zhu et al., 2013; Stephan et al., 2016). Initially, the signal is generated in root cells and subsequently propagated towards shoot tissues (Choi et al., 2014). Among other players, the vacuole localized TWO PORE CHANNEL 1 (TPC1) is involved in the generation of rising $[Ca]_{cyt}$ after exposure to salt. Consequently, in *tpc1* mutants, propagation of the Ca^{2+} wave was severely limited, and the systemic, genetic responses to salt stress were lacking (Choi et al., 2014). The genetic responses include upregulation of several stress defense genes, including *TPC1* itself. Surprisingly, *tpc1* loss-of-function mutants did not exhibit a penalty to plant growth (Peiter et al., 2005). The Ca^{2+} signatures, in part generated by TPC1, are decoded by a toolkit of Ca^{2+} interacting proteins such as calmodulin (CaM), calcium-dependent protein kinases (CDPKs), and calcineurin B-like proteins (CBLs) with CBL-interacting protein kinases (CIPKs). These proteins may function as molecular switches, and their activity can result in changes in gene expression and protein activity (Weinl and Kudla, 2009; Boudsocq and Sheen, 2013). However, many players involved in the signaling cascades remain unknown and uncharacterized.

Even though levels of free Ca^{2+} in most cellular environments are kept at nanomolar levels to avoid precipitation of phosphates, the importance of this ion on plant health and physiology should not be underestimated. Besides being able to bind to and gate channels, Ca^{2+} serves as a ubiquitous secondary messenger. Thus, in response to either developmental factors (Scheible and McCubbin, 2019) or biotic and abiotic stress (Nomura et al., 2012), subcellular Ca^{2+} concentrations can rise amplitudes higher than resting levels. Intriguingly, both amplitude and frequency of spikes are elicitor-specific.

It is expected that plants precisely employ Ca^{2+} transients to encode and communicate different types of stress triggers, which have been observed in all parts of the cell and are distinct depending on the compartment or organelle (Resentini et al., 2021). Research has been done on

Ca^{2+} transients in the cytosol (Knight et al., 1996, 1997; Qudeimat et al., 2008; Tanaka et al., 2010), mitochondria (Logan and Knight, 2003), endoplasmatic reticulum (Bonza et al., 2013), peroxisomes (Costa et al., 2010; Corso et al., 2018), nucleus (Charpentier et al., 2008; Leitao et al., 2019), and the plastid (Nomura et al., 2012; Pottosin and Dobrovinskaya, 2015). In most cases, Ca^{2+} transients in these compartments occur after the rise in $[Ca]_{cyt}$. Therefore, it was suggested that these compartments act as sinks to shape the cytosolic Ca^{2+} transient. Interestingly, chloroplasts create their own Ca^{2+} signatures that do not transmit into the cytosol in the form of Ca^{2+} (Pottosin and Dobrovinskaya, 2015; Lenzoni and Knight, 2019), suggesting that chloroplasts function as a central hub in detecting and fending off various environmental stressors.

1.4 Plastid signaling and ion transport.

Plastid origin and integration into plants.

The chloroplast, a specialized plastid type, is one of the defining features of plant cells. It is home to photosynthesis in which atmospheric CO_2 is fixed and oxygen (O_2) released, thereby providing the foundation for higher life on earth. Plastids are a group of organelles in plants that, like mitochondria, originated from an endosymbiotic event. In the case of mitochondria, a prokaryotic cell able to perform aerobic respiration was likely ingested *via* phagocytosis into a larger eukaryotic cell more than 1.45 billion years ago (Embley and Martin, 2006). The ancestor of today's plastids was a photoautotrophic cyanobacterium. This prokaryote was engulfed by a cell that already harbored mitochondria about 1.2 billion years ago (Gould et al., 2008). Over time, both endosymbionts became intertwined with the host cell, becoming organelles. As a result, mitochondria and plastids transferred most of their circular genome into the host's nuclear

genome, a process known as horizontal gene transfer. However, a strongly reduced genome remains in plant mitochondria and plastids until today (Timmis et al., 2004).

Mitochondria and plastids lost the ability to reproduce independently (Andersson et al., 2003; Richly and Leister, 2004). In the case of plastids, some genes involved in photosynthesis, gene expression, and genome duplication are encoded on the plastid genome (plastome). Nevertheless, even those genes are thought to be under nuclear control via anterograde signaling (Woodson and Chory, 2008). For instance, many plastid mRNA editing components are encoded in the nucleus and need to be imported into the organelle (DeTar et al., 2021). Similarly, the chloroplast also engages in retrograde signaling, controlling, or at least influencing, nuclear gene expression (Kleine and Leister, 2016). For example, reactive oxygen species (ROS) are formed in the chloroplast in response to pathogenic elicitors, leading to downregulation of nuclear-encoded genes. Genes under the influence of the plastid include, for example, genes responsible for the biosynthesis of transcription factors or the various phytohormones that originate from the chloroplast (Nomura et al., 2012). In addition to influencing gene expression networks, chloroplasts are the primary source of cellular ROS and biosynthesize precursors of phytohormones, amino acids, and lipids.

In contrast to other compartments inside the plant cell, organelles of endosymbiotic origin retained their original membranes, and therefore possess an outer and inner envelope membrane with an intermembrane space in between. In addition, chloroplasts harbor stacked, compressed internal membranes, the thylakoid. The outer envelope membrane is composed of the phospholipids phosphatidylcholine and phosphatidylglycerol. Besides this, the composition of these three membranes is very similar. They mainly consist of two types of lipids, monogalactosyldiacylglycerol (MGDG) and digalactosyldiacylglycerol (DGDG). Galactolipids

are synthesized in the plastid and, in healthy plants, rarely found outside of the organelle. In contrast, envelope and thylakoid membranes contain only trace amounts of phospholipids that represent the main component of all other plant membranes (Block et al., 2007).

Because the plastid lost or transferred most of its genome into the nucleus, it must be supplied with thousands of different proteins to function properly. Therefore, plastids were outfitted with a protein import system called the TRANSLOCON AT THE OUTER CHLOROPLAST ENVELOPE - TRANSLOCON AT THE INNER CHLOROPLAST ENVELOPE (TOC-TIC) complex (Jarvis and Soll, 2001; Woodson and Chory, 2008). Most plastid-targeted proteins contain cleavable N-terminal plastid transit peptides (pTPs), which direct the proteins to the organelle after translation in the cytosol. The exceptions are integral proteins of the outer envelope membrane (outside of TOC75) which maintain their pTP in the mature protein. The multiprotein TOC complex recognizes pTPs, importing proteins into the intermembrane space. They are further processed into the stroma by the TIC under ATP consumption (Pain and Blobel, 1987; Kouranov and Schnell, 1997). IMPs of the inner envelope membrane are imported into the stroma in their entirety. These are processed to their mature forms by a stromal processing peptidase and then reinserted into the membrane they just passed (Schwenkert et al., 2011). This is different for thylakoid proteins which carry a bipartite pTP that directs them to the thylakoid membrane. Their processing is realized by a thylakoid processing peptidase (Richter and Lamppa, 2002). Discovery of chloroplast membrane proteins has been greatly simplified since the early 2000s through proteomics efforts and *in silico* prediction of pTPs (Ferro et al., 2002; Ferro et al., 2003; Sun et al., 2009). Nevertheless, many players involved in core chloroplast function, such as cation transport and ion homeostasis, have not been identified or characterized thus far and are the focus of this dissertation.

K^+ exchange at chloroplast membranes is multifaceted.

Even though K^+ has significant implications for physiology, the identity of potential K^+ transport mechanisms embedded in plastid membranes is under debate. Like in the rest of the plant, K^+ plays a pivotal role in chloroplast biology. Early studies on isolated chloroplasts revealed that K^+ transport across the inner envelope is accompanied by proton exchange (Demmig and Gimmler, 1983) and that the stroma is negatively charged (-70 to -110 mV) (Wu et al., 1991). This proton dependency is critical in the stroma, which exhibits a stark pH gradient (ΔpH) across the thylakoid membrane. Furthermore, the proton motive force (*pmf*), which drives ATP production *via* the F_1F_0-ATP synthase, relies on both the pH component ΔpH and electric component $\Delta\Psi$ (Mitchell, 1966; Witt, 1979). Thus, chloroplast envelope membrane K^+ transport is linked to *pmf* generation and ATP production, impacting carbon fixation *via* the Calvin-Benson-Bassham cycle.

Thirty years after the connection between plastid K^+ and H^+ exchange was established, K^+ EFFLUX ANTIPORTER 1 and 2 (KEA1/2) of the CPA family were characterized (Aranda-Sicilia et al., 2012; Zheng et al., 2013; Kunz et al., 2014). KEA1 and KEA2 were shown to facilitate the electroneutral antiport of K^+ and H^+ (Tsujii et al., 2019). Mutants lacking both copies of these inner envelope localized transporters are severely stunted, display variegated leaves, swollen chloroplasts with obvious deficiencies in development, photosynthesis, and osmoregulation (Kunz et al., 2014; DeTar et al., 2021). Surprisingly, light salt stress alleviates phenotypic defects in *Arabidopsis* seedlings, restoring development and photosynthesis. Intriguingly, similar morphological defects can be observed in plastids of mutants lacking both MscS-LIKE (MSL) plastid members, MSL2 and MSL3. In *msl2msl3* double mutants, plastids are swollen, and plants are smaller than the wild-type. The plastid phenotype can also be restored

by adding external osmolytes, similar to the effect observed in *kea1kea2* (Wilson et al., 2014). However, many aspects of this phenomenon remain vaguely understood. This emphasizes our lack of knowledge of chloroplast osmoregulation and ion transport proteins, which has substantial implications for overall plant health and physiology. The interaction between plastid envelope KEA and MSL members is the focus of Chapter Three.

Apart from envelope transporters KEA1/2, much research has been done lately to understand the function of KEA3, the only thylakoid membrane member of the KEA family. Here, KEA3 imports K^+ into the thylakoid lumen in exchange for protons, influencing both aspects of the *pmf* (Armbruster et al., 2014; Kunz et al., 2014; Armbruster et al., 2016). Increased light intensities lead to a high concentration of protons in the lumen, creating a steep ΔpH. A low luminal pH in the light is critical to activate non-photochemical quenching (NPQ) processes. NPQ protects photosystems by dissipating excess energy as heat. Activation of NPQ can be realized within seconds, while relaxation takes much longer (Muller et al., 2001). Cloud movement or shading of leaves creates sunflecks, leading to constant activation and inactivation of NPQ (Kaiser et al., 2018). While photosystem protection is vital in minimizing light-induced damage to plants, slow NPQ relaxation also reduces the amount of ATP or reducing power generated. When switching from high to low light, the lumen pH becomes more alkaline due to H^+ efflux through ATP synthase, lowered activity of water-splitting reactions, and lowered cytochrome b_6f activity (Tikhonov, 2014; Armbruster et al., 2017). Here, relaxation of NPQ is of high importance to maximize photosynthetic production of leaves. Consequently, the export of H^+ facilitated by KEA3 is of particular interest in regulation of ΔpH in *pmf,* as loss-of-function *kea3* mutants display a reduction in growth under fluctuating light conditions (Armbruster et al., 2014; Aranda-Sicilia et al., 2016).

Outside of KEA transporters, only one protein associated with K^+ transport, the ion channel TWO PORE K^+ CHANNEL3 (TPK3), has been linked to the plastid thus far (Carraretto et al., 2013). Nevertheless, our extensive studies give strong evidence for a tonoplast localization of TPK3 (Höhner et al., 2019), which is in accordance with proteomics data (Sun et al., 2009; Tomizioli et al., 2014; Hooper et al., 2017). Chapter Two presents a novel family of K^+-permeable channel proteins localizing to the envelope membrane of chloroplasts (Völkner et al., 2021).

Plastid Ca^{2+} transients ask for uptake mechanisms.

The role of chloroplasts in plant defense signaling has been under heavy investigation since discovering the CALCIUM-SENSING RECEPTOR (CaS) protein. Initially, *At*CaS was thought to localize to the plasma membrane because of reduced $[Ca]_{cyt}$ transients after application of external Ca^{2+} (Chou et al., 2003). However, other studies have since presented strong evidence for a thylakoid membrane-localization of CaS (Nomura et al., 2008; Vainonen et al., 2008; Weinl et al., 2008). Since then, CaS activity has been connected to stomatal closure, phytohormone biosynthesis, and plant immunity *via* retrograde signaling (Nomura et al., 2008; Vainonen et al., 2008; Weinl et al., 2008; Nomura et al., 2012). Intriguingly, *cas* mutants lack any visible phenotypes and do not show strong stromal Ca^{2+} ($[Ca]_{str}$) signaling alterations. Still, loss-of-function *cas* mutants display reduced transients in response to bacterial elicitors and light-to-dark transition. At the same time, higher $[Ca]_{str}$ transients in response to cold shock were reported, which makes CaS unlikely to be involved in stromal Ca^{2+} transport (Nomura et al., 2012). The fast timescale of $[Ca]_{str}$ transients requires rapid uptake mechanisms, which indicates an involvement of unknown Ca^{2+}-permeable ion channels.

Similar to K^+ transport proteins, Ca^{2+} transport mechanisms in plastids are obscure. Initially, a study reported that the previously plasma-membrane localized Ca^{2+} channel GLUTAMATE-RECEPTOR LIKE3.4 (GLR3.4) (Meyerhoff et al., 2005; Vincill et al., 2012) has an alternative localization to chloroplasts, yet no data were presented showing if the lack of GLR3.4 affects $[Ca]_{str}$ (Teardo et al., 2011). Later, two previously characterized manganese (Mn) transporters, PHOTOSYNTHESIS-AFFECTED MUTANT71 (PAM71) (Schneider et al., 2016) and CHLOROPLAST MANGANESE TRANSPORTER1 (CMT1) (Wang et al., 2009), were again described as chloroplast Ca^{2+} transporters (Frank et al., 2019). Loss of inner envelope carrier *BIVALENT CATION TRANSPORTER2* (*BICAT2*), previously *CMT1*, caused plants to die under short-day conditions while portraying severely stunted rosette and root growth under long-day conditions (Frank et al., 2019). Besides affecting the chloroplast generated $[Ca]_{str}$ changes in response to light-to-dark transitions, no other effects were reported (Frank et al., 2019). Lastly, a protein from the MITOCHONDRIAL CALCIUM UNIPORTER (MCU) family was recently suggested to be dual targeted to mesophyll chloroplasts and mitochondria and termed cMCU (Teardo et al., 2019). *cmcu* loss-of-function mutants exhibited a lowered $[Ca]_{str}$ response after H_2O_2 application and osmotic stress. Nevertheless, neither *bicat2* nor *cmcu* mutants showed a flatline response, indicating an involvement of other channel candidates contributing to the fast response of $[Ca]_{str}$.

As mentioned before, a variety of elicitors can elevate $[Ca]_{str}$. These include bacterial peptide flg22, NaCl, sorbitol, and cold and heat shock, each substance causing distinct kinetic responses of Ca^{2+} elevation (Manzoor et al., 2012; Nomura et al., 2012; Sello et al., 2018; Lenzoni and Knight, 2019). A lack of knowledge about these mechanisms underpins the need for further studies into the chloroplast transportome.

Context of candidate proteins of this dissertation.

The proteins studied in the frame of this dissertation all localize to chloroplast membranes of *A. thaliana* and function in ion transport. Beyond that, all candidate proteins have additional roles in maintaining chloroplast functions. Those roles were explored in Chapters Two, Three, and Four, using a variety of molecular, biochemical, and spectroscopy-based approaches. This last section aims at giving specific context for each chapter (Fig. 1.2).

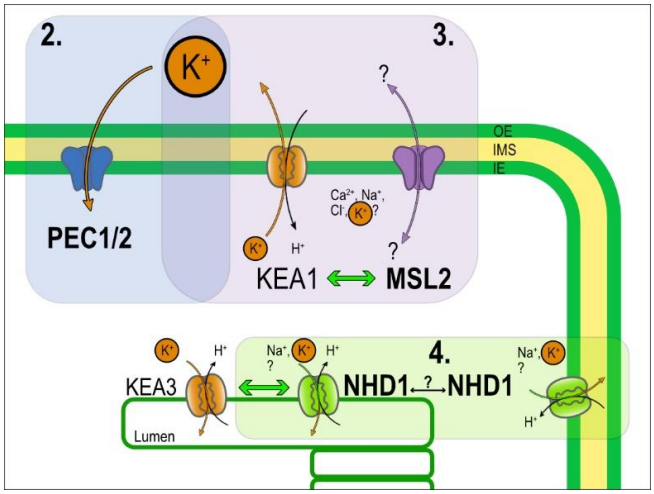

Figure 1.2 Model of candidate plastid proteins investigated in the frame of this dissertation. K^+ illustrates the overlap between candidate proteins of Chapters Two, Three, and Four as a central aspect of this dissertation. OE=outer envelope membrane, IMS=Intermembrane space, IE=Inner envelope membrane

The presence of K^+ export mechanisms in the inner envelope membrane calls for a pathway to import K^+ and other cations (Bernardi, 1999). Cation channel activity across the envelope membrane was measured independently in the past, using patches of isolated *Spinacia oleracea* (spinach) or *Pisum sativum* (pea) chloroplasts (Wang et al., 1993; Pottosin et al., 2005). Eventually, the identified protein was coined fast-activating chloroplast cation (FACC) channel. FACC showed little selectivity between the physiologically essential cations K^+, Na^+, Ca^{2+}, and Mg^{2+} (Pottosin et al., 2005). Our studies of publicly available proteome data sets from pea chloroplast envelope fractions (Brautigam et al., 2008; Gutierrez-Carbonell et al., 2014) revealed distant homologs of the earlier mentioned CASTOR/POLLUX/DMI protein family in plastids of *A. thaliana*. We termed the proteins PLASTID ENVELOPE ION CHANNEL1 (PEC1) and PEC2. PEC1 and PEC2 share high homology, localize to the chloroplast envelope membrane,

and possess K^+ permeability in heterologous systems. While homologs are implicated in the formation of nuclear Ca^{2+} transients, we propose a similar role for PEC1/2 in the chloroplast. Our studies reveal that loss-of-function mutants show the most robust reduction in stress-induced $[Ca]_{str}$ transients reported thus far, tying in both K^+ exchange at the inner envelope membrane and chloroplast Ca^{2+} signaling (Chapter Two). Chapter Two has recently been published in *Plant Physiology* (Völkner et al., 2021).

As mentioned previously, KEA1/2 proteins are involved in K^+ ion- and osmohomeostasis in the chloroplast. Similarly, two chloroplast envelope membrane-localized members of the MSL protein family, MSL2 and MSL3, were implied to function in this process (Haswell and Meyerowitz, 2006). Mechanosensitive channels are of prokaryotic origin and activated by membrane tension (Zhang et al., 2021). In bacteria, a sudden increase in the osmotic potential of the environment can lead to cell rupture due to water influx (Levina et al., 1999). Due to the myriads of processes happening simultaneously inside chloroplasts, content of solutes (and thereby osmotic potential) must be readily adjustable at all stages of chloroplast development. By crossing *msl2* and *kea1* single mutants, we tested whether a functional interaction between the two unrelated protein families exists. We were able to show that in an *msl2* background, the loss of KEA1 resulted in mutants displaying disturbed plant growth, chlorophyll content, and photosynthetic efficiency. We thereby add to the knowledge about chloroplast ion- and osmohomeostasis (Chapter 3).

Finally, a carrier of the NHAD transporter family, NHD1, has previously been localized to chloroplast envelope membranes (Furumoto et al., 2011; Muller et al., 2014). However, proteomics studies identified *At*NHD1 in thylakoid membrane fractions, opening the possibility for another or a dual-localization of the carrier. Additionally, our studies of *nhd1* loss-of-function

mutants revealed photosystem II (PS II) related alterations from WT during fluctuating light conditions, indicating a localization to the thylakoid membrane. Therefore, we decided to pursue localization studies using orthogonal approaches in two different systems. Indeed, our results suggest a thylakoid membrane localization for NHD1, connecting another ion transport protein to *pmf* modulation under fluctuating light (Chapter Four).

The topic of this dissertation revolves around the role of ion transport proteins in chloroplast signaling, ion homeostasis, osmoregulation, and photosynthetic processes at the thylakoid membrane. This dissertation was broken down into the following aims: 1) Identify the role of CASTOR/POLLUX/DMI family proteins in plastid K^+ homeostasis and Ca^{2+} signaling. 2) Study interactions of KEA and MSL family proteins in osmoregulation of the chloroplast. 3) Investigate the localization of NHD1 and its role in photosynthesis during fluctuating light (Fig. 1.2). Altogether, this dissertation adds important knowledge to chloroplast physiology and furthers our understanding of how plants use ion transport proteins and the K^+ cation.

1.5 References

Aiyar J, Rizzi JP, Gutman GA, Chandy KG (1996) The signature sequence of voltage-gated potassium channels projects into the external vestibule. J Biol Chem **271:** 31013-31016

Alberts B (2015) Molecular biology of the cell, Ed Sixth edition. Garland Science, Taylor and Francis Group, New York, NY

Amtmann A, Fischer M, Marsh EL, Stefanovic A, Sanders D, Schachtman DP (2001) The wheat cDNA LCT1 generates hypersensitivity to sodium in a salt-sensitive yeast strain. Plant Physiol **126:** 1061-1071

Amtmann A, Sanders D (1999) Mechanisms of Na(+) uptake by plant cells. Advances in Botanical Research Incorporating Advances in Plant Pathology, Vol 29 **29:** 75-112

Ane JM, Kiss GB, Riely BK, Penmetsa RV, Oldroyd GE, Ayax C, Levy J, Debelle F, Baek JM, Kalo P, Rosenberg C, Roe BA, Long SR, Denarie J, Cook DR (2004) Medicago truncatula DMI1 required for bacterial and fungal symbioses in legumes. Science **303:** 1364-1367

Andersson SGE, Karlberg O, Canback B, Kurland CG (2003) On the origin of mitochondria: a genomics perspective. Philosophical Transactions of the Royal Society B-Biological Sciences **358:** 165-177

Aranda-Sicilia MN, Aboukila A, Armbruster U, Cagnac O, Schumann T, Kunz HH, Jahns P, Rodriguez-Rosales MP, Sze H, Venema K (2016) Envelope K+/H+ Antiporters AtKEA1 and AtKEA2 Function in Plastid Development. Plant Physiol **172:** 441-449

Aranda-Sicilia MN, Cagnac O, Chanroj S, Sze H, Rodriguez-Rosales MP, Venema K (2012) Arabidopsis KEA2, a homolog of bacterial KefC, encodes a K(+)/H(+) antiporter with a chloroplast transit peptide. Biochim Biophys Acta **1818:** 2362-2371

Armbruster U, Carrillo LR, Venema K, Pavlovic L, Schmidtmann E, Kornfeld A, Jahns P, Berry JA, Kramer DM, Jonikas MC (2014) Ion antiport accelerates photosynthetic acclimation in fluctuating light environments. Nat Commun **5:** 5439

Armbruster U, Correa Galvis V, Kunz HH, Strand DD (2017) The regulation of the chloroplast proton motive force plays a key role for photosynthesis in fluctuating light. Curr Opin Plant Biol **37:** 56-62

Armbruster U, Leonelli L, Galvis VC, Strand D, Quinn EH, Jonikas MC, Niyogi KK (2016) Regulation and Levels of the Thylakoid K+/H+ Antiporter KEA3 Shape the Dynamic Response of Photosynthesis in Fluctuating Light. Plant and Cell Physiology **57:** 1557-1567

Ayres RU, Ayres LW, Warr B (2003) Exergy, power and work in the US economy, 1900-1998. Energy **28:** 219-273

Bailey-Serres J, Parker JE, Ainsworth EA, Oldroyd GED, Schroeder JI (2019) Genetic strategies for improving crop yields. Nature **575:** 109-118

Bar-Yosef O (1998) The Natufian culture in the Levant, threshold to the origins of agriculture. Evolutionary Anthropology **6:** 159-177

Benito B, Haro R, Amtmann A, Cuin TA, Dreyer I (2014) The twins K+ and Na+ in plants. Journal of Plant Physiology **171:** 723-731

Bernardi P (1999) Mitochondrial transport of cations: channels, exchangers, and permeability transition. Physiol Rev **79:** 1127-1155

Bhuiyan MJAN, Dutta D (2012) Assessing impacts of sea level rise on river salinity in the Gorai river network, Bangladesh. Estuarine Coastal and Shelf Science **96:** 219-227

Block MA, Douce R, Joyard J, Rolland N (2007) Chloroplast envelope membranes: a dynamic interface between plastids and the cytosol. Photosynthesis Research **92:** 225-244

Blumwald E, Aharon GS, Apse MP (2000) Sodium transport in plant cells. Biochimica Et Biophysica Acta-Biomembranes **1465:** 140-151

Bocquet-Appel JP (2011) When the world's population took off: the springboard of the Neolithic Demographic Transition. Science **333:** 560-561

Bonza MC, Loro G, Behera S, Wong A, Kudla J, Costa A (2013) Analyses of Ca2+ Accumulation and Dynamics in the Endoplasmic Reticulum of Arabidopsis Root Cells Using a Genetically Encoded Cameleon Sensor. Plant Physiology **163:** 1230-1241

Boudsocq M, Sheen J (2013) CDPKs in immune and stress signaling. Trends in Plant Science **18:** 30-40

Boyden SV (2004) The biology of civilisation : understanding human culture as a force in nature. UNSW Pess, Sydney

Brautigam A, Hoffmann-Benning S, Weber AP (2008) Comparative proteomics of chloroplast envelopes from C3 and C4 plants reveals specific adaptations of the plastid envelope to C4 photosynthesis and candidate proteins required for maintaining C4 metabolite fluxes. Plant Physiol **148:** 568-579

Brett CL, Donowitz M, Rao R (2005) Evolutionary origins of eukaryotic sodium/proton exchangers. American Journal of Physiology-Cell Physiology **288:** C223-C239

Brownell PF, Crossland CJ (1972) Requirement for Sodium as a Micronutrient by Species Having C4 Dicarboxylic Photosynthetic Pathway. Plant Physiology **49:** 794-797

Carraretto L, Formentin E, Teardo E, Checchetto V, Tomizioli M, Morosinotto T, Giacometti GM, Finazzi G, Szabó I (2013) A thylakoid-located two-pore K+ channel controls photosynthetic light utilization in plants. Science **342:** 114-118

Charpentier M, Bredemeier R, Wanner G, Takeda N, Schleiff E, Parniske M (2008) Lotus japonicus CASTOR and POLLUX are ion channels essential for perinuclear calcium spiking in legume root endosymbiosis. Plant Cell **20:** 3467-3479

Charpentier M, Sun J, Vaz Martins T, Radhakrishnan GV, Findlay K, Soumpourou E, Thouin J, Very AA, Sanders D, Morris RJ, Oldroyd GE (2016) Nuclear-localized cyclic nucleotide-gated channels mediate symbiotic calcium oscillations. Science **352:** 1102-1105

Choi WG, Toyota M, Kim SH, Hilleary R, Gilroy S (2014) Salt stress-induced Ca2+ waves are associated with rapid, long-distance root-to-shoot signaling in plants. Proceedings of the National Academy of Sciences of the United States of America **111:** 6497-6502

Chou ML, Fitzpatrick LM, Tu SL, Budziszewski G, Potter-Lewis S, Akita M, Levin JZ, Keegstra K, Li HM (2003) Tic40, a membrane-anchored co-chaperone homolog in the chloroplast protein translocon. EMBO J **22:** 2970-2980

Corso M, Doccula FG, de Melo JRF, Costa A, Verbruggen N (2018) Endoplasmic reticulum-localized CCX2 is required for osmotolerance by regulating ER and cytosolic Ca2+ dynamics in Arabidopsis. Proceedings of the National Academy of Sciences of the United States of America **115:** 3966-3971

Costa A, Drago I, Behera S, Zottini M, Pizzo P, Schroeder JI, Pozzan T, Lo Schiavo F (2010) H2O2 in plant peroxisomes: an in vivo analysis uncovers a Ca2+-dependent scavenging system. Plant Journal **62:** 760-772

Cotsaftis O, Plett D, Shirley N, Tester M, Hrmova M (2012) A two-staged model of Na+ exclusion in rice explained by 3D modeling of HKT transporters and alternative splicing. PLoS One **7:** e39865

Demmig B, Gimmler H (1983) Properties of the Isolated Intact Chloroplast at Cytoplasmic K Concentrations : I. Light-Induced Cation Uptake into Intact Chloroplasts is Driven by an Electrical Potential Difference. Plant Physiol **73:** 169-174

DeTar RA, Barahimipour R, Manavski N, Schwenkert S, Höhner R, Bölter B, Inaba T, Meurer J, Zoschke R, Kunz H-H (2021) Loss of inner-envelope K+/H+ exchangers impairs plastid rRNA maturation and gene expression. The Plant Cell

Diallinas G (2014) Understanding transporter specificity and the discrete appearance of channel-like gating domains in transporters. Front Pharmacol **5:** 207

Duggleby RG, Dennis DT (1973) Pyruvate-Kinase, a Possible Regulatory Enzyme in Higher-Plants. Plant Physiology **52:** 312-317

Embley TM, Martin W (2006) Eukaryotic evolution, changes and challenges. Nature **440:** 623-630

EPA (2019) United States Environmental Protection Agency. Inventory of US greenhouse gas emissions and sinks: 1990–2019. EPA 430-R-21-005

Epstein E, Rains DW, Elzam OE (1963) Resolution of Dual Mechanisms of Potassium Absorption by Barley Roots. Proc Natl Acad Sci U S A **49:** 684-692

Essah PA, Davenport R, Tester M (2003) Sodium influx and accumulation in Arabidopsis. Plant Physiol **133:** 307-318

Evenson RE, Gollin D (2003) Assessing the impact of the green revolution, 1960 to 2000. Science **300:** 758-762

Eynard A, Lal R, Wiebe K (2005) Crop response in salt-affected soils. Journal of Sustainable Agriculture **27:** 5-50

Ferro M, Salvi D, Brugiere S, Miras S, Kowalski S, Louwagie M, Garin J, Joyard J, Rolland N (2003) Proteomics of the chloroplast envelope membranes from Arabidopsis thaliana. Molecular & Cellular Proteomics **2:** 325-345

Ferro M, Salvi D, Riviere-Rolland H, Vermat T, Seigneurin-Berny D, Grunwald D, Garin J, Joyard J, Rolland N (2002) Integral membrane proteins of the chloroplast envelope: Identification and subcellular localization of new transporters. Proceedings of the National Academy of Sciences of the United States of America **99:** 11487-11492

Flowers TJ, Hajibagheri MA, Yeo AR (1991) Ion accumulation in the cell walls of rice plants growing under saline conditions—evidence for the Oertli hypothesis. Plant Cell Environ **14**:319–325

Flowers TJ, Munns R, Colmer TD (2015) Sodium chloride toxicity and the cellular basis of salt tolerance in halophytes. Annals of Botany **115:** 419-431

Frank J, Happeck R, Meier B, Hoang MTT, Stribny J, Hause G, Ding H, Morsomme P, Baginsky S, Peiter E (2019) Chloroplast-localized BICAT proteins shape stromal calcium signals and are required for efficient photosynthesis. New Phytol **221:** 866-880

Furumoto T, Yamaguchi T, Ohshima-Ichie Y, Nakamura M, Tsuchida-Iwata Y, Shimamura M, Ohnishi J, Hata S, Gowik U, Westhoff P, Brautigam A, Weber APM, Izui K (2011) A plastidial sodium-dependent pyruvate transporter. Nature **478:** 274-274

Galloway JN, Aber JD, Erisman JW, Seitzinger SP, Howarth RW, Cowling EB, Cosby BJ (2003) The nitrogen cascade. Bioscience **53:** 341-356

Gierth M, Maser P (2007) Potassium transporters in plants - Involvement in K+ acquisition, redistribution and homeostasis. Febs Letters **581:** 2348-2356

Gierth M, Maser P, Schroeder JI (2005) The potassium transporter AtHAK5 functions in K+ deprivation-induced high-affinity K+ uptake and AKT1 K+ channel contribution to K+ uptake kinetics in Arabidopsis roots. Plant Physiology **137:** 1105-1114

Glenn EP, Brown JJ, Blumwald E (1999) Salt Tolerance and Crop Potential of Halophytes. Critical Reviews in Plant Sciences **18:** 227-255

Glover JD, Reganold JP (2010) Perennial grains: Food security for the future. Issues in Science and Technology **26:** 41-47

Golldack D, Quigley F, Michalowski CB, Kamasani UR, Bohnert HJ (2003) Salinity stress-tolerant and -sensitive rice (Oryza sativa L.) regulate AKT1-type potassium channel transcripts differently. Plant Molecular Biology **51:** 71-81

Gomez-Porras JL, Riano-Pachon DM, Benito B, Haro R, Sklodowski K, Rodriguez-Navarro A, Dreyer I (2012) Phylogenetic analysis of K+ transporters in bryophytes, lycophytes, and flowering plants indicates a specialization of vascular plants. Frontiers in Plant Science **3:** 167

Gouaux E, Mackinnon R (2005) Principles of selective ion transport in channels and pumps. Science **310:** 1461-1465

Gould SB, Waller RR, McFadden GI (2008) Plastid evolution. Annual Review of Plant Biology **59:** 491-517

Guerrero-Mendiola C, Garcia-Trejo JJ, Encalada R, Saavedra E, Ramirez-Silva L (2017) The contribution of two isozymes to the pyruvate kinase activity of Vibrio cholerae: One K (+)- dependent constitutively active and another K (+)- independent with essential allosteric activation. Plos One **12**

Gutierrez-Carbonell E, Takahashi D, Lattanzio G, Rodriguez-Celma J, Kehr J, Soll J, Philippar K, Uemura M, Abadia J, Lopez-Millan AF (2014) The distinct functional roles of the inner and outer chloroplast envelope of Pea (Pisum sativum) as revealed by proteomic approaches. J Proteome Res **13:** 2941-2953

H Greenway a, Munns R (1980) Mechanisms of Salt Tolerance in Nonhalophytes. Annual Review of Plant Physiology **31:** 149-190

Haswell ES, Meyerowitz EM (2006) MscS-like proteins control plastid size and shape in Arabidopsis thaliana. Curr Biol **16:** 1-11

Hanin M, Ebel C, Ngom M, Laplaze L, Masmoudi K (2016) New Insights on Plant Salt Tolerance Mechanisms and Their Potential Use for Breeding. Frontiers in Plant Science **7**

Hedrich R (2012) Ion channels in plants. Physiol Rev **92:** 1777-1811

Hirsch RE, Lewis BD, Spalding EP, Sussman MR (1998) A role for the AKT1 potassium channel in plant nutrition. Science **280:** 918-921

Höhner R, Galvis VC, Strand DD, Völkner C, Kramer M, Messer M, Dinc F, Sjuts I, Bolter B, Kramer DM, Armbruster U, Kunz HH (2019) Photosynthesis in Arabidopsis Is Unaffected by the Function of the Vacuolar K(+) Channel TPK3. Plant Physiol **180:** 1322-1335

Hooper CM, Castleden IR, Tanz SK, Aryamanesh N, Millar AH (2017) SUBA4: the interactive data analysis centre for Arabidopsis subcellular protein locations. Nucleic Acids Res **45:** D1064-D1074

Jarvis P, Soll J (2001) Toc, Tic, and chloroplast protein import. Biochim Biophys Acta **1541:** 64-79

Kaiser E, Morales A, Harbinson J (2018) Fluctuating Light Takes Crop Photosynthesis on a Rollercoaster Ride. Plant Physiol **176:** 977-989

Kayne FJ (1971) Thallium (I) Activation of Pyruvate Kinase. Archives of Biochemistry and Biophysics **143:** 232-&

Kim S, Zeng W, Bernard S, Liao J, Venkateshwaran M, Ane JM, Jiang Y (2019) Ca(2+)-regulated Ca(2+) channels with an RCK gating ring control plant symbiotic associations. Nat Commun **10:** 3703

Kim TH, Bohmer M, Hu HH, Nishimura N, Schroeder JI (2010) Guard Cell Signal Transduction Network: Advances in Understanding Abscisic Acid, CO2, and Ca2+ Signaling. Annual Review of Plant Biology, Vol 61 **61:** 561-591

Kim TH, Kunz HH, Bhattacharjee S, Hauser F, Park J, Engineer C, Liu A, Ha T, Parker JE, Gassmann W, Schroeder JI (2012) Natural variation in small molecule-induced TIR-NB-LRR signaling induces root growth arrest via EDS1- and PAD4-complexed R protein VICTR in Arabidopsis. Plant Cell **24:** 5177-5192

Kleine T, Leister D (2016) Retrograde signaling: Organelles go networking. Biochim Biophys Acta **1857:** 1313-1325

Knight H, Trewavas AJ, Knight MR (1996) Cold calcium signaling in Arabidopsis involves two cellular pools and a change in calcium signature after acclimation. Plant Cell **8:** 489-503

Knight H, Trewavas AJ, Knight MR (1997) Calcium signalling in Arabidopsis thaliana responding to drought and salinity. Plant Journal **12:** 1067-1078

Kouranov A, Schnell DJ (1997) Analysis of the interactions of preproteins with the import machinery over the course of protein import into chloroplasts. Journal of Cell Biology **139:** 1677-1685

Kronzucker HJ, Coskun D, Schulze LM, Wong JR, Britto DT (2013) Sodium as nutrient and toxicant. Plant and Soil **369:** 1-23

Kunz HH, Gierth M, Herdean A, Satoh-Cruz M, Kramer DM, Spetea C, Schroeder JI (2014) Plastidial transporters KEA1, -2, and -3 are essential for chloroplast osmoregulation, integrity, and pH regulation in Arabidopsis. Proc Natl Acad Sci U S A **111:** 7480-7485

Larsen TM, Benning MM, Rayment I, Reed GH (1998) Structure of the Bis(Mg2+)-ATP-oxalate complex of the rabbit muscle pyruvate kinase at 2.1 angstrom resolution: ATP binding over a barrel. Biochemistry **37:** 6247-6255

Lebaudy A, Very AA, Sentenac H (2007) K+ channel activity in plants: genes, regulations and functions. FEBS Lett **581:** 2357-2366

Lebergott S (1966) Labor force and employment, 1800–1960. *In* Output, employment, and productivity in the United States after 1800. NBER, pp 117-204

Leigh RA, Jones RGW (1984) A Hypothesis Relating Critical Potassium Concentrations for Growth to the Distribution and Functions of This Ion in the Plant-Cell. New Phytologist **97:** 1-13

Leitao N, Dangeville P, Carter R, Charpentier M (2019) Nuclear calcium signatures are associated with root development. Nat Commun **10:** 4865

Lenzoni G, Knight MR (2019) Increases in Absolute Temperature Stimulate Free Calcium Concentration Elevations in the Chloroplast. Plant Cell Physiol **60:** 538-548

Levina N, Totemeyer S, Stokes NR, Louis P, Jones MA, Booth IR (1999) Protection of Escherichia coli cells against extreme turgor by activation of MscS and MscL mechanosensitive channels: identification of genes required for MscS activity. EMBO J **18:** 1730-1737

Logan DC, Knight MR (2003) Mitochondrial and cytosolic calcium dynamics are differentially regulated in plants. Plant Physiology **133:** 21-24

Maathuis FJM (2009) Physiological functions of mineral macronutrients. Current Opinion in Plant Biology **12:** 250-258

Malagoli P, Britto DT, Schulze LM, Kronzucker HJ (2008) Futile Na+ cycling at the root plasma membrane in rice (Oryza sativa L.): kinetics, energetics, and relationship to salinity tolerance. J Exp Bot **59:** 4109-4117

Manzoor H, Chiltz A, Madani S, Vatsa P, Schoefs B, Pugin A, Garcia-Brugger A (2012) Calcium signatures and signaling in cytosol and organelles of tobacco cells induced by plant defense elicitors. Cell Calcium **51:** 434-444

Marcel D, Muller T, Hedrich R, Geiger D (2010) K+ transport characteristics of the plasma membrane tandem-pore channel TPK4 and pore chimeras with its vacuolar homologs. Febs Letters **584:** 2433-2439

Marschner H, Marschner P (2012) Marschner's mineral nutrition of higher plants, Ed 3rd. Elsevier/Academic Press, London ; Waltham, MA

Maser P, Thomine S, Schroeder JI, Ward JM, Hirschi K, Sze H, Talke IN, Amtmann A, Maathuis FJM, Sanders D, Harper JF, Tchieu J, Gribskov M, Persans MW, Salt DE, Kim SA, Guerinot ML (2001) Phylogenetic relationships within cation transporter families of Arabidopsis. Plant Physiology **126:** 1646-1667

Mengel K, Arneke WW (1982) Effect of Potassium on the Water Potential, the Pressure Potential, the Osmotic Potential and Cell Elongation in Leaves of Phaseolus-Vulgaris. Physiologia Plantarum **54:** 402-408

Meyerhoff O, Muller K, Roelfsema MR, Latz A, Lacombe B, Hedrich R, Dietrich P, Becker D (2005) AtGLR3.4, a glutamate receptor channel-like gene is sensitive to touch and cold. Planta **222:** 418-427

Millar N, Robertson GP, Grace PR, Gehl RJ, Hoben JP (2010) Nitrogen fertilizer management for nitrous oxide (N2O) mitigation in intensive corn (Maize) production: an emissions reduction protocol for US Midwest agriculture (vol 15, pg 185, 2010). Mitigation and Adaptation Strategies for Global Change **15:** 411-411

Milo R, Phillips R (2016) Cell biology by the numbers. Garland Science, Taylor & Francis Group, New York, NY

Mitchell P (1966) Chemiosmotic Coupling in Oxidative and Photosynthetic Phosphorylation. Biological Reviews of the Cambridge Philosophical Society **41:** 445-502

Moller IS, Gilliham M, Jha D, Mayo GM, Roy SJ, Coates JC, Haseloff J, Tester M (2009) Shoot Na+ exclusion and increased salinity tolerance engineered by cell type-specific alteration of Na+ transport in Arabidopsis. Plant Cell **21:** 2163-2178

Muller M, Kunz HH, Schroeder JI, Kemp G, Young HS, Neuhaus HE (2014) Decreased capacity for sodium export out of Arabidopsis chloroplasts impairs salt tolerance, photosynthesis and plant performance. Plant J **78:** 646-658

Muller P, Li XP, Niyogi KK (2001) Non-photochemical quenching. A response to excess light energy. Plant Physiol **125:** 1558-1566

Munns R, James RA, Xu B, Athman A, Conn SJ, Jordans C, Byrt CS, Hare RA, Tyerman SD, Tester M, Plett D, Gilliham M (2012) Wheat grain yield on saline soils is improved by an ancestral Na(+) transporter gene. Nat Biotechnol **30:** 360-364

Nomura H, Komori T, Kobori M, Nakahira Y, Shiina T (2008) Evidence for chloroplast control of external Ca2+-induced cytosolic Ca2+ transients and stomatal closure. Plant J **53:** 988-998

Nomura H, Komori T, Uemura S, Kanda Y, Shimotani K, Nakai K, Furuichi T, Takebayashi K, Sugimoto T, Sano S, Suwastika IN, Fukusaki E, Yoshioka H, Nakahira Y, Shiina T (2012) Chloroplast-mediated activation of plant immune signalling in Arabidopsis. Nat Commun **3:** 926

Oertli J (1968) Extracellular salt accumulation a possible mechanism of salt injury in plants. Agrochimica **12:** 461-469

Ohnishi J, Flugge UI, Heldt HW, Kanai R (1990) Involvement of Na+ in Active Uptake of Pyruvate in Mesophyll Chloroplasts of Some C4 Plants - Na+/Pyruvate Cotransport. Plant Physiology **94:** 950-959

Ohnishi J, Kanai R (1990) Pyruvate Uptake Induced by a Ph Jump in Mesophyll Chloroplasts of Maize and Sorghum, Nadp-Malic Enzyme Type-C4 Species. Febs Letters **269:** 122-124

Organisation for Economic Co-operation and Development (2017) Water risk hotspots for agriculture. OECD Publishing, Paris

Pain D, Blobel G (1987) Protein Import into Chloroplasts Requires a Chloroplast Atpase. Proceedings of the National Academy of Sciences of the United States of America **84:** 3288-3292

Peiter E, Maathuis FJM, Mills LN, Knight H, Pelloux J, Hetherington AM, Sanders D (2005) The vacuolar Ca2+-activated channel TPC1 regulates germination and stomatal movement. Nature **434:** 404-408

Pottosin, II, Muniz J, Shabala S (2005) Fast-activating channel controls cation fluxes across the native chloroplast envelope. J Membr Biol **204:** 145-156

Pottosin I, Dobrovinskaya O (2015) Ion Channels in Native Chloroplast Membranes: Challenges and Potential for Direct Patch-Clamp Studies. Front Physiol **6:** 396

Qudeimat E, Faltusz AMC, Wheeler G, Lang D, Brownlee C, Reski R, Frank W (2008) A P-IIB-type Ca2+-ATPase is essential for stress adaptation in Physcomitrella patens. Proceedings of the National Academy of Sciences of the United States of America **105:** 19555-19560

Ray DK, Mueller ND, West PC, Foley JA (2013) Yield Trends Are Insufficient to Double Global Crop Production by 2050. PLoS One **8:** e66428

Resentini F, Ruberti C, Grenzi M, Bonza MC, Costa A (2021) The signatures of organellar calcium. Plant Physiol

Richly E, Leister D (2004) An improved prediction of chloroplast proteins reveals diversities and commonalities in the chloroplast proteomes of Arabidopsis and rice. Gene **329:** 11-16

Richter S, Lamppa GK (2002) Determinants for removal and degradation of transit peptides of chloroplast precursor proteins. Journal of Biological Chemistry **277:** 43888-43894

Rubio F, Nieves-Cordones M, Aleman F, Martinez V (2008) Relative contribution of AtHAK5 and AtAKT1 to K(+) uptake in the high-affinity range of concentrations. Physiologia Plantarum **134:** 598-608

Santa-Maria GE, Rubio F, Dubcovsky J, Rodriguez-Navarro A (1997) The HAK1 gene of barley is a member of a large gene family and encodes a high-affinity potassium transporter. Plant Cell **9:** 2281-2289

Shabala S, Demidchik V, Shabala L, Cuin TA, Smith SJ, Miller AJ, Davies JM, Newman IA (2006) Extracellular Ca2+ ameliorates NaCl-induced K+ loss from Arabidopsis root and leaf cells by controlling plasma membrane K+-perme- able channels. Plant Physiol **141**:1653–1665

Schachtman DP, Kumar R, Schroeder JI, Marsh EL (1997) Molecular and functional characterization of a novel low-affinity cation transporter (LCT1) in higher plants. Proc Natl Acad Sci U S A **94:** 11079-11084

Scheible N, McCubbin A (2019) Signaling in Pollen Tube Growth: Beyond the Tip of the Polarity Iceberg. Plants-Basel **8**

Schneider A, Steinberger I, Herdean A, Gandini C, Eisenhut M, Kurz S, Morper A, Hoecker N, Ruhle T, Labs M, Flugge UI, Geimer S, Schmidt SB, Husted S, Weber AP, Spetea C, Leister D (2016) The Evolutionarily Conserved Protein PHOTOSYNTHESIS AFFECTED MUTANT71 Is Required for Efficient Manganese Uptake at the Thylakoid Membrane in Arabidopsis. Plant Cell **28:** 892-910

Schroeder JI, Delhaize E, Frommer WB, Guerinot ML, Harrison MJ, Herrera-Estrella L, Horie T, Kochian LV, Munns R, Nishizawa NK, Tsay YF, Sanders D (2013) Using membrane transporters to improve crops for sustainable food production. Nature **497:** 60-66

Schwacke R, Schneider A, van der Graaff E, Fischer K, Catoni E, Desimone M, Frommer WB, Flugge UI, Kunze R (2003) ARAMEMNON, a novel database for Arabidopsis integral membrane proteins. Plant Physiol **131:** 16-26

Schwender J, Goffman F, Ohlrogge JB, Shachar-Hill Y (2004) Rubisco without the Calvin cycle improves the carbon efficiency of developing green seeds. Nature **432:** 779-782

Schwenkert S, Soll J, Bolter B (2011) Protein import into chloroplasts-How chaperones feature into the game. Biochimica Et Biophysica Acta-Biomembranes **1808:** 901-911

Sello S, Moscatiello R, Mehlmer N, Leonardelli M, Carraretto L, Cortese E, Zanella FG, Baldan B, Szabo I, Vothknecht UC, Navazio L (2018) Chloroplast Ca2+ Fluxes into and across Thylakoids Revealed by Thylakoid-Targeted Aequorin Probes. Plant Physiology **177:** 38-51

Sharma T, Dreyer I, Riedelsberger J (2013) The role of K+ channels in uptake and redistribution of potassium in the model plant Arabidopsis thaliana. Frontiers in Plant Science **4:**224

Smil V (2001) Enriching the earth : Fritz Haber, Carl Bosch, and the transformation of world food production. MIT Press, Cambridge, Mass.

Stephan AB, Kunz HH, Yang E, Schroeder JI (2016) Rapid hyperosmotic-induced Ca2+ responses in Arabidopsis thaliana exhibit sensory potentiation and involvement of plastidial KEA transporters. Proc Natl Acad Sci U S A **113:** E5242-5249

Stringer CB, Andrews P (1988) Genetic and fossil evidence for the origin of modern humans. Science **239:** 1263-1268

Subbarao GV, Ito O, Berry WL, Wheeler RM (2003) Sodium - A functional plant nutrient. Critical Reviews in Plant Sciences **22:** 391-416

Sun Q, Zybailov B, Majeran W, Friso G, Olinares PD, van Wijk KJ (2009) PPDB, the Plant Proteomics Database at Cornell. Nucleic Acids Res **37:** D969-974

Tanaka K, Swanson SJ, Gilroy S, Stacey G (2010) Extracellular Nucleotides Elicit Cytosolic Free Calcium Oscillations in Arabidopsis. Plant Physiology **154:** 705-719

Teardo E, Carraretto L, Moscatiello R, Cortese E, Vicario M, Festa M, Maso L, De Bortoli S, Cali T, Vothknecht UC, Formentin E, Cendron L, Navazio L, Szabo I (2019) A chloroplast-localized mitochondrial calcium uniporter transduces osmotic stress in Arabidopsis. Nat Plants **5:** 581-588

Teardo E, Formentin E, Segalla A, Giacometti GM, Marin O, Zanetti M, Lo Schiavo F, Zoratti M, Szabo I (2011) Dual localization of plant glutamate receptor AtGLR3.4 to plastids and plasmamembrane. Biochim Biophys Acta **1807:** 359-367

Tikhonov AN (2014) The cytochrome b6f complex at the crossroad of photosynthetic electron transport pathways. Plant Physiol Biochem **81:** 163-183

Timmis JN, Ayliffe MA, Huang CY, Martin W (2004) Endosymbiotic gene transfer: organelle genomes forge eukaryotic chromosomes. Nat Rev Genet **5:** 123-135

Tomizioli M, Lazar C, Brugiere S, Burger T, Salvi D, Gatto L, Moyet L, Breckels LM, Hesse AM, Lilley KS, Seigneurin-Berny D, Finazzi G, Rolland N, Ferro M (2014) Deciphering thylakoid sub-compartments using a mass spectrometry-based approach. Mol Cell Proteomics **13:** 2147-2167

Tsujii M, Kera K, Hamamoto S, Kuromori T, Shikanai T, Uozumi N (2019) Evidence for potassium transport activity of Arabidopsis KEA1-KEA6. Sci Rep **9:** 10040

Vainonen JP, Sakuragi Y, Stael S, Tikkanen M, Allahverdiyeva Y, Paakkarinen V, Aro E, Suorsa M, Scheller HV, Vener AV, Aro EM (2008) Light regulation of CaS, a novel phosphoprotein in the thylakoid membrane of Arabidopsis thaliana. FEBS J **275:** 1767-1777

van Meer G, Voelker DR, Feigenson GW (2008) Membrane lipids: where they are and how they behave. Nat Rev Mol Cell Biol **9:** 112-124

Van Zanden JL (1991) The 1st Green-Revolution - the Growth of Production and Productivity in European Agriculture, 1870-1914. Economic History Review **44:** 215-239

Vincill ED, Bieck AM, Spalding EP (2012) Ca(2+) conduction by an amino acid-gated ion channel related to glutamate receptors. Plant Physiol **159:** 40-46

Voelker C, Gomez-Porras JL, Becker D, Hamamoto S, Uozumi N, Gambale F, Mueller-Roeber B, Czempinski K, Dreyer I (2010) Roles of tandem-pore K plus channels in plants - a puzzle still to be solved. Plant Biology **12:** 56-63

Völkner C, Holzner LJ, Day PM, Ashok AD, Vries Jd, Bölter B, Kunz H-H (2021) Two plastid POLLUX ion channel-like proteins are required for stress-triggered stromal Ca2+ release. Plant Physiology

von Heijne G (2006) Membrane-protein topology. Nature reviews Molecular cell biology **7:** 909-918

Wang CM, Zhang JL, Liu XS, Li Z, Wu GQ, Cai JY, Flowers TJ, Wang SM (2009) Puccinellia tenuiflora maintains a low Na+ level under salinity by limiting unidirectional Na+ influx resulting in a high selectivity for K+ over Na+. Plant Cell Environ **32:** 486-496

Wang X, Berkowitz GA, Peters JS (1993) K+-conducting ion channel of the chloroplast inner envelope: functional reconstitution into liposomes. Proc Natl Acad Sci U S A **90:** 4981-4985

Ward JM (2001) Identification of novel families of membrane proteins from the model plant Arabidopsis thaliana. Bioinformatics **17:** 560-563

Weinl S, Held K, Schlucking K, Steinhorst L, Kuhlgert S, Hippler M, Kudla J (2008) A plastid protein crucial for Ca2+-regulated stomatal responses. New Phytol **179:** 675-686

Weinl S, Kudla J (2009) The CBL-CIPK Ca2+-decoding signaling network: function and perspectives. New Phytologist **184:** 517-528

Wetson AM, Flowers TJ (2010) The effect of saline hypoxia on growth and ion uptake in Suaeda maritima. Functional Plant Biology **37:** 646-655

Wilson ME, Basu MR, Bhaskara GB, Verslues PE, Haswell ES (2014) Plastid osmotic stress activates cellular stress responses in Arabidopsis. Plant Physiol **165:** 119-128

Witt HT (1979) Energy-Conversion in the Functional Membrane of Photosynthesis - Analysis by Light-Pulse and Electric Pulse Methods - Central Role of the Electric-Field. Biochimica Et Biophysica Acta **505:** 355-427

Woodson JD, Chory J (2008) Coordination of gene expression between organellar and nuclear genomes. Nature Reviews Genetics **9:** 383-395

Wu W, Peters J, Berkowitz GA (1991) Surface Charge-Mediated Effects of Mg on K Flux across the Chloroplast Envelope Are Associated with Regulation of Stromal pH and Photosynthesis. Plant Physiol **97:** 580-587

Zhang YX, Daday C, Gu RX, Cox CD, Martinac B, de Groot BL, Walz T (2021) Visualization of the mechanosensitive ion channel MscS under membrane tension. Nature **590:** 509-514

Zheng S, Pan T, Fan L, Qiu QS (2013) A novel AtKEA gene family, homolog of bacterial K+/H+ antiporters, plays potential roles in K+ homeostasis and osmotic adjustment in Arabidopsis. PLoS One **8:** e81463

Zhu JK (2002) Salt and drought stress signal transduction in plants. Annu Rev Plant Biol **53:** 247-273

Zhu XH, Feng Y, Liang GM, Liu N, Zhu JK (2013) Aequorin-Based Luminescence Imaging Reveals Stimulus- and Tissue-Specific Ca2+ Dynamics in Arabidopsis Plants. Molecular Plant **6:** 444-455

CHAPTER TWO: TWO PLASTID POLLUX ION CHANNEL-LIKE PROTEINS ARE REQUIRED FOR STRESS-TRIGGERED STROMAL CA^{2+} RELEASE

This chapter was previously published in the journal *Plant Physiology* with co-authors Lorenz Josef Holzner, Philip M. Day, Amra Dhabalia Ashok, Jan de Vries, Bettina Bölter, and Hans-Henning Kunz.

Received: 09 March 2021. Accepted: 11 August 2021. Published: 07 September 2021

DOI: https://doi.org/10.1093/plphys/kiab424

An addendum was added at the end of this chapter which contains noteworthy unpublished data on the putative role of the candidate proteins.

2.1 Abstract

Two decades ago, large cation currents were discovered in the envelope membranes of *Pisum sativum* L. (pea) chloroplasts. The deduced K^+-permeable channel was coined fast-activating chloroplast cation (FACC) channel but its molecular identity remained elusive. To reveal candidates, we mined proteomic datasets of isolated pea envelopes. Our search uncovered distant members of the nuclear POLLUX ion channel family. Since pea is not amenable to molecular genetics, we used *Arabidopsis thaliana* to characterize the two gene homologs. Using several independent approaches, we show that both candidates localize to the chloroplast envelope membrane. The proteins, designated PLASTID ENVELOPE ION CHANNELS (PEC1/2), form oligomers with regulator of K^+ conductance (RCK) domains protruding into the intermembrane space. Heterologous expression of PEC1/2 rescues yeast mutants deficient in K^+ uptake. Nuclear POLLUX ion channels cofunction with Ca^{2+} channels to generate Ca^{2+} signals, critical for establishing mycorrhizal symbiosis and root development. Chloroplasts also exhibit Ca^{2+} transients in the stroma, probably to relay abiotic and biotic cues between plastids and the

nucleus via the cytosol. Our results show that *pec1pec2* loss-of-function double mutants fail to trigger the characteristic stromal Ca^{2+} release observed in wild-type plants exposed to external stress stimuli. Besides this molecular abnormality, *pec1pec2* double mutants do not show obvious phenotypes. Future studies of PEC proteins will help to decipher the plant's stress-related Ca^{2+} signaling network and the role of plastids. More importantly, the discovery of PECs in the envelope membrane is another critical step towards completing the chloroplast ion transport protein inventory.

2.2 Introduction

Land plants cannot escape from environmental challenges collectively known as abiotic and biotic stress. Consequently, evolutionary innovations in the molecular mechanisms to sense and respond to rapidly changing conditions likely played a key role in the success of land plants (Furst-Jansen et al., 2020). Leaf plastids are optimized for light harvesting, rendering the organelle a sensory hub to collect information about the plant's environment. Chloroplasts employ several mechanisms to transmit environmental information to the nucleus to adjust gene expression. These include changes in metabolite and hormone levels, redox potential, reactive oxygen species (ROS) production, and ion flux. Through the action of ion channels and carriers, signals - encoded as ion transients - can be relayed within seconds. The best-known ion signals are Ca^{2+} transients which exist in plastids and several other organelles, including the nucleus (Resentini et al., 2021).

In the nuclear envelope, Ca^{2+} and K^{+} transport are coupled (Charpentier et al., 2016). The Ca^{2+} channel CYCLIC NUCLEOTIDE GATED CHANNEL 15 (CNGC15) functionally interacts with DMI, a member of the CASTOR/POLLUX/DMI ion channel family. Both channels work in concert to trigger Ca^{2+} transients critical for root development and in some

species mycorrhizal symbiosis (Charpentier et al., 2016; Leitao et al., 2019). In the plastid envelope, a similar system may exist as the organelle elicits stromal Ca^{2+} transients in responds to various triggers such as NaCl and osmotic shock (Nomura et al., 2012), temperature changes (Lenzoni and Knight, 2019), and circadian rhythms (Marti Ruiz et al., 2020). However, the inventory of ion transport proteins in the inner envelope (IE) membrane of plastids is still incomplete. Only recently, the dual-targeted ion channel cMCU was discovered, and reportedly plays a role in Ca^{2+} flux into mitochondria and mature chloroplasts (Teardo et al., 2019). Indeed, *cmcu* loss-of-function mutants show dampened stromal Ca^{2+} flux in response to osmotic but not salt-stress (Teardo et al., 2019). Because significant stromal Ca^{2+} transients remain in *cmcu*, other ion channels and/ or Ca^{2+} transporters are expected in the plastid IE membrane (Resentini et al., 2021). The CMT1/BICAT2 transporter was suggested as an alternative IE Ca^{2+} transporter as its absence impacts the shape of stromal Ca^{2+} release after dark transition (Frank et al., 2019). However, other data indicate that this particular carrier may primarily transport Mn^{2+} ions (Eisenhut et al., 2018; Zhang et al., 2018).

Knowledge about plastid K^+ flux across the IE is similarly limited. Thus far, only two K^+/H^+ exchangers from the KEA family have been characterized in more detail (Aranda-Sicilia et al., 2012; Kunz et al., 2014). Both carriers (KEA1 and KEA2) physiologically function in pH and ion homeostasis which is critical for plastid gene expression and development (Aranda Sicilia et al., 2021; DeTar et al., 2021). The IE membrane potential of at least -70 mV on the stromal side (Wu et al., 1991) makes K^+/H^+ valves such as KEA1/2 a necessity for osmoregulation to balance K^+ influx and prevent rupture of plastids (Bernardi, 1999). To functionally describe IE cation channel(s) that aid in ion influx, reconstituted proteins from *Spinacia oleracea* L. (spinach) (Wang et al., 1993; Mi et al., 1994) or *Pisum sativum* L. (pea)

(Pottosin et al., 2005) chloroplasts were employed in electrophysiological studies; these efforts resulted in the characterization of the voltage-dependent FACC channel of pea chloroplasts (Pottosin et al., 2005). The channel exhibits conductivity for $K^+ > Na^+ > Ca^{2+} \geq Mg^{2+}$ ions. While the experimental setup seemed to assure that the channel(s)' activity originated from the IE membrane (Pottosin and Dobrovinskaya, 2015), it is not entirely clear if the currents came exclusively from a single channel type. Fifteen years later no FACC channel gene candidate(s) has emerged to explain what protein(s) may have caused the recorded K^+ currents in patch-clamped pea chloroplasts.

In this study, we set out to identify first candidate proteins and their corresponding genetic loci that may explain the recorded K^+ and other cation currents in the chloroplast IE membrane. By mining proteomic data on pea and *A. thaliana* leaf plastids, distant members of the CASTOR/POLLUX/DMI ion channel family emerged as potential FACC candidates. Therefore, the goal of this study was to a) determine if leaf plastids indeed possess members from the CASTOR/POLLUX ion channel family, b) gain initial insights into their physiological relevance through heterologous expression in yeast and the study of *A. thaliana* loss-of-function mutants, and c) test if plastid Ca^{2+} transients depend on the activity of CASTOR/POLLUX-like ion channels.

2.3 Results and Discussion

The family of CASTOR/POLLUX cation channels contains functionally similar members with plastid transit peptides

To identify potential FACC candidates, we mined published pea chloroplast envelope proteome datasets (Brautigam et al., 2008; Gutierrez-Carbonell et al., 2014). Only four different protein types related to ion transport were found: PAA1 (copper transporting ATPase),

Glutathione-regulated potassium-efflux system protein (KEA), Voltage-dependent anion-selective channel protein (VDAC), and probable ion channel CASTOR-like (Psat6g113560). PAA1 and KEA represent well-characterized carriers (Shikanai et al., 2003; Aranda-Sicilia et al., 2012; Kunz et al., 2014; Tsujii et al., 2019) and are therefore unlikely responsible for FACC-mediated currents. VDAC, a frequent contaminant in plastid proteomics, is an anion-selective channel in the mitochondrial outer membrane (Clausen et al., 2004). However, a protein annotated "probable ion channel CASTOR-like" was intriguing as CASTOR/POLLUX/DMI have been described as nuclear cation channels with conductance for K^+, Rb^+, Na^+, and Ca^{2+} (Charpentier et al., 2008; Venkateshwaran et al., 2012; Kim et al., 2019). We designated the candidate plastid envelope ion channel, PEC. To understand the evolutionary history of PEC, POLLUX, and CASTOR, we performed a phylogenetic analysis (Fig. 2.1). We used: (i) POLLUX, CASTOR, and DMI proteins from *Lotus japonicus*, *Medicago truncatula*, *Pisum sativum*, and *Oryza sativa*; (ii) PEC proteins from *Arabidopsis thaliana* (At5g02940, At5g43745) as query in a BLASTp search against a dataset of 17 land plants, eleven streptophyte algae, and four chlorophyte algae. Among these 31 Chloroplastida, we detected 157 homologs with a minimum length of 700 amino acids. These long homologs were used in all following analyses; the topology stayed robust when we included shorter sequences (Suppl. Fig. S2.1). PEC's structural similarity to the SLO big potassium (BK) channel family (Roy et al., 2010), led us to add 13 animal SLO sequences as an outgroup.

All homologs of PEC, POLLUX, and CASTOR fell into a fully-supported clade of diverse sequences from Chloroplastida (Fig. 2.1). In this large Chloroplastida clade, a few chlorophyte homologs branch sister to all other streptophyte sequences. The sequences from streptophytes (forming a sub-clade, bootstrap support of 87) were distributed over two major

clades: a PEC clade and a CASTOR/POLLUX clade. Homologs of PEC fell into a fully-supported clade that included sequences spanning the diversity of streptophytes; we detected PEC homologs in all major classes of streptophyte algae—from those most divergent from land plants, represented by *Chlorokybus atmophyticus* and *Mesostigma viride* (Wang et al., 2020)—and diverse land plants. Nested within this clade of putative streptophyte PEC proteins was an angiosperm-specific sub-clade, in which a PEC homolog from *Amborella trichopoda* (see (Amborella Genome, 2013)) branched sister to homologs from all other angiosperms—which is in line with its position in the species phylogeny. A duplication that gave rise to *At*PEC1 and *t*PEC2 appears specific to the genus *Arabidopsis*.

The large CASTOR/POLLUX clade (ultrafast bootstrap support of 91) also contained homologs from across the diversity of streptophytes; the topology of this clade largely followed the species phylogeny. Clear orthogroups of solely CASTOR and solely POLLUX first appeared in angiosperms; in each of these two clades, *Amborella* sequences branch sister to the other angiosperm sequences, suggesting a duplication event that occurred in a common ancestor of all extant angiosperms. It is noteworthy that, branching sister to the streptophyte CASTOR/POLLUX clade, we recovered a fully-supported clade that contained homologs from diverse non-vascular streptophytes (including representatives of all streptophyte algae); this suggests that there was another very early duplication of the CASTOR/POLLUX ortholog followed by a loss early during vascular evolution—or euphyllophyte evolution (see Suppl. Fig. S2.1, where a *Selaginella* homolog falls into this clade).

In sum, it appears that there was a single PEC/CASTOR/POLLUX ortholog in the last common ancestor of Chloroplastida when the green lineage was in its infancy. At the base of Streptophyta, this ortholog duplicated, giving rise to the clade of PECs and the clade of

CASTOR/POLLUX proteins. During the course of evolution, there were some lineage-specific duplications in each of the orthogroups—including the duplication in a common ancestor of angiosperms that gave rise to the separate POLLUX and CASTOR clades. From a bird's eye view, the orthogroups of PEC and CASTOR/POLLUX are each likely as old as Streptophyta.

We compared functional domains of *At*PEC1/2 with the nuclear member DMI1 using InterPro (Suppl. Fig. S2.2A). All three proteins contain a well-conserved C-terminal CASTOR/POLLUX domain (IPR010420). This stretch includes a tandem RCK domain (IPR036721), previously determined as functionally relevant for the nuclear members (Kim et al., 2019). In the N-terminal regions the three members differ. Only PEC1/2 possess a voltage-gated potassium channel superfamily domain (SSF81324) which was not identified in DMI1. Additionally, both PEC members contain a predicted plastid transit peptide (pTP)(Schwacke et al., 2003; Sun et al., 2009) and were identified in recent envelope proteomes from *Arabidopsis* (Bouchnak et al., 2019; Trentmann et al., 2020).

Figure 2.1 Phylogenetic tree of PEC/CASTOR/ POLLUX family members. (Next page) A) Phylogenetic framework for the evolutionary history of PEC, CASTOR, and POLLUX. Homologs of PEC, CASTOR, and POLLUX were sampled from genomes of 17 land plants, seven streptophyte algae, and four chlorophytes. We further added in silico translated homologs from the transcriptomes of *Spirogyra pratensis* (de Vries et al., 2020), *Coleochaete scutata* and *Zygnema circumcarinatum* (de Vries et al., 2018), and *Coleochaete orbicularis* (Ju et al., 2015). 13 animal SLO1 sequences were included as an outgroup (blue). Only protein sequences longer than 700 amino acids were included in the analysis. A rooted maximum likelihood phylogeny of all 170 sequences was computed using LG+F+R7 as model for protein evolution (chosen according to BIC). 1000 ultrafast bootstrap (UFBoot2, (Hoang et al., 2018)) replicates were computed. Only ultrafast bootstrap values ≥50 are shown and full support (ultrafast bootstrap values of 1000) is depicted by a filled dot. PEC, CASTOR, and POLLUX sequences are found across the green lineage (fully-supported yellow clade) and were likely present as a single-copy ortholog in the last common ancestor of Chloroplastida. Early during streptophyte evolution, the PEC / CASTOR / POLLUX ortholog duplicated, giving rise to the clade of streptophyte PECs (hues of orange) and CASTOR / POLLUX (hues of teal green). Scale bar length corresponds to 2.0 expected substitutions per site.


2.0
PEC2 PEC1
angiosperm PEC
bryophyte PEC
streptophyte PEC
CASTOR
POLLUX
streptophyte CASTOR / POLLUX
Chloroplastida CASTOR / POLLUX / PEC
non-vascular streptophyte CASTOR / POLLUX likes
animal Slo1

Heterologous expression of PEC1 and PEC2 rescues a K^+ transport deficient yeast mutant

Nuclear envelope members of the CASTOR/POLLUX cation channel family exhibit conductivity for K^+, Rb^+, Na^+, and Ca^{2+} ions (Charpentier et al., 2008; Kim et al., 2019). Initially, we injected PEC1/2-YFP (-pTPs) cRNA into Xenopus oocytes to perform electrophysiology. However, oocytes did not synthesize the candidate proteins and PEC1/2-YFP was not detectable at the plasma membrane.

Therefore, we employed *yeast* in which the plasma membrane K^+-transportome is well-established (reviewed in (Arino et al., 2019)) and that had been successfully used as a model to study POLLUX family channels (Charpentier et al., 2008). Heterologous expression of *Lj*POLLUX restored growth of MAB2d, a yeast mutant defective in K^+ uptake and K^+ efflux across the plasma membrane (Maresova and Sychrova, 2005), at low K^+ (Charpentier et al., 2008). PEC1/2 (-pTPs) were cloned into the constitutive expression yeast vector pYeT. As a control, we cloned DMI1, the closest Arabidopsis homolog to *Lj*POLLUX. Resulting strains were grown overnight in K^+ supplemented media and washed extensively. OD_{600} was adjusted and cells were spotted side-by-side on media plates supplemented with increasing K^+ amounts from 0 mM to 25 mM KCl (Fig. 2.2A). While the WT strain W303 showed strong growth at all K^+ levels, MAB2d +pYeT-empty vector cells were severely growth limited below 25 mM KCl in the growth medium. DMI1, the Arabidopsis homolog of *Lj*POLLUX, did not robustly restore MAB2d mutant growth at low (<25 mM) KCl levels. In contrast, PEC1 and PEC2 transformed cells were able to grow on media even without additional KCl. PEC1/2 outperformed DMI1 in the MAB2d background, suggesting that PEC1 and PEC2 may possess higher K^+ permeability than DMI1 in this setup.

Independent studies confirm PEC1 and PEC2 as proteins of the plastid envelope membrane

For subcellular localization studies, PEC1/2 full-length cDNA YFP fusions were co-injected with plastid envelope marker TIC40-CFP into N. benthamiana leaves. The PEC1/2-YFP fluorescence signals appeared ring-shaped and overlayed with the IE marker TIC40-CFP (Fig. 2.2B). Both signals surrounded the chlorophyll (Chl a) fluorescence from the thylakoids. Line plots for each fluorescence channel confirmed the spatial signal overlay (Suppl. Fig. S2.3A). Truncated PEC1/2 variants lacking pTPs did not exhibit YFP signal around chl fluorescence but at the cell periphery (Suppl. Fig. S2.3B). We also attempted to establish stable full-length PEC1/2-YFP overexpressor mutants in *A. thaliana*. In successfully isolated T1 individuals YFP signal co-localized with the chl fluorescence (Suppl. Fig. S2.3C). Unfortunately, both constructs underwent transgene silencing in the T_2 generation.

Next, we radiolabeled PEC1/2 and DMI1 proteins with ^{35}S-Met. Isolated intact chloroplasts were incubated with labeled proteins and half of each reaction thermolysin treated to degrade non-imported substrate. After electrophoresis, protein bands were visualized using a phosphorimager (Suppl. Fig. S2.3D). For the two candidate plastid proteins PEC1/2 an additional smaller sized band was detectable in the plus and minus thermolysin lanes (see asterisks) which was absent in DMI1 lanes. The results confirm that only PEC1/2 carry plastid transit peptides which are processed by the TOC-TIC complex after import into the organelle. In summary, independent assays led us to conclude that PEC1/2 reside in leaf plastids. It is noteworthy that the DMI homolog was initially also suggested as a plastid channel (Imaizumi-Anraku et al., 2005). However, later it was shown that this was caused by a promoter artifact and that the nuclear membrane is the genuine CASTOR/POLLUX/DMI localization (Charpentier et al., 2008).

The C-terminal RCK domains of PEC1 reside in the envelope intermembrane space

To realize PEC1/2 immunolabeling studies we used the well-conserved C-terminal soluble stretch (≈ 64 kDa) harboring the RCK domain of PEC1 to raise serum (Suppl. Fig. S2.2B and S2.4A). The resulting α-PEC1 almost exclusively recognized PEC1, but not PEC2 or DMI1 (Suppl. Fig. S2.4B). Initially, we produced suborganellar fractions from A. thaliana chloroplasts. immunoblotting of established marker proteins confirmed fraction purity (Fig. 2.2C, Suppl. Fig. S2.4C). A strong enrichment of PEC1 was identified only in the plastid envelope fraction. To probe the topology of PEC1 and the localization of the functionally critical RCK domain, intact chloroplasts were isolated from WT plants. Subsequently, isolated plastids were incubated with increasing amounts of trypsin (Fig. 2.2D, Suppl. Fig. S2.4D). Trypsin accesses the intermembrane space (IMS) but does not cross the IE as long as the plastids remain intact (Froehlich, 2011). TOC64, which expands from the outer envelope membrane into the cytosol, served as a control to monitor proper function of the peptidase at the cytosolic surface of the outer envelope, while KEA1/2 was used to show that trypsin entered the IMS. TIC40 is a plastid intactness indicator. The bulk of the TIC40 protein resides in the stroma and therefore only remains stable in the presence of trypsin if the IE membrane remains intact. In untreated chloroplasts, native PEC1 protein was detected at 75 kDa. In the presence of trypsin, TOC64, KEA1/2, and PEC1 were rapidly degraded while TIC40 signal remained unchanged. Because no stable PEC1 degradation product of ≈ 64 kDa accumulated, our results suggest that the long soluble PEC1 C-terminus harboring the RCK domain resides in the envelope IMS. In line with this, the heterologously expressed soluble PEC1 C-terminus was also trypsin-sensitive (Suppl. Fig. S2.4E). It follows that PEC1 monomers likely possess an uneven number of transmembrane domains.

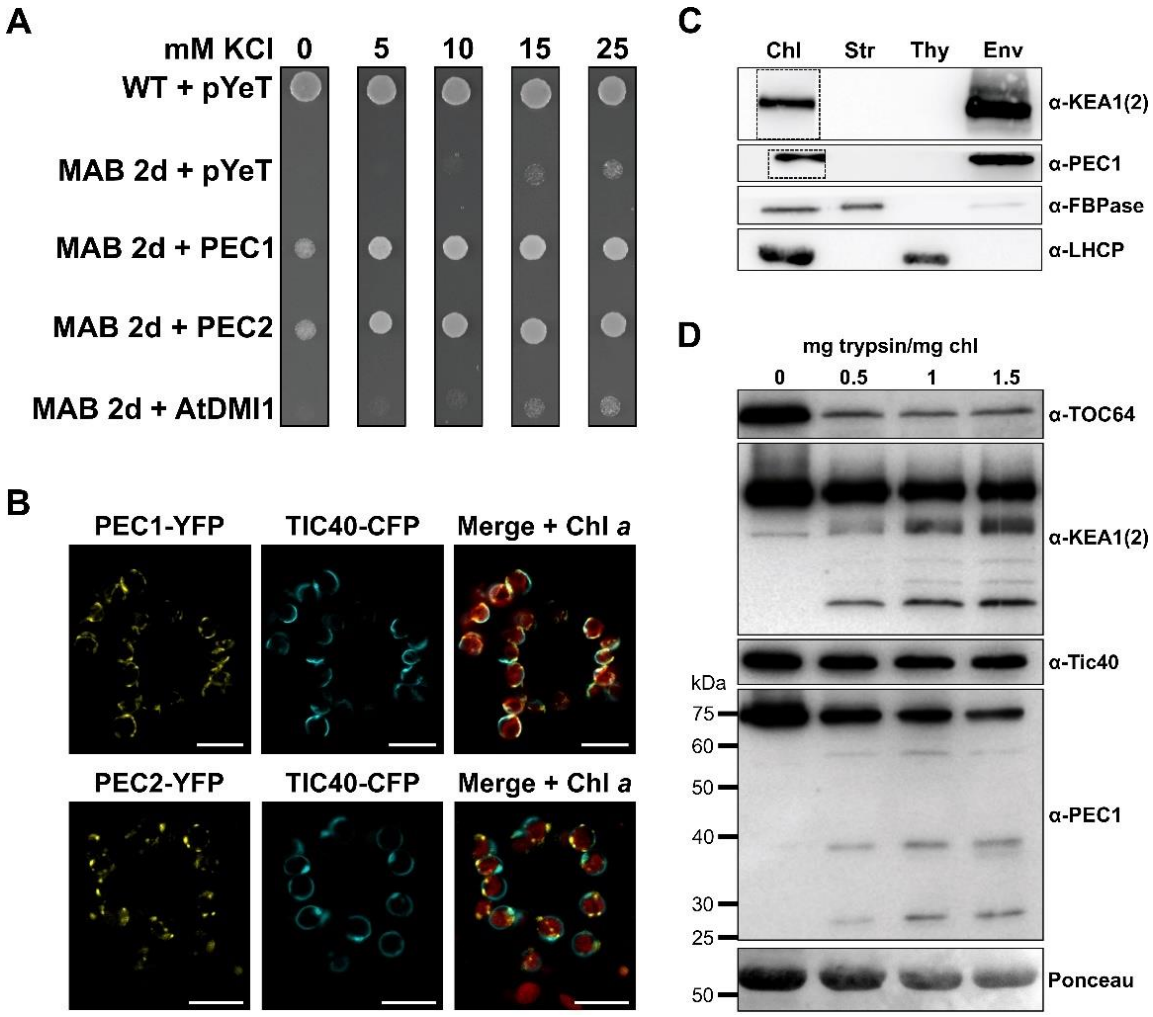

Figure 2.2 PEC1 and PEC2 functional protein characterization. A) Complementation of K^+-uptake deficient S. cerevisiae strain MAB2d with Arabidopsis POLLUX members. WT W303 cells transformed with empty pYeT vector show growth regardless of KCl concentration whereas MAB2d cells with empty pYeT vector cannot grow. PEC1 and PEC2 complement the K+ uptake deficient MAB2d strain, indicating K^+ permeability for PEC1 and PEC2 proteins. Shown is OD 0.01 after 48 h at 30°C. B) Localization of PEC cDNA-YFP fusions to the chloroplast envelope membrane in N. benthamiana. Positive controls TIC40-CFP and Chl a confirm colocalization of PEC1 and PEC2 with the IE (scale bars = 10 µm). C) Immunoblotting of isolated chloroplast membrane fractions. Boxes indicate separate exposure time to account for relative protein abundance (Original figure Suppl. Fig. S2.4C). Chl=Entire chloroplast, Str=Stroma, Thy=Thylakoid membrane, Env=Envelope membranes D) Protease treatment of intact WT chloroplasts. Samples were treated with 0-1.5 mg trypsin*mg-1 chl. Samples corresponding to 10 µg chl were separated on SDS gels, blotted onto PVDF and individually immunolabeled with α-PEC1, α-KEA1(2), α-Tic40, and α-Toc64. Molecular size markers are displayed on the left of the α-PEC1 blot.

In planta characterization of PEC1/2 genes and loss-of-function mutants

Initially, we inserted 2 kB PEC1/2 promoter fragments directly upstream of a GUS reporter gene. Several independent Arabidopsis lines were tested for consistent staining patterns

to gain insights into what plastid types harbor PEC1 and PEC2, respectively (Fig. 2.3A). No unspecific blue GUS staining was observed when the WT plants were incubated with X-Glu, while the *pUBQ10::GUS* positive control line displayed dark blue GUS stain throughout all tissues. *PEC1* and *PEC2* were robustly expressed at plant ages 10, 28, and 35 days (Fig. 2.3A and Suppl. Fig. S2.5C). While *PEC1* seemed exclusively expressed in aerial tissue, *pPEC2::GUS* reporter lines also showed staining in seedling roots. Both loci were expressed in mature leaf and flower tissue which is in line with the robust immunoblot signal we observed when probing isolated chloroplasts with α-PEC1 (Fig. 2.2C-D). The GUS tissue expression patterns were generally in line with publicly available transcriptomic data (Suppl. Fig. S2.5A-B (Kilian et al., 2007; Zhang et al., 2020)) although these suggest higher *PEC1* expression in mature leaves compared to *PEC2*.

Subsequently, we isolated T-DNA insertion mutants in *PEC1* and *PEC2* loci (Fig. 2.3B, Suppl. Fig. S2.6A-B). None of the independent *pec1* and *pec2* single mutants displayed obvious phenotypes (Suppl. Fig. S2.6C). Therefore, two independent *pec1pec2* double mutant lines were isolated by crossing respective single mutants. In both double mutants the absence of detectable gene-specific transcripts and PEC protein was confirmed by means of RT-PCR and immunoblotting respectively (Fig. 2.3C-D). CASTOR/POLLUX/DMI form tetramers in *in vivo* (Kim et al., 2019). Thus, we probed the oligomeric state of PEC1 using isolated WT and *pec1pec2* mutant chloroplasts separated on blue native (BN) page (Fig. 2.3E). Indeed, PEC1 protein gave several higher molecular bands above the 440 kDa marker, suggesting that also the distantly-related POLLUX member PEC1 exists as a multimer *in vivo* and potentially in complex(es) with other binding partners. To characterize the *pec* single and double loss-of-

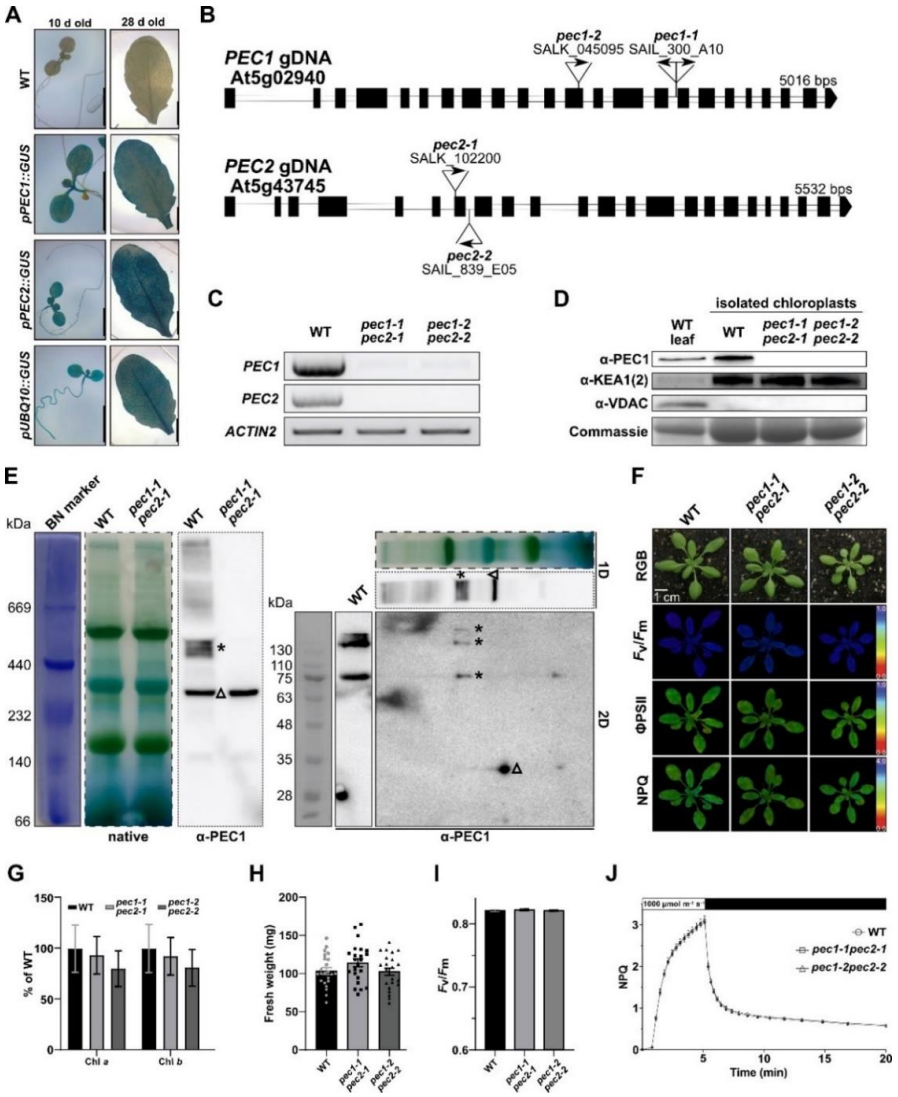

Figure 2.3 *PEC* Expression and loss-of-function mutant characterization. A) Promotor studies of pPEC1/2::GUS constructs indicate strong expression in *A. thaliana* tissues. Left panel shows 10-d-old seedlings, right panel leaves of 28-d-old plants. Experiments were repeated three times with similar results. Representative images are shown (scale bars = 5 mm). B) PEC1 and PEC2 locus information, including T-DNA insertion sites for all pec mutants isolated in this study. Border sequences of T-DNA insertion sites are provided in Supplemental Fig S2.6. C) Full length semi-quantitative reverse transcriptase PCR shows absence of *PEC1* and *PEC2* transcripts in the two independent *pec1pec2* lines. D) Immunoblotting of WT and *pec1pec2* mutant proteins validates lack of PEC1(2) in the mutant plastids. α-KEA1(2) and commassie are presented as loading controls, α-VDAC confirms absence of mitochondrial contamination in the isolated chloroplast fraction. E) BN-PAGE of WT and *pec1-1pec2-1* isolated chloroplasts. Specific signals in WT samples detected by α-PEC1 are marked with asterisks (*). An unspecific band appearing in WT and knockout lanes was marked with triangle (Δ), which was confirmed by 2D SDS-PAGE of the WT BN lane (striped border). F) RBG and false color panel of photosynthesis measurements of WT and two *pec1pec2* double mutants. No obvious phenotypes could be detected when grown under long day conditions at 150 µmol m^{-2} s^{-1} (scale bar = 1 cm). G) Normalized chlorophyll values are unchanged when compared to the WT as determined by ANOVA and Dunn's multiple comparisons test (p>0.05, mean ± SEM, n=9). H) Loss of PEC1/2 does not affect plant fresh weight. Shown are pooled results of three independent experiments (Mean ± SEM, n=23). Photosynthetic parameters (F_v/F_m (I) and NPQ kinetics (J)) are unchanged in *pec1pec2* mutants (Mean ± SD, n=8, a representative result of three experiments is shown).

function lines, mutant plants and WT controls were grown under long-day conditions (16h / 8h day-night cycle, 150 µmol photons m^{-2} s^{-1}). While some mutant individuals appeared slightly smaller, no statistical differences from WT were found for fresh weight and chlorophyll content (Fig. 2.3F-H) Additionally, several basic photosynthesis parameters (F_v/F_M, NPQ, and ΦPSII) were recorded by Pulse-Amplitude-Modulation (PAM) fluorometry (Fig. 2.3I-J). Again, we detected no differences from WT in any of the photosystem-II-related parameters. This indicates that the lack of PEC1 and PEC2 neither impacts photosynthesis nor chloroplast function under normal growth conditions – a striking difference from envelope K^+/H^+ exchanger mutants *kea1kea2* (Kunz et al., 2014; DeTar et al., 2021) but also from Mn^{2+}/Ca^{2+} carrier deficient *cmt1/bicat2* lines (Eisenhut et al., 2018; Zhang et al., 2018; Frank et al., 2019). Because of the importance of plastid ion carriers and their impact on the leaf ionome, several mutants show aberrations from the WT in ionomics experiments (Shikanai et al., 2003; Eisenhut et al., 2018; Zhang et al., 2018; Höhner et al., 2019). Therefore, we analyzed leaf element levels but did not find significant changes between WT and the two *pec1pec2* loss-of-function lines (Table 2.1).

Table 2.1 Leaf-level concentrations of elements(mg*g DW $^{-1}$)
Mean leaf concentration of assorted elements normalized to dry weight (mg*g DW^{-1}) (± SEM, *n*=6-7). No significance was determined using ANOVA and Tukey's multiple comparisons test (p>0.05).

	WT		***pec1-1pec2-1***		***pec1-2pec2-2***	
Element	Mean	SEM	Mean	SEM	Mean	SEM
P	10.233	0.305	10.432	0.247	10.369	0.205
S	10.184	0.279	9.902	0.220	10.444	0.254
Cl	0.101	0.007	0.104	0.01	0.144	0.013
K	38.482	0.502	40.222	0.707	40.544	1.352
Ca	49.014	1.231	51.130	0.87	51.160	2.282
Mn	0.028	0.004	0.03	0.005	0.03	0.005
Fe	0.083	0.006	0.08	0.006	0.079	0.004
Cu	0.004	0.000	0.005	0.001	0.008	0.003
Zn	0.097	0.003	0.095	0.003	0.108	0.004
Rb	0.021	0.005	0.023	0.006	0.025	0.006
Sr	0.143	0.014	0.15	0.016	0.147	0.016

We reckoned that the lack of phenotypic abnormalities and quantitative changes of leaf elements along with intact photosynthesis may point towards a more specialized role for PEC1/2 channels such as in signaling pathways triggered by specific stress conditions.

The loss of PEC1/PEC2 function affects stress induced stromal Ca^{2+} transients

Chloroplasts harbor the Ca^{2+} sensor protein CaS and are therefore an integral part of cellular Ca^{2+} signaling (Weinl et al., 2008). Because of the involvement of CASTOR/POLLUX channels in the formation of nuclear Ca^{2+} transients, it was important to test if PEC proteins may function in plastid Ca^{2+} signaling.

A homozygous WT reporter line expressing stromal targeted YFP-AEQUORIN (NADPH-DEPENDENT THIOREDOXIN REDUCTASE C (NTRC) pTP fused to YFP-AEQUORIN, therefore NTRC-YA (Mehlmer et al., 2012)) was introgressed into *pec1* and *pec2* single mutants and into both *pec1pec2* double mutant lines. The same sensor line was also crossed into the *cas-1* (Nomura et al., 2012) mutant to aid as an assay control. Proper stromal localization and homogenous expression of the stromal Ca^{2+} reporter was verified for all lines by microscopy (Fig. 2.4A, Suppl. Fig. S2.7C. Additionally, we verified similar YFP-AEQUORIN levels via RT-PCR and immunoblotting in isolated *pec1pec2* double mutants (Fig. 2.4B-C).

A plate reader-based seedling assay was used to quantify free stromal Ca^{2+} levels through the bioluminescence signal emitted by AEQUORIN. After overnight dark incubation with the substrate coelenterazine, each well was measured to check for background luminescence which was negligible throughout (Supp. Fig. S2.7A). Under the assumption that *pec* single mutants are largely redundant, we first focused on characterizing *pec1pec2* double mutants. Initially, we applied an equal volume of room temperature buffer to the seedlings to observe changes in Ca^{2+} levels merely triggered by the injection method. The result was a slight increase of free stromal Ca^{2+} similar in all genotypes tested (Fig. 2.4D).

Next, we tested the two strong Ca^{2+} triggers NaCl and Mannitol, and observed large Ca^{2+} transients maxing out at about 550 nM in the WT. Interestingly, both independent *pec1pec2*

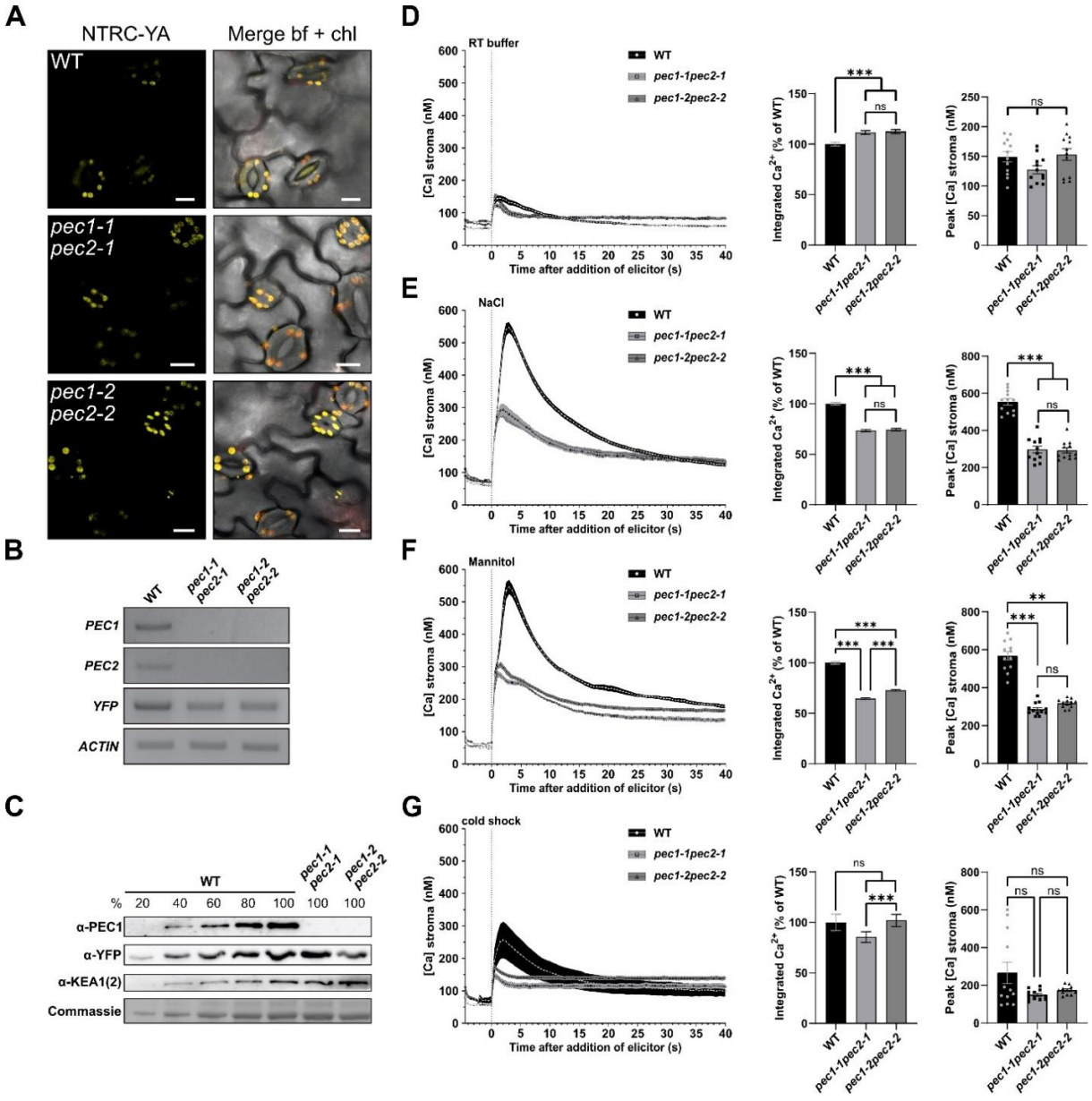

Figure 2.4 Stress-triggered stromal Ca^{2+} transients are diminished in *pec1pec2*. A) Plastid localization of the NTRC-YFP-AEQUORIN construct in WT and *pec1pec2* backgrounds. Representative images are shown, (scale bars = 10 µm). B) Full length semi-quantitative reverse transcriptase PCR shows absence of either PEC transcript in the two independent *pec1pec2* lines and shows similar expression of the YFP fragment attached to AEQUORIN. C) Immunoblotting of WT and *pec1pec2* mutant total leaf proteins shows similar YFP-AEQUORIN levels and confirms absence of PEC in *pec1pec2* mutants. Commassie and α-KEA1(2) validate similar loading for all samples. D-G) Ca^{2+} transients are decreased in plants lacking plastid PEC proteins. 6-d-old seedlings were triggered with room temperature (RT) buffer (D), 200 mM NaCl (E), 400 mM Mannitol (F) or ice-cold buffer (G). Shown in the kinetics are the mean Ca^{2+} concentrations (calculated according to Knight et. al, 1996) in the stroma of 12 individuals (± SEM in the shaded area, n=12). Bar graphs highlight changes in response to the respective elicitors, *i.e.*, Ca^{2+} taken up into the chloroplast during the measurement (integration, relative to WT, left) and peak Ca^{2+} values of the corresponding seedlings (right). Statistical differences were determined by one-way ANOVA followed by Tukey's multiple comparisons test (Mean ± SEM, n=12 **p<0.01, ***p<0.001). Experiments were repeated multiple times with similar results.

double mutant lines exhibited a drastically lower Ca^{2+} response upon elicitor application compared to WT but also compared to *pec* single mutants (Fig. 2.4E-F, Suppl. Fig. S2.7D-E). In addition to the time course, we further evaluated response parameters, such as total free stromal Ca^{2+} during our measurement in the form of Ca^{2+} integration and peak Ca^{2+} levels. Both double mutant lines showed nearly identical but significantly lower values compared to WT regardless of parameter or elicitor. As opposed to osmotic and salt stress, cold stress response was not as uniform in the WT. Only 4 of 12 seedlings showed a distinct peak in response to the addition of ice-cold buffer, ranging from 400-620 nM (Fig. 2.4G). In contrast, *pec1pec2* double knockout lines never peaked higher than 390 nM in our tests (n=36, Suppl. Fig. S2.7B). In line with prior work (Nomura et al., 2012), the Ca^{2+} response in the *cas-1* control was also dampened, yet not as extreme as reported previously. This could be explained by the differing specimen types employed (leaf discs, Nomura et al., 2012 vs seedlings, this study). Interestingly, the decrease in stromal Ca^{2+} transients in *cas-1* was less pronounced than in *pec1pec2*. When the same *pec1pec2* double mutant lines were backcrossed to WT, resulting F1 progenies exhibited a clear but not full recovery of the Ca^{2+} (Suppl. Fig. S2.7F-G) transients, confirming that PEC proteins play a critical role in stromal Ca^{2+} kinetics. Interestingly, none of the tested stress elicitors affected homozygous *pec1pec2* double mutant growth more severely than WT (Suppl. Fig. S2.8).

Based on the obtained results, we compiled a working model which integrates PEC1/2's suggested function with previously described K^+ and Ca^{2+} transport proteins in the plastid IE (Fig. 2.5). All our experiments confirmed PEC1/2 as an IE protein which is in line with several proteomics studies from pea and Arabidopsis. *PEC1/2* expression rescues K^+-uptake deficient yeast mutants. Consequently, we propose that PEC1/2 can facilitate K^+ influx into the stroma. According to the literature chloroplasts have a membrane potential of at least -70 mV across the

IE (Wu et al., 1991), allowing for cation influx through an opened, cation-selective pore down the electrical gradient. KEA1/2 balance the K^+ influx through K^+/H^+ exchange to avoid osmotic stress. Akin to the nuclear CASTOR/POLLUX/DMI cation channels, PEC1/2 function is highly relevant for organellar stress-triggered Ca^{2+} transients. Regardless of the elicitor, Ca^{2+} transients remained at a very low level in *pec1pec2* double mutants. Comparing the here observed Ca^{2+} readings with the published data on *cmcu* and *cmt1*/*bicat2* null mutants it appears that the loss of PECs has a more general and severe impact on stromal Ca^{2+} transients. This indicates two non-mutually exclusive scenarios: Firstly, PEC proteins themselves might also facilitate Ca^{2+} flux. Secondly, PEC proteins may affect the activity of envelope Ca^{2+} transport proteins (cMCU, BICAT2 and/ or unknown ones).

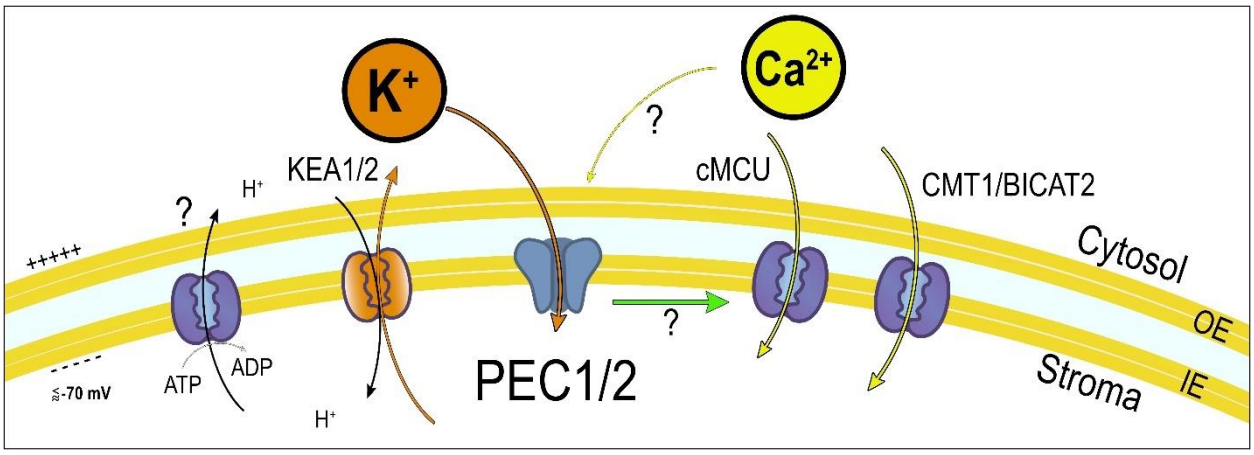

Figure 2.5 Working model of K^+ and Ca^{2+} transport mechanisms across the outer and inner envelope (OE and IE) membrane of *A. thaliana* chloroplasts. KEA1/2 facilitate K^+-efflux across the IE membrane (Kunz et al., 2014). cMCU (Teardo et al., 2019) and potentially CMT1/BICAT2 (Eisenhut et al., 2018, Frank et al., 2019) aid in Ca^{2+} import. PEC1/2 possess K^+-permeability and may impact Ca^{2+} transients in the stroma through a) having Ca^{2+} conductance themselves or b) their activity influences other envelope Ca^{2+} transport proteins.

In regards to scenario 1: Independent studies suggest Ca^{2+} permeability for nuclear CASTOR-type cation channels albeit with different quantities. While two studies found

moderate preference for K^+ over Rb^+, Na^+, and Ca^{2+} (Charpentier et al., 2008; Venkateshwaran et al., 2012), a recent structural work suggested preference for Ca^{2+} over K^+ ions (Kim et al., 2019). Each study had to overcome technical challenges; Charpentier and Venkateshwara et al. reconstituted *in vitro* translated protein, whereas Kim et al. expressed CASTOR/DMI without the first two membrane domains. These limitations make it difficult to draw strong conclusions regarding the *in vivo* substrate of CASTOR/POLLUX/DMI cation channels. This also pertains to their plastid homologs, the PEC proteins, for which we unsuccessfully attempted electrophysiology. However, the rescue of a K^+ uptake deficient yeast mutant indicates that K^+ can pass through the PEC pore. Given the very low level free Ca^{2+} in the cytosol and stroma (low nM) it seems reasonable that highly abundant K^+ ions (50-100 mM) represent the main PEC1/2 substrate *in vivo*. Notably, also the enigmatic FACC channel from pea exhibits K^+ and Ca^{2+} conductivity (Pottosin et al., 2005).

In regards to scenario 2: PEC function may control activity of envelope Ca^{2+} transport proteins. The mechanism proposed for the nuclear Ca^{2+} transients controlled by CASTOR/POLLUX/DMI cation channels is unlikely to occur at the IE. In the nucleus CASTOR/POLLUX/DMI cation channels were suggested to carry counterions for the inward rectifying Ca^{2+} flux. Given the literature values for the IE membrane potential of at least -70 mV the flux direction for chloroplasts should be different. Here, K^+ and Ca^{2+} should both be drawn into the stroma by its negative voltage if facilitated by a cation channel. Therefore, the exact mechanism by which PEC activity may trigger Ca^{2+} influx via the two suggested and potentially additional envelope Ca^{2+} transport proteins, remains to be investigated in detail. Notably, while PEC1/2 and CMT1/BICAT2 were highly abundant in the plastid envelope proteome of Arabidopsis mesophyll chloroplasts, cMCU was not identified (Bouchnak et al., 2019;

Trentmann et al., 2020). Because of cMCU's suggested cell-specific dual-targeting, the highly abundant PEC1/2 may not exert a strong impact on cMCU activity. In the future, detailed co-localization studies using endogenous promoter-driven fluorescence protein fusions and native antibodies for respective membrane proteins are needed to resolve this question.

2.4 Conclusions

In this study, we set out to find candidate genes encoding for the enigmatic FACC channel. While we cannot say with certainty that PEC1/2 represent FACC it is likely that they contribute to the measured FACC conductance. PEC1/2 reside in the IE membrane of pea and Arabidopsis chloroplasts and possess all characteristic functional domains of an ion channel. Similar to their homologs, the nuclear CASTOR/POLLUX/DMI cation channels, PEC1/2 restore K^+ flux in yeast mutants and affect the formation of organellar Ca^{2+} transients. PEC1/2 might have Ca^{2+} conductance themselves or their activity influences other envelope Ca^{2+} transport proteins and thus impact stromal Ca^{2+} transients indirectly. To resolve this, electrophysiology on reconstituted PEC proteins, colocalization, and interaction studies are needed. The discovery of PEC1/2 adds members to the chloroplast transportome and enables the understanding of Ca^{2+} signaling in future work.

2.5 Materials and Methods

Phylogenetic analysis

We downloaded protein data from (*i*) genomes of seventeen land plants: *Anthoceros agrestis* as well as *Anthoceros punctatus* (Li et al., 2020), *Amborella trichopoda* (Amborella Genome, 2013), *Arabidopsis thaliana* (Lamesch et al., 2012), *Arabidopsis lyrata* (Hu et al., 2011), *Brachypodium distachyon (International Brachypodium, 2010), Brassica rapa* (*Brassica*

rapa FPsc v1.3, DOE-JGI, http://phytozome.jgi.doe.gov/), *Gnetum montanum* (Wan et al., 2018), *Lotus japonicus* (Li et al., 2020), *Marchantia polymorpha* (Bowman et al., 2017), *Oryza sativa* (Ouyang et al., 2007), *Physcomitrium patens* (Lang et al., 2018), *Pisum sativum* (Kreplak et al., 2019), *Selaginella moellendorffii* (Banks et al., 2011), and *Sphagnum fallax* (*Sphagnum fallax* v0.5, DOE-JGI, http://phytozome.jgi.doe.gov/); protein data for *Spinacia oleracea* were obtained from (Dohm et al., 2014); (*ii*) the genomes of seven streptophyte algae: *Chlorokybus atmophyticus* (Wang et al., 2020), *Chara braunii* (Nishiyama et al., 2018), *Klebsormidium nitens (Hori et al., 2014), Mesotaenium endlicherianum* (Cheng et al., 2019), *Mesostigma viride* (Wang et al., 2020), *Penium margaritaceum* (Jiao et al., 2020), *Spirogloea muscicola* (Cheng et al., 2019)—additionally, we included sequences found in the transcriptomes of *Spirogyra pratensis* (de Vries et al., 2020), *Zygnema circumcarinatum* and *Coleochaete scutata* (de Vries et al., 2018), and *Coleochaete orbicularis* (Ju et al., 2015); (iii) the genomes of four chlorophytes: *Chlamydomonas reinhardtii* (Merchant et al., 2007), *Coccomyxa subellipsoidea* (Blanc et al., 2012), *Micromonas pusilla* (Worden et al., 2009), *Ulva mutabilis* (De Clerck et al., 2018).

We used (i) seed sequences from *Lotus japonicus, Medicago truncatula, Pisum sativum* and *Oryza sativa* and (ii) animal Slo1 protein homologs from *Caenorhabditis elegans, Acanthaster planci, Danio rerio,* N*ematostella vectensis, Pomacea canaliculate, Echinococcus granulosus, Parasteatoda tepidariorum, Lingula anatine, Biomphalaria glabrata, Homo sapiens, Drosophila mojavensis,* and *Mus musculus* as a query sequence for a BLASTp against this dataset. Initially, we considered all homologs recovered at a cutoff level of 10^{-5} Alignments were generated using MAFFT v7.475 (Katoh and Standley, 2013) with an L-INS-I approach. Alignments are provided in Supplemental Datasets S1 and S2. We computed maximum likelihood phylogenies using IQ-TREE 2.0.3 (Minh et al., 2020), with 1000 ultrafast (UFBoot2;

(Hoang et al., 2018)) bootstrap replicates. To determine the best model, we used ModelFinder (Kalyaanamoorthy et al., 2017) and picked LG+F+R7 for Figure 2.1 (Le and Gascuel, 2008) and WAG+R8 (Whelan and Goldman, 2001) for Supp. Fig. S2.1 as the best models based on the Bayesian Information Criterion.

Alignment and domain structure

Full-length amino acid sequences of PEC1, PEC2, and DMI1 were submitted to the InterPro protein families and domains database (https://www.ebi.ac.uk/interpro/). Figures were created using Affinity Designer (serif).

Plant growth and isolation of Arabidopsis thaliana mutant lines

Wild-type (WT) and mutant seeds from accession Columbia-0 (Col-0) were surface-sterilized, stratified in the dark (48 h at 4°C), and then germinated for seven days on ½ strength Murashige & Skoog (MS) 0.8% (w/v) phytoagar plates (pH 5.8) at 150 µmol photons m^{-2} s^{-1} in long day conditions (16 h/8 h at 22ºC). On day seven seedlings were transferred to soil (Sungro Professional Growing Mix #1, Sun Gro Horticulture, Agawam, MA, USA) and grown under 150 µmol photons m^{-2} s^{-1} illumination in 16 h / 8 h day-night cycle at 22ºC. Rosettes of 3-week-old plants were used for all experiments if not stated differently, except for chloroplast isolation where seeds were sown directly onto soil. All T-DNA insertion mutants were ordered from the ABRC stock center. Homozygous genotypes were confirmed by PCR using primers detailed in Supplemental Tables S1 and S2.

Yeast complementation assay

For *Saccharomyces cerevisiae* assays, we used the MAB2d mutant (Maresova and Sychrova, 2005) and the corresponding WT strain W303. PEC1, PEC2 and DMI1 coding sequences without stop codon were cloned into the yeast expression vector pYeT, harboring a

GAP promoter for strong expression and a C-terminal YFP and were transformed according *via* lithium acetate method (Gietz and Woods, 2001). To minimize mislocalization, the N-terminal plastid transit peptide of PEC1 and PEC2 were truncated. According to predictions of the plant proteome database (Sun et al., 2009) 44 amino acids (AAs) were truncated in the case of PEC1 and 50 AAs for PEC2, respectively. We observed more consistent localization of DMI1 to the plasma membrane in yeast cells, which prompted us to use the putative DMI1 signal peptide (SP, 70 AAs) as an N-terminal fusion to the PEC1/2 CDS. Strains were grown overnight in K^+-supplemented dropout media, washed extensively, and shaken at 30°C for 30 min in K^+-free media. OD_{600} was adjusted to 0.1 in water and cells were spotted side-by-side on media plates supplemented with increasing K^+ amounts.

Transient Nicotiana benthamiana infiltration and confocal microscopy for protein localization studies

For localization studies in *N. benthamiana, Agrobacterium tumefaciens* strains carrying respective vectors (Supplemental Table S3) were co-injected with the 19k vector (Voinnet et al., 2003) according to (Waadt et al., 2014). Images were taken on a Leica SP8 Confocal Laser Scanning Microscope equipped with a supercontinuum laser and hybrid detectors. In co-localization experiments employing YFP and chlorophyll autofluorescence (chl *a*), both fluorophores were excited at 514 nm and recorded at 524-560 nm and 627-700 nm, respectively. CFP was excited with a pulsed laser at 405 nm and emission was sequentially recorded at 465 - 492 nm.

Promoter-GUS-activity staining

For GUS promoter fusion constructs (Supplemental Table S3), 2000 bps 5' fragments upstream from the respective ATG were amplified from gDNA and cloned into pGreenII 0179-

derived vectors harboring the GUS reporter gene (Pratt et al., 2020). *Agrobacterium* containing the respective plasmids were transformed into WT plants according to (Clough and Bent, 1998). GUS staining was performed as described in (Höhner et al., 2019). Representative images are shown, experiments were carried out three times with similar results.

Generation of α-PEC1(2) immunoglobulin

To maximize chance of recognition of the antibody against PEC1, the entire soluble domain (M244 until stop codon, ≈ 64 kDa) was cloned into pET16b and transformed into BLR 21 for expression in *Escherichia coli*. Purification of the antigen was performed as described in (Höhner et al., 2021). An antigen solution at 0.49 mg/mL was flash-frozen on dry ice and sent for antibody generation. The PEC1 antiserum was raised in rabbits (YenZym Antibodies, San Francisco, CA, USA).

Immunoblotting

Arabidopsis leaf tissue frozen in liquid N_2 was powderized using mortar and pestle. Total protein was extracted in extraction buffer (200 mM tris pH 8.0, 4% (w/v) sodium dodecyl sulfate (SDS), 20 mM dithiothreitol (DTT)) to 0.5 g fresh weight/mL, followed by heating at 80°C for 10 min and removing insoluble debris by centrifugation at 21,000*g* for 8 min. Supernatant was mixed with Laemmli buffer and loaded on 8-10% (w/v) acrylamide gels. A voltage of 120 V was applied until the loading dye had left the gel. Gels were either commassie stained or electroblotted onto PVDF or nitrocellulose membranes (0.45 µm pore size) by applying 70 V for 45 min. Subsequently, the membrane was incubated with blocking buffer (tris-buffered saline with 0.05% (w/v) tween (TBS-T), 5% (w/v) nonfat dry milk) for up to one hour at RT and incubated overnight in blocking buffer plus primary antibody at indicated dilutions, gently rocking at 4°C. Primary antibodies used in this study were α-PEC1 (this study), α-KEA1(2)

(Bolter et al., 2020), α-LHCP, α-VDAC (both (Clausen et al., 2004)), α-FPBase (Benz et al., 2009), α-TIC40 (Stahl et al., 1999), α-TOC64 (Sohrt and Soll, 2000) and a commercial α-GFP antibody (Roche, Basel, Switzerland). The membrane was washed 4 times for 5 min in TBS-T and subsequently incubated with HRP conjugated secondary antibody (goat-anti-rabbit (Proteintech Cat# SA00001-2) or goat-anti-mouse in case of anti-GFP), diluted 1:10,000 in blocking buffer for 1 h at room temperature. The blot was rinsed 4 times with TBS-T, 10 min each, and then developed with Biorad clarity ECL substrates (Cat#1705060) for 2-5 min. Signal was detected using a ImageQuant LAS 4000 (GE Healthcare, Chalfont St Giles, UK) with the precision setting and automatic exposure.

Chloroplast subfractionation

Initially, chloroplasts were isolated according to (Bolter et al., 2020). Chloroplast subfractionation was performed as described in (Flores-Perez and Jarvis, 2017), with slight modifications. Intact chloroplasts were isolated, then incubated in 10 mM HEPES/KOH, 5 mM $MgCl_2$ plus complete protease inhibitor (cpi) at a concentration of 1mg/ml chl for 30 min on ice and then ruptured by 50 strokes in a dounce homogenizer. The homogenate was loaded onto a step sucrose gradient (0.46 M, 1.0 M, 1.2 M sucrose in lysis buffer) and centrifuged at 58,000*g* for 2 h at 4°C. Stroma was collected from the top and directly used for SDS PAGE. The envelope fraction was taken from the interface between 0.46 M and 1.0 M sucrose, diluted 1:4 with lysis buffer and centrifuged for 30 min at 256.000*g* at 4°C. The resulting pellet was resuspended in loading buffer. Thylakoids were recovered from the pellet of the gradient, washed 5 times in lysis buffer. Loading was adjusted to total protein.

Protease treatments of chloroplasts

For trypsin treatment of intact chloroplasts an equivalent of 100 µg chl was pelleted and resuspended in 100 µl wash buffer supplemented with 0.5 mM $CaCl_2$. Trypsin was added in the indicated amounts per mg chl and incubated for 45 min at 23°C. The treatment was terminated by addition of 1 × cpi, chloroplasts were reisolated by centrifugation and washed once with wash buffer + 1 × cpi. The final pellet was solubilized in Laemmli loading buffer containing 2 M urea and 1 × cpi, heated at 65°C for 5 min and plastids equivalent to 10 µg chl were loaded onto an SDS gel followed by immunoblotting as described above. All experiments were at least done in triplicates giving the same results. Shown here are representative blots.

Blue-native PAGE

BN-PAGE experiments of total enriched chloroplast membrane fractions were carried out as described by (Nickel et al., 2016), with minor modifications. Samples equal to 15 µg chl were solubilized with 5% β-dodecylmaltoside for 15 min and separated on a 5-15% acrylamide gradient overnight. For subsequent western blotting, lanes were incubated in Towbin buffer (25 mM Tris pH 8.3, 192 mM glycine, 0.1% (w/v) SDS, 20% (v/v) MeOH) with additional 0.9% (w/v) SDS for 1 h prior to blotting. For 2D experiments, the respective BN gel lane was incubated for 30 min in BN-denaturation buffer (1% (w/v) SDS, 50 mM DTT, 25 mM Tris, 192 mM glycine), washed, and afterwards assembled on top of an SDS-PAGE. Total enriched chloroplast membrane fractions equal to 15 µg chl were loaded as a control and separated on the same SDS-PAGE.

Photosynthetic parameters and chlorophyll quantification

Plants were dark-adapted for 20 min. Subsequently, chlorophyll *a* fluorescence was measured with a Walz IMAGING-PAM M-Series MAXI version (Walz, Effeltrich, Germany).

False-color images were exported using the ImagingWinGigE software. Total chlorophyll was extracted from 5–10 mg of N_2-frozen powderized plant material in prechilled reaction tubes. After addition of 1 mL 80% (v/v) acetone, samples were incubated for at least 30 min on ice in the dark interrupted by occasional vortexing. Samples were centrifuged at 10,000*g* for 5 min at 4°C to pellet debris. Chlorophyll determination was performed trough photometry on the clear supernatant (Porra et al., 1989). Obtained values were normalized to fresh weight, and then to the WT. A representative result of three independent experiments is shown.

Generation of stable Aequorin reporter mutants and Ca^{2+} assays

Aequorin lines were generated by using the floral dip method with *Agrobacterium tumefaciens* strains harboring the plasmid pBINU-CHYA(K) (Mehlmer et al., 2012). Homozygous T_3 individuals were introgressed into mutant lines and homozygosity of the reporter lines was confirmed in the F_3 generation. Aequorin assays were performed according to (Tanaka et al., 2013), with minor changes to the CTZ buffer. In brief, five days old seedlings were transferred from ½ MS plates to white 96-well plates filled with 50 µl CTZ buffer (1.4 mM $CaCl_2$, 20 mM KCl, 5 mM MES pH5.7) containing 10 µM coelenterazine (NanoLight Technologies, USA, CAS#55779-48-1). Seedlings were kept in the dark overnight at 22ºC. Luminescence was recorded in a TECAN SPARK plate reader (Tecan, Männedorf, Switzerland) with 500 ms integration time (400 ms in supplementary experiments). Total, reconstituted AEQUORIN amounts were calculated by discharging with 10% (v/v) ethanol and 1 M $CaCl_2$. Calibrations were performed according to (Knight et al., 1996). Graphs were plotted with GraphPad Prism. A representative result of at least three experiments is shown. Statistical significance was tested using ANOVA followed by Tukey's multiple comparisons test.

Elemental analysis

Leaf elements analyzed by Total Reflection X-ray Fluorescence (TXRF) spectroscopy. All procedures were previously described in detail (Höhner et al., 2016). In brief, 21 days old plants were harvested, pooled in groups of three, and dried completely in an oven at 80°C. To avoid elemental contamination, tissue was ground into fine powder using a zirconia mortar and pestle (Stanford Advanced Materials, Lake Forest, USA). 5-10 mg dry weight tissue was digested by boiling in 1 mL 70% (v/v) HNO_3 (analytical grade). 100 µL of the digested tissue was mixed with internal quantitative Ga and Sc standards to final concentrations of 1 ppm Ga and 50 ppm Sc. 10 µL of the mixture was spotted onto quartz disc carriers and dried before measuring on a S4 T-STAR TXRF spectrometer (Bruker, Berlin, Germany).

Accession numbers

PEC1 (At5g02940), *PEC2* (At5g43745), *DMI1* (At5g49960), *TIC40* (At5g16620), *NTRC* (AT2G41680), *pec1-1* (SAIL_300_A10, CS72537), *pec1-2* (SALK_045095, CS72538), *pec2-1* (SALK_102200, CS72539), *pec2-2* (SAIL_839_E05, CS72540), *pec1-1pec2-1* (CS72541), *pec1-2pec2-2* (CS72542), *cas-1* (SALK_070416).

Acknowledgements

We thank Prof. Dr. Ute Vothknecht (University of Bonn) for kindly providing NTRC-YA vector DNA and the respective Arabidopsis Ca^{2+} reporter line. We thank Dr. Myriam Charpentier (John Innes Centre) for early advice on the yeast K^+ assays and Dr. Sychrová Hana (Czech Academy of Sciences at Prague) for sharing the MAB2d mutant strain. Many thanks to Drs. Michael Varnum (Washington State University) and Miguel Piñeros (Cornell University) for tremendous support in trying to establish electrophysiology assays on PECs in Xenopus ooyctes. We are very thankful for many helpful aequorin-related discussions with Drs. Tanaka

and Jewell (both WSU) and their insights on plate-reader based luminescence assays. Lots of thanks to A.H. Howell for confocal microscopy assistance, to Dr. DeTar for help in ionomics sample preparation and evaluation, to A.I. Pratt (all WSU) for early discussions on Ca^{2+} assays, and to Dr. Jordan Zager (Dewey Scientific) for discussion on various parts of the project. C.M. and C.L. Lewis (Alumni WSU Honors College), and K. Bünger (LMU Munich) supported various aspects of the projects. A.M. Garbers (WSU) assisted early in the project. C.V. is grateful for travel support through the WSU Elling and Higinbotham scholarship program and support for microscopy work through the WSU Franceschi training grant.

2.6 Supplemental Material

Supplemental Data and Tables

Supplemental Datasets S1 and S2 can be accessed from the following link:

https://academic.oup.com/plphys/advance-article/doi/10.1093/plphys/kiab424/6365950

Supplemental Table S2.1 Oligonucleotide combinations used in genotyping PCRs.

Line name:	Stock nr.:	WT PCR primers	WT product size	KO PCR primers	~KO product size
pec1-1	SAIL_300_A10	HKPP336/HKPP337	2335	HKP10/HKP337	1500
pec1-2	SALK_045095	HKP336/HKP337	2335	HKP366/HKP370	1500
pec2-1	SALK_102200	HKP419/HKP339	1904	HKP366/HKP339	780
pec2-2	SAIL_839_E05	HKP419/HKP339	1904	HKP419/HKP10	1700
cas-1	SALK_070416	HKP350/HKP351	1650	HKP366/HKP351	1500

Supplemental Table S2.2 List of oligonucleotides used in this study.

Primer name	Oligonucleotide sequence	Used for:
Sail LB3	tagcatctgaatttcataaccaatctcgatacac	genotyping
Venus as	gtttacgtcgccgtccag	genotyping/sequencing
pUBQ10_SeqF	gtcgaataattactcttcgatttg	genotyping
Salk LBb1.3	attttgccgatttcggaac	genotyping

PEC1 fwd + BamHI **(HKP334)**	ggatccaaaatggtggctgttcagttgtttac	genotyping, full length cDNA clone and RT-PCR
PEC1 rev + XmaI **(HKP337)**	cccgggtagtgtgataacttggtctccttc	genotyping, full length cDNA clone and RT-PCR
PEC2 fwd + BamHI **(HKP338)**	ggatccaaaatgatggtggctgttcagttg	genotyping, full length cDNA clone and RT-PCR
PEC2 rev + XmaI **(HKP341)**	cccgggtagtgtgattggttggtctcc	genotyping, full length cDNA clone and RT-PCR
PEC1 fwd 5 **(HKP336)**	gatggaatccatcccaacc	genotyping
PEC2 rev 5 **(HKP339)**	cggacatgagcagaagtc	genotyping
PEC1 rev 6 **(HKP370)**	gtcgacaatttcagaggctag	genotyping
PEC1 fwd + XmaI **(HKP419)**	cccccgggatgagagggaccttcaaagtc	genotyping
CaS fwd + BamHI	ggatccaaaatggctatggcggaaatg	*cas-1* genotyping
CaS rev + XmaI	cccggggtcggagctaggaaggaact	*cas-1* genotyping
DMI1 fwd + SalI	gagtcgacaaaatgccgattcatacccctag	full length cDNA clone AtDMI1
DMI1 rev + XmaI	cccgggctgacttgaggcgatgacaac	full length cDNA clone AtDMI1
DMI1 Gibson Frag Fwd	gccatggccgcgggatatcactagtatgccgattc atacccc	in vitro expression vector pGEM-5Zf
DMI1 Gibson Frag Rev	ttgggagctctcccatatggtcgacttactgacttga ggcgatgac	in vitro expression vector pGEM-5Zf
PEC2 Gibson Frag Fwd	gccatggccgcgggatatcactagtatgatggtgg ctgttcag	in vitro expression vector pGEM-5Zf
PEC2 Gibson Frag Rev	ttgggagctctcccatatggtcgactcatagtgtgat tggttggtct	in vitro expression vector pGEM-5Zf
PEC1 Gibson Frag Fwd	gccatggccgcgggatatcactagtatggtggctg ttcagttg	in vitro expression vector pGEM-5Zf
PEC1 Gibson Frag Rev	ttgggagctctcccatatggtcgactcatagtgtgat aacttggtctcc	in vitro expression vector pGEM-5Zf
PEC1P + pG2.0 fwd	cgaaattacccttttgttgaaaagtctcaataacttctg ggagagaagccaggg	Gibson pPEC1 into pG2.0
PEC1P + pG2.0_GUS rev	ggggtttctacaggacgtaacatcctttcttaatcttc tccttgatttatcttacgctc	Gibson pPEC1 into pG2.0_GUS
PEC2P + pG2.0 fwd	cgaaattacccttttgttgaaaagtctcaataagagct gcacaggtttctatatgatcattac	Gibson pPEC2 into pG2.0
PEC2P + pG2.0_GUS rev	gttggggtttctacaggacgtaacatcttatctcttct cctcgctctctctttgtttc	Gibson pPEC2 into pG2.0_GUS
DMI1SP Gibson pYeT fwd	ggcgcgccactagtggatccatgccgattcatacc	gibson DMI1SP to pYe-T (for both PEC1 and PEC2)

DMI1SP_gibson_PEC1 rev	gaagtttttattaggggattgactcggcaccgg	gibson DMI1SP to PEC1
DMI1SP_gibson_PEC1 fwd	gtgccgagtcaatcccctaataaaaacttcaaagatttaaattcc	gibson DMI1SP to PEC1
PEC1 cDNA Gibson mVenus rev	cgcccttgctcaccatcccgggtagtgtgataacttgg	gibson PEC1 to mVenus
DMI1SP_gibson_PEC2 rev	cactagaagaaggggattgactcggcac	DMI1SP-PEC2 clone
DMI1SP_gibson_PEC2 fwd	caatccccttcttctagtgtcaacctgaatgatttcagttcc	DMI1SP-PEC2 clone
PEC2 rev gibson mVenus	gcccttgctcaccatcccgggtagtgtgattggttg	DMI1SP-PEC2 clone
PEC1+pET16b fwd	aggtcgtcatatgaaaaaagtgagggaaggggcacatatg	Gibson primer PEC1noTMs into pET16b
PEC1+pET16b rev	cggatcctctcatagtgtgataacttggtctccttcaagctctgatataaca	Gibson primer PEC1noTMs into pET16b
pET16b+PEC1 fwd	acactatgagaggatccggctgctaacaaag	Gibson primer for PEC1 noTMs into pET16b
pET16b+PEC1 rev	actttttttcatatgacgaccttcgatatggcc	Gibson primer for PEC1 noTMs into pET16b

Supplemental Table S2.3 Constructs used in this study and their origin.

Name	**External source (if not this work)**
pHygIIUT-YFP	(Kunz et al., 2014)
19K	(Voinnet et al., 2003)
W303	(Wallis et al., 1989)
Mab2D yeast strain	(Maresova and Sychrova, 2005)
pYe-T-YFP empty	Kudla lab (University Münster)
pBINU-CHYA(K)	(Mehlmer et al., 2012)
pG2.0_GUS	(Pratt et al., 2020)
DMI1 cDNA-stop + pYe-T-YFP	This work
P3SP + PEC1cDNA-stop chimera + pYe-T-YFP	
P3SP + PEC2cDNA-stop chimera + pYe-T-YFP	
PEC1-stop cDNA + pHygIIUT-YFP	
PEC2-stop cDNA + pHygIIUT-YFP	
PEC1 cDNA noTP -stop + pHygIIUT-YFP	
PEC2 cDNA noTP -stop + pHygIIUT-YFP	
pPEC1 + pG2.0_GUS	
pPEC2 + pG2.0_GUS	
pUBQ10 + pG2.0_GUS	
PEC1 cDNA + pGEM5zf+	
PEC2 cDNA + pGEM5zf+	
DMI1 cDNA + pGEM5zf+	
PEC1noTMs+pET16b	

Supplemental Figures

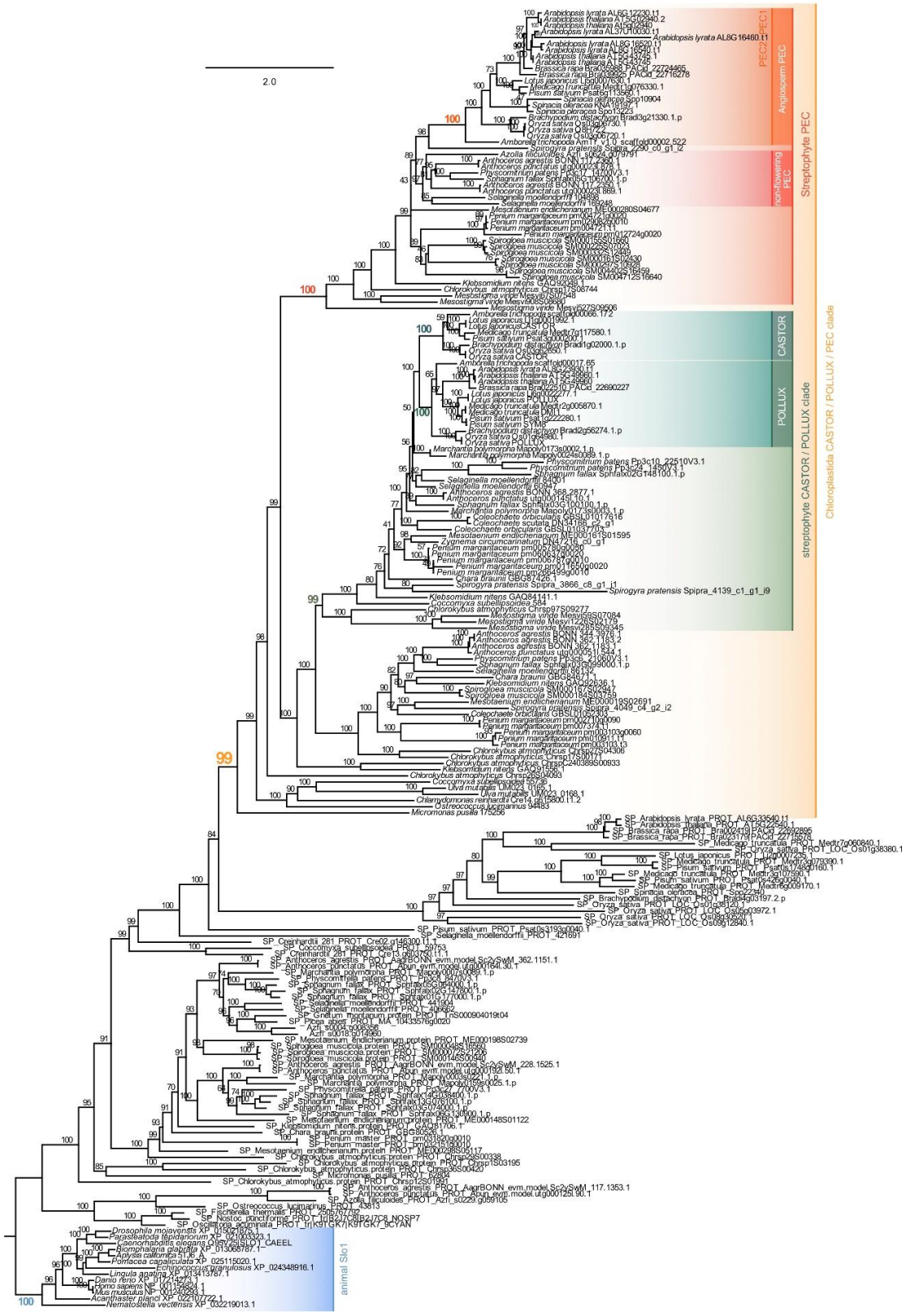

Supplemental Figure S2.1 Phylogeny of PEC, CASTOR, and POLLUX homologs (previous page). Homologs of PEC, CASTOR, and POLLUX were sampled from genomes of 17 land plants, seven streptophyte algae, and four chlorophytes. We further added in silico translated homologs from the transcriptomes of Spirogyra pratensis (de Vries et al., 2020), *Coleochaete scutata* and *Zygnema circumcarinatum* (de Vries et al., 2018), and *Coleochaete orbicularis* (Ju et al., 2015). 13 animal SLO1 sequences were included as an outgroup (blue). A rooted maximum likelihood phylogeny of all 211 sequences was computed using WAG+R8 as model for protein evolution (chosen according to BIC). 1000 ultrafast bootstrap (UFBoot2, Hoang et al., 2018) replicates were computed. Only ultrafast bootstrap values ≥50 are shown and full support (ultrafast bootstrap values of 1000) is depicted by a filled dot. Scale bar length corresponds to 2.0 expected substitutions per site.

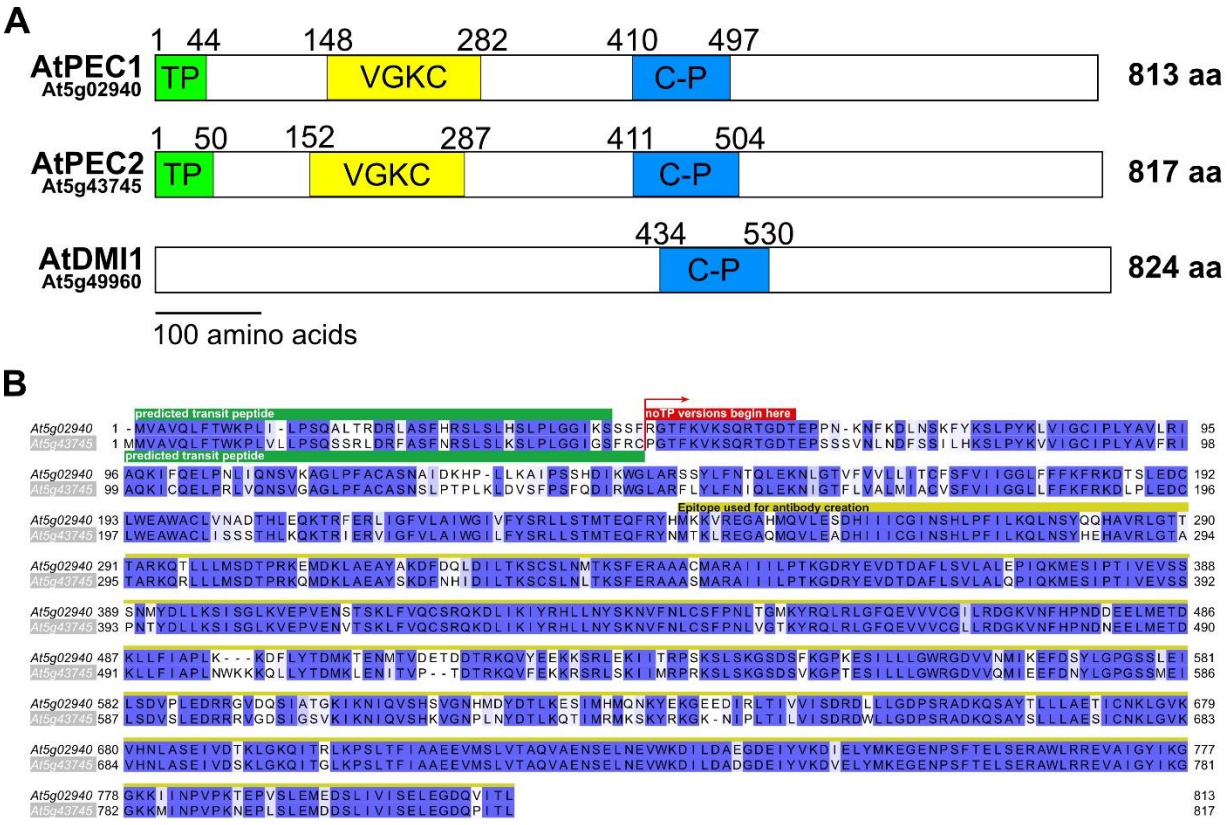

Supplemental Figure S2.2 PEC domains and construct information. A) PEC architecture and annotated domains according to InterPro. Shown in green are predicted transit peptides, recognized by the plastid protein import machinery. PEC1 and PEC2 possess an annotated voltage gated potassium channel (yellow box, VKGC) superfamily domain (SSF81324). All POLLUX family members share the CASTOR-POLLUX domain (blue box, IPR036721). B) Alignment of PEC1 and PEC2 and construct information. Amino acids with dark blue backdrop are identical, light blue backdrop indicates similar amino acids. Predicted transit peptide from S1A is marked in green, the start of the 'noTP versions' marked with a red arrow and the epitope used α-PEC antibody creation is marked with a yellow bar above the amino acid sequence of PEC1

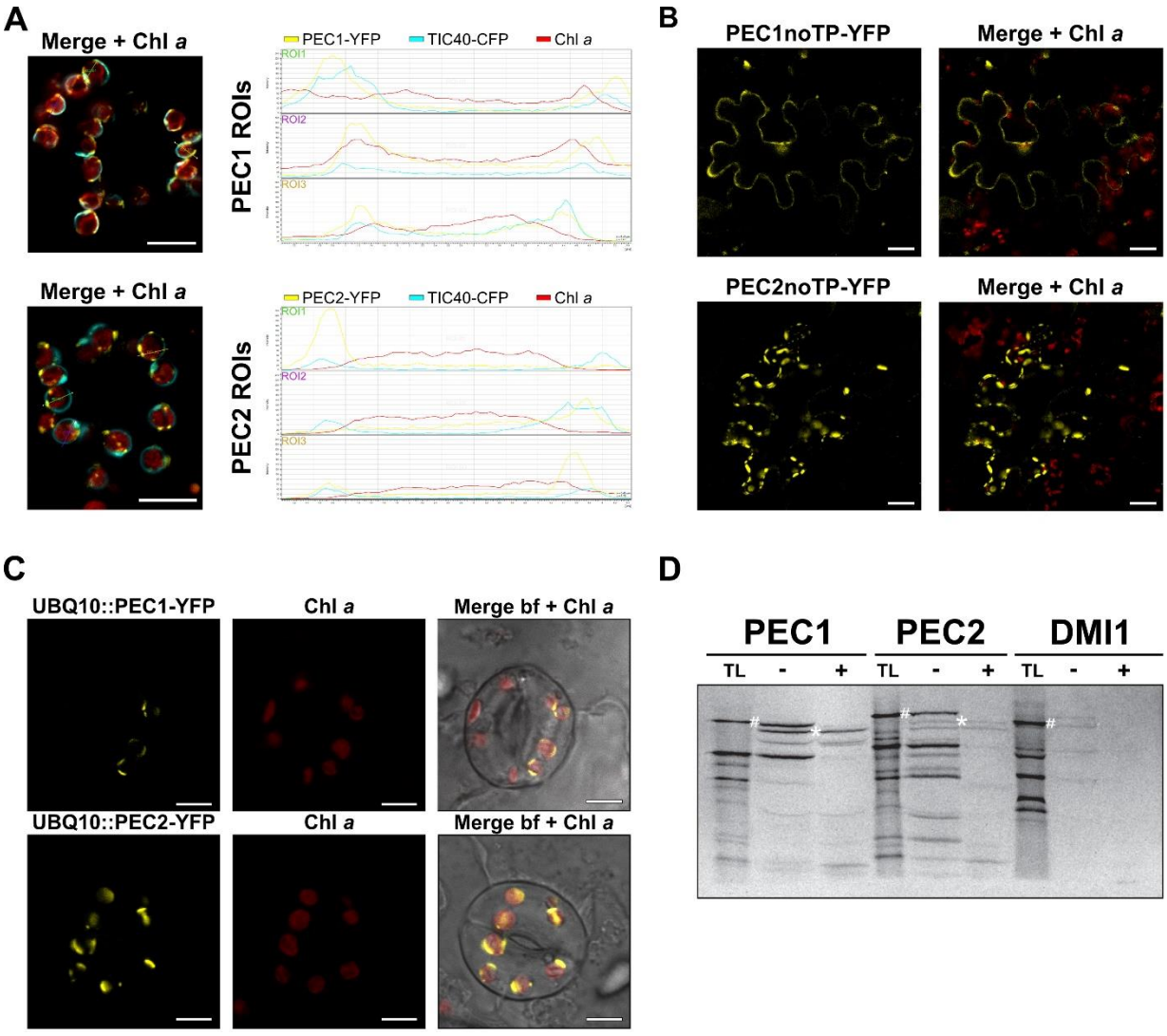

Supplemental Figure S2.3 Localization studies of PEC proteins in *N. benthamiana* and *A. thaliana*.
A) Regions of interest overlayed over Fig. 2.2B. Line plots indicate fluorescence intensity along the ROI (scale bars = 5 µm). B) Transient infiltration of truncated PEC-YFP fusions into *N. benthamiana* leaves. (scale bars = 20 µm). C) PEC-cDNA-YFP constructs localize to guard cell chloroplast envelope membranes in *A. thaliana* T1 transformants (scale bars = 5 µm). D) Radiolabelled proteins imaged with a phoshoimager. Shown are total translation product after 25 minutes (TL), chloroplast suspension without thermolysin (-) and with thermolysin treatment (+). # marks the preprotein including transit peptide, * marks the mature, cleaved protein that was processed by the TOC-TIC complex.

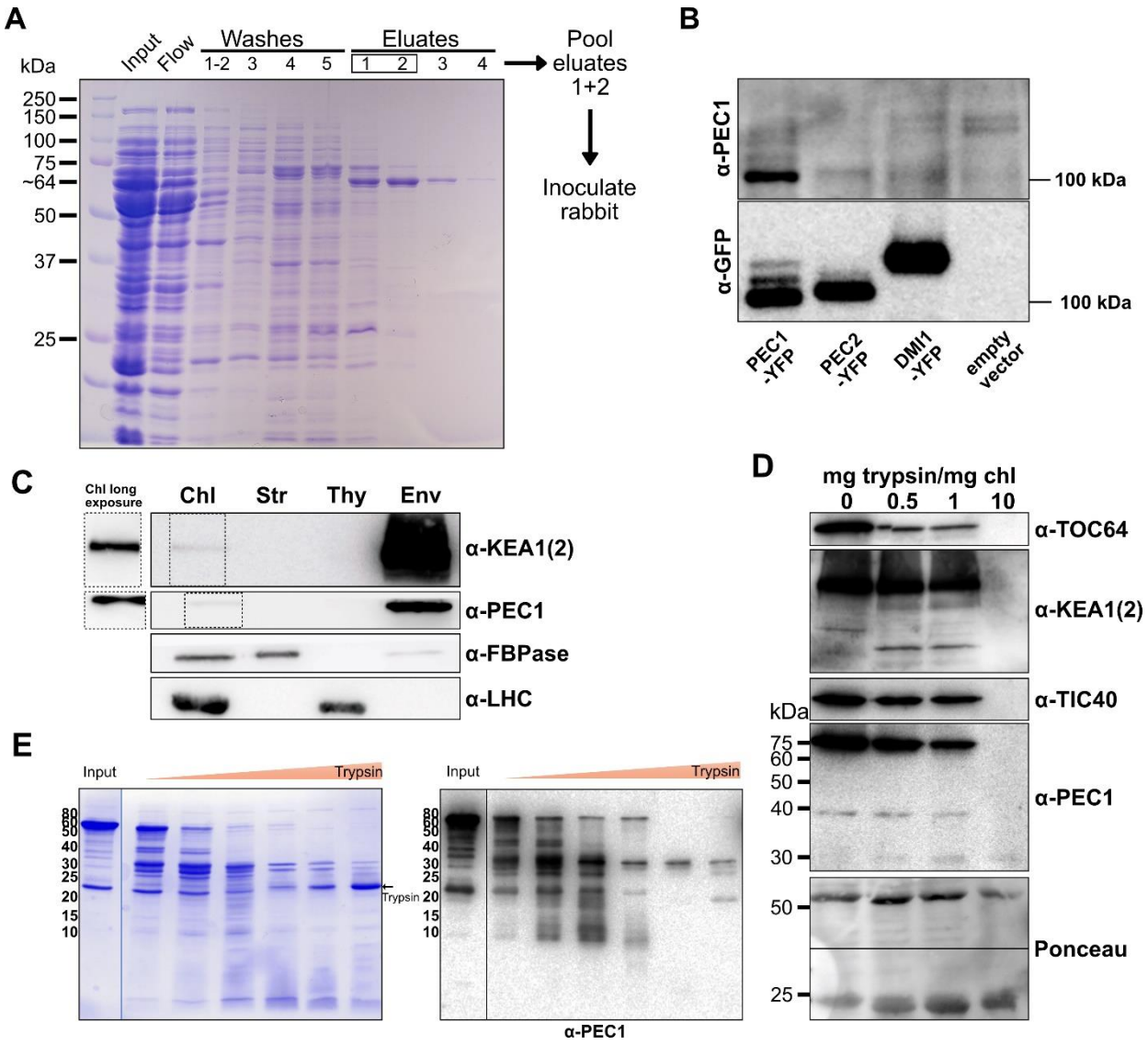

Supplemental Figure S2.4 α-PEC1 antibody design and application in localization studies. A) Commassie-stained SDS page of E. coli lysates taken during purification of the antigen. Shown are E. coli lysate before mixing with Ni-NTA (Input), unbound proteins after incubation with Ni-NTA (Flow) and eluates. B) N. benthamiana protein extracts probed with α-PEC1 (1:1000) and α-GFP (1:2000) primary antibodies and labelled with a secondary antibody with conjugated horseradish peroxidase. C) Immunoblotting of isolated chloroplast fractions. Chl=Entire chloroplast, Str=Stroma, Thy=Thylakoid membrane, Env=Envelope membranes. Original image from Fig. 2.2C. Dotted boxes indicate longer exposure time during detection. D) Intact WT chloroplasts were treated with 0, 0.5, 1 or 10 mg trypsin/mg chlorophyll. Samples corresponding to 10 µg chl were separated on SDS gels, blotted onto PVDF and individually immunolabeled with α-PEC1, α-KEA1(2), α-Tic40, and α-Toc64. Markers for molecular sizes are displayed on the left. E) Heterologous expression of the PEC1 soluble c-term (M244 through stop-1, 64.4 kDa) in E. coli and digest with increasing amounts of trypsin. Commassie stained SDS-PAGE (left) and α-PEC1 labelled western blot (right) reveal trypsin sensitivity.

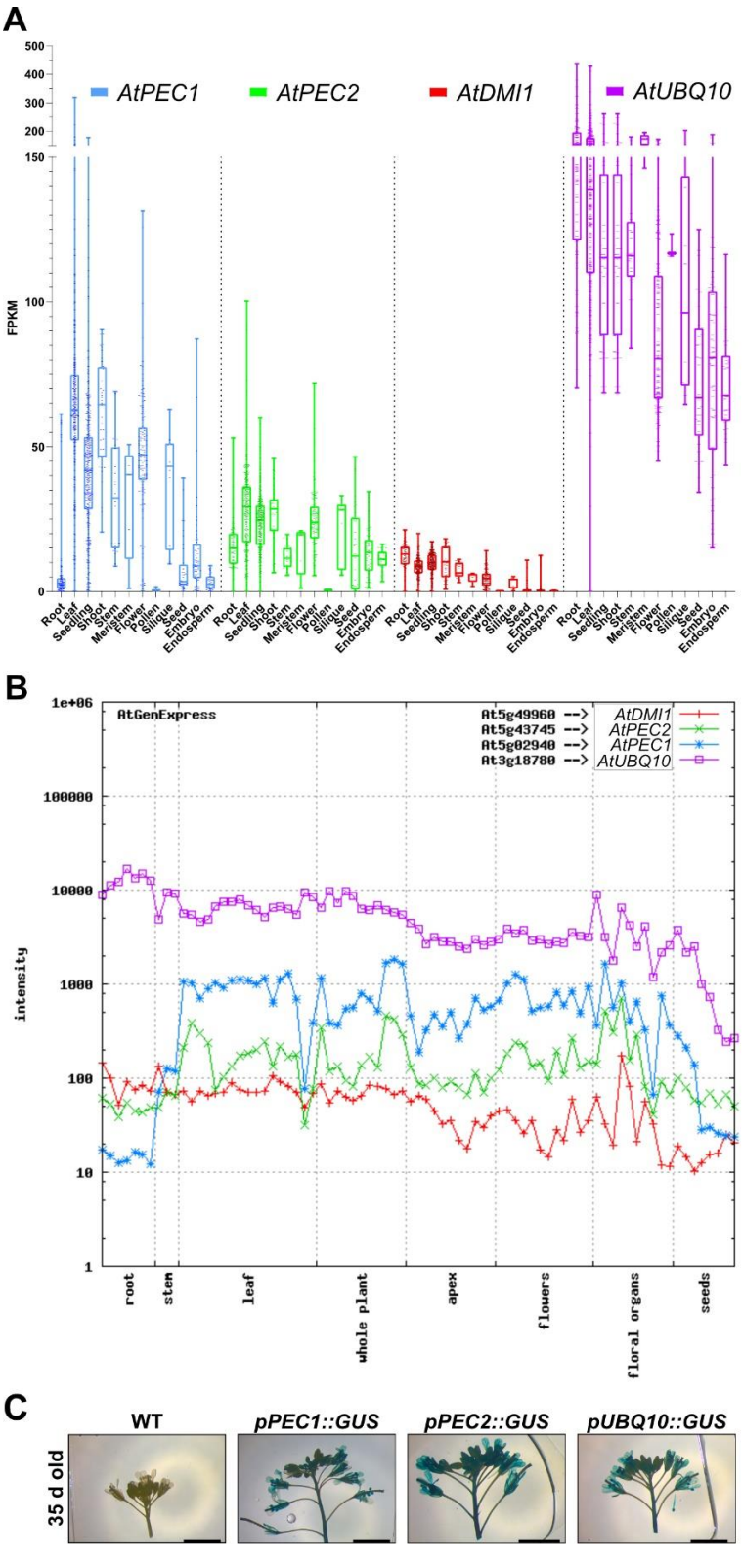

Supplemental Figure S2.5 Extended *PEC* expression information. A) RNA-seq data sets showing expression of AtPEC1 (blue), AtPEC2 (green), AtDMI1 (red), and AtUBQ10 (purple) (Zhang et al., 2020) show in fragments per kilobase of transcript per Million mapped reads (FKPM). Boxplot indicates upper and lower quartile with median as center line. Whiskers go from min to max, showing all individual experiments. B) In-silico microarray expression data as shown on weigelworld.org (accessed May 2019, (Kilian et al., 2007)). C) Additional GUS stained images from 35d old plants. Representative images are shown (scale bars = 5 mm).

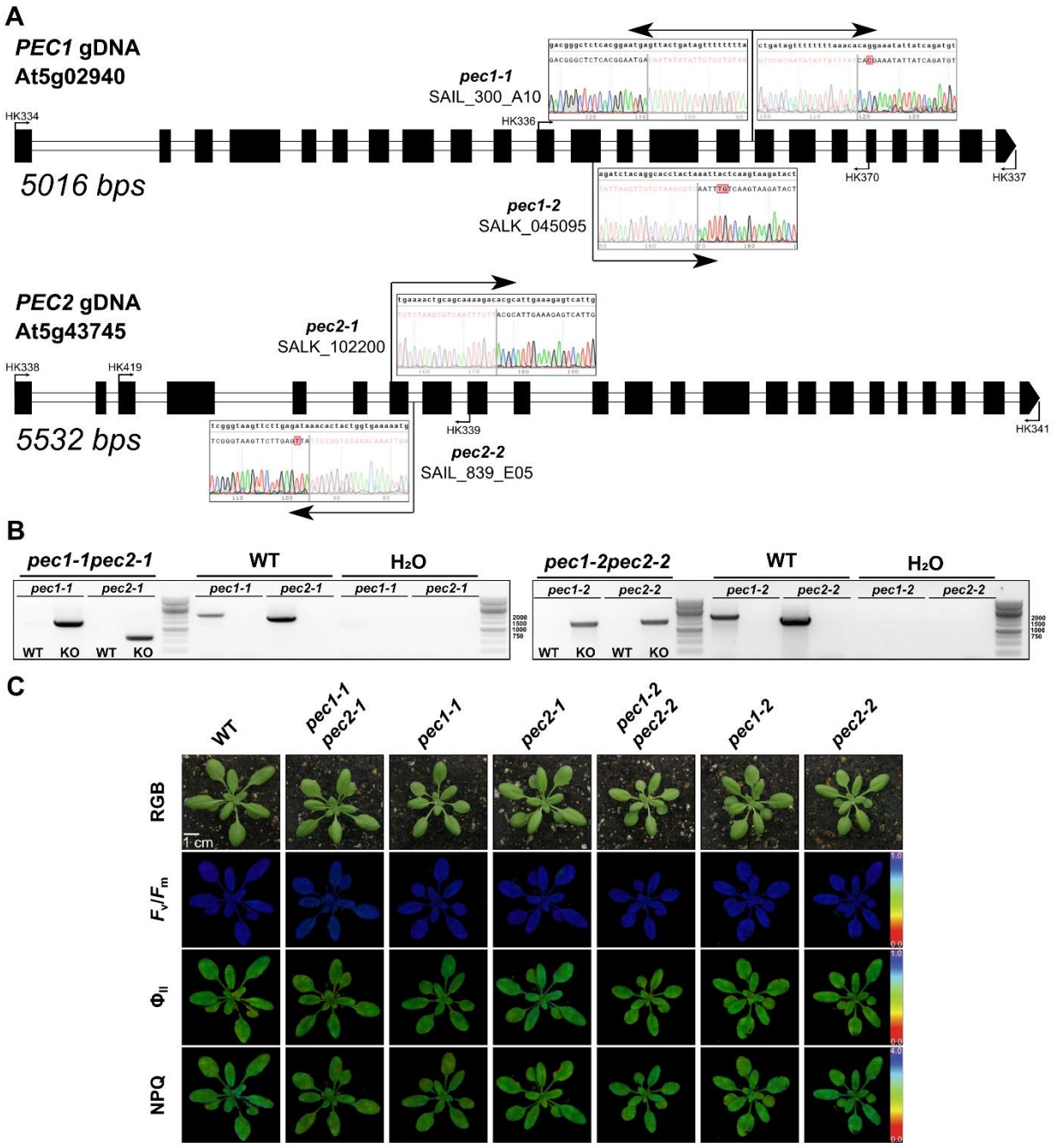

Supplemental Figure S2.6 *PEC* locus information and *pec* single mutant characterization. A) PEC locus and T-DNA insertion site information. Borders were sequenced using NGS and commercial T-DNA LB primers. B) Genotyping PCRs on indicated *pec1pec2* double mutants. The pipetting scheme marked on the first lanes carries on through the entire gel. Thermo Fischer's 1kb+ ladder was used and a few bands were marked with their respective sizes. C) RBG and false color panel of photosynthesis measurements of all *pec* single and *pec1pec2* double mutants. No obvious phenotypes could be detected when grown under long day conditions at 150 µmol m^{-2} s^{-1} (scale bar = 1 cm).

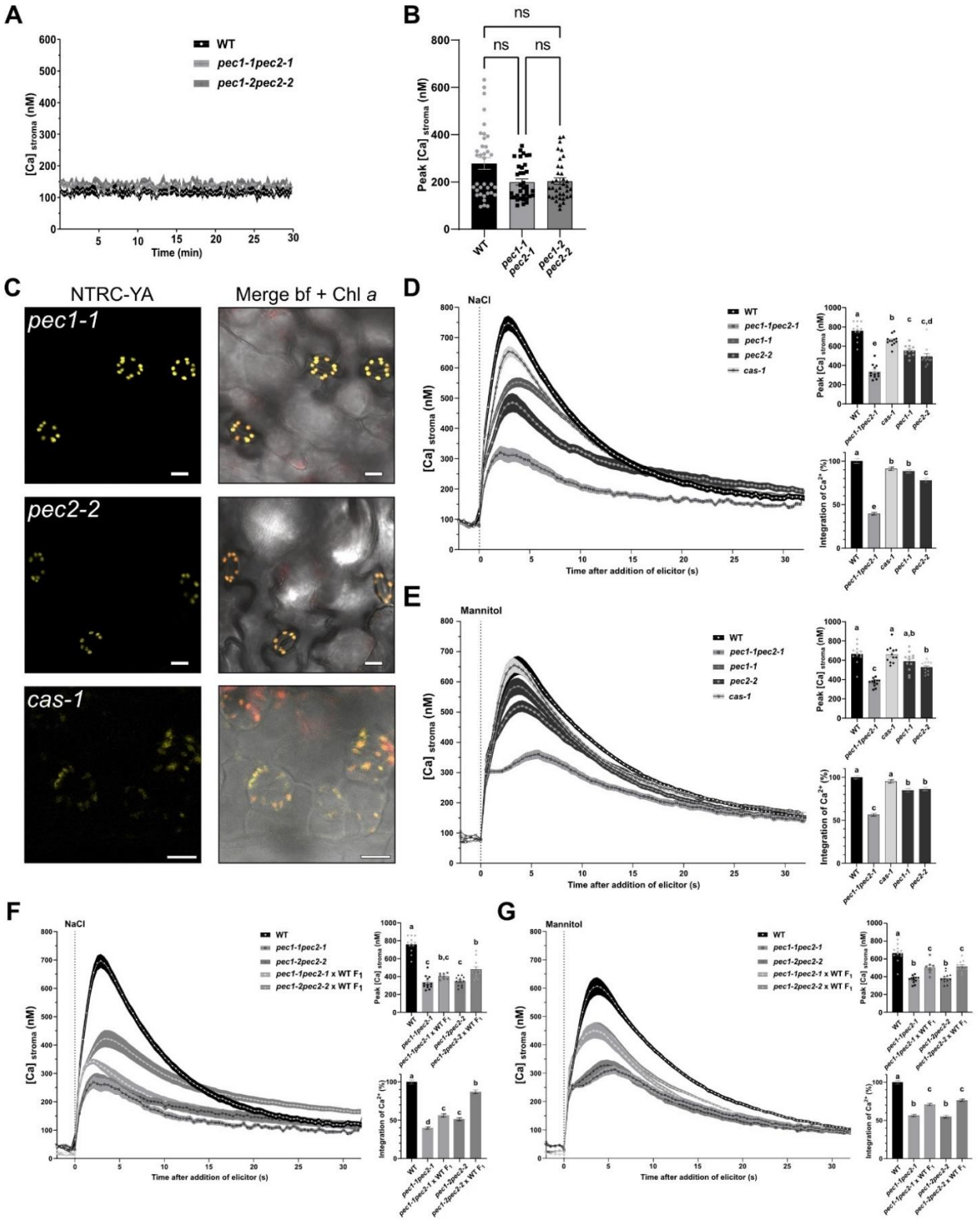
A
WT
pec1-1pec2-1
pec1-2pec2-2
[Ca] stroma (nM)
Time (min)
B
ns
ns
ns
Peak [Ca] stroma (nM)
WT
pec1-1 pec2-1
pec1-2 pec2-2
C
NTRC-YA
Merge bf + Chl a
pec1-1
pec2-2
cas-1
D
NaCl
WT
pec1-1pec2-1
pec1-1
pec2-2
cas-1
[Ca] stroma (nM)
Time after addition of elicitor (s)
Peak [Ca] stroma (nM)
Integration of Ca2+ (%)
E
Mannitol
WT
pec1-1pec2-1
pec1-1
pec2-2
cas-1
[Ca] stroma (nM)
Time after addition of elicitor (s)
Peak [Ca] stroma (nM)
Integration of Ca2+ (%)
F
NaCl
WT
pec1-1pec2-1
pec1-2pec2-2
pec1-1pec2-1 x WT F1
pec1-2pec2-2 x WT F1
[Ca] stroma (nM)
Time after addition of elicitor (s)
Peak [Ca] stroma (nM)
Integration of Ca2+ (%)
G
Mannitol
WT
pec1-1pec2-1
pec1-2pec2-2
pec1-1pec2-1 x WT F1
pec1-2pec2-2 x WT F1
[Ca] stroma (nM)
Time after addition of elicitor (s)
Peak [Ca] stroma (nM)
Integration of Ca2+ (%)

Supplemental Figure S2.7 Background AEQUORIN and additional cold shock measurements, single mutant readings, and complementation by backcross into the WT (previous page). A) Representative AEQUORIN background readings from WT and pec1pec2 double mutants. Shown are means of 12 individuals, shaded areas indicate SEM. B) Combined results from three independent cold shock treatments as shown in and including Fig 2.4G. Shown are mean ± SEM of 36 individuals. No significant difference was determined by one-way ANOVA and Tukey's multiple comparisons test (p>0.05). C) Localization of NTRC-YA in *pec1-1*, *pec2-2*, and *cas-1* mutants (scale bar = 5 µm). D-G) Ca^{2+} transients in *pec1-1*, *pec2-2*, *cas-1* mutants (D+E), and *pec1pec2* x WT F_1 backcrosses (F+G). Shown is the mean Ca^{2+} concentration in the stroma of 8-12 individuals, shaded areas indicate SEM. Bar graphs (Mean ± SEM) highlight changes of responses to the respective elicitors, i.e. total Ca^{2+} taken up into the chloroplast during the measurement (integration, relative to WT, bottom) peak Ca^{2+} values of the corresponding seedlings (top). Experiments with backcrosses were repeated twice with similar results. Different letters indicate different levels of significance (p<0.05) as determined by one-way ANOVA and Tukey's multiple comparisons test. C) RBG and false color panel of photosynthesis measurements of all pec single and pec1pec2 double mutants. No obvious phenotypes could be detected when grown under long day conditions at 150 µmol m^{-2} s^{-1} (scale bar = 1 cm).

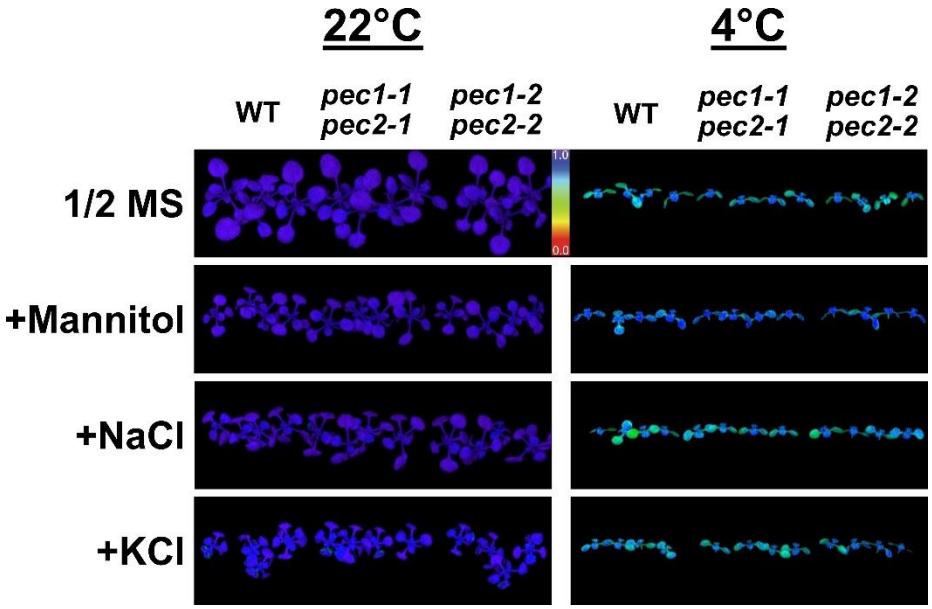

Supplemental Figure S2.8 Lack of stromal Ca^{2+} transients in *pec1pec2* mutants does not correspond with additional growth defects under abiotic stress conditions. *Arabidopsis* seedlings were germinated and grown for 7 days on solid 1/2 MS media and then transferred to control or effector plates (50 mM Mannitol, 75 mM NaCl or 75 KCl). Plates were grown either at 22°C or 4°C. Shown are false-color images of F_v/F_m after 1 week.

2.7 References

Amborella Genome P (2013) The Amborella genome and the evolution of flowering plants. Science **342:** 1241089

Aranda-Sicilia MN, Cagnac O, Chanroj S, Sze H, Rodriguez-Rosales MP, Venema K (2012) Arabidopsis KEA2, a homolog of bacterial KefC, encodes a K(+)/H(+) antiporter with a chloroplast transit peptide. Biochim Biophys Acta **1818:** 2362-2371

Aranda Sicilia MN, Sanchez Romero ME, Rodriguez Rosales MP, Venema K (2021) Plastidial transporters KEA1 and KEA2 at the inner envelope membrane adjust stromal pH in the dark. New Phytol **229:** 2080-2090

Arino J, Velazquez D, Casamayor A (2019) Ser/Thr protein phosphatases in fungi: structure, regulation and function. Microb Cell **6:** 217-256

Banks JA, Nishiyama T, Hasebe M, Bowman JL, Gribskov M, dePamphilis C, Albert VA, Aono N, Aoyama T, Ambrose BA, Ashton NW, Axtell MJ, Barker E, Barker MS, Bennetzen JL, Bonawitz ND, Chapple C, Cheng C, Correa LG, Dacre M, DeBarry J, Dreyer I, Elias M, Engstrom EM, Estelle M, Feng L, Finet C, Floyd SK, Frommer WB, Fujita T, Gramzow L, Gutensohn M, Harholt J, Hattori M, Heyl A, Hirai T, Hiwatashi Y, Ishikawa M, Iwata M, Karol KG, Koehler B, Kolukisaoglu U, Kubo M, Kurata T, Lalonde S, Li K, Li Y, Litt A, Lyons E, Manning G, Maruyama T, Michael TP, Mikami K, Miyazaki S, Morinaga S, Murata T, Mueller-Roeber B, Nelson DR, Obara M, Oguri Y, Olmstead RG, Onodera N, Petersen BL, Pils B, Prigge M, Rensing SA, Riano-Pachon DM, Roberts AW, Sato Y, Scheller HV, Schulz B, Schulz C, Shakirov EV, Shibagaki N, Shinohara N, Shippen DE, Sorensen I, Sotooka R, Sugimoto N, Sugita M, Sumikawa N, Tanurdzic M, Theissen G, Ulvskov P, Wakazuki S, Weng JK, Willats WW, Wipf D, Wolf PG, Yang L, Zimmer AD, Zhu Q, Mitros T, Hellsten U, Loque D, Otillar R, Salamov A, Schmutz J, Shapiro H, Lindquist E, Lucas S, Rokhsar D, Grigoriev IV (2011) The Selaginella genome identifies genetic changes associated with the evolution of vascular plants. Science **332:** 960-963

Benz JP, Stengel A, Lintala M, Lee YH, Weber A, Philippar K, Gugel IL, Kaieda S, Ikegami T, Mulo P, Soll J, Bolter B (2009) Arabidopsis Tic62 and ferredoxin-NADP(H) oxidoreductase form light-regulated complexes that are integrated into the chloroplast redox poise. Plant Cell **21:** 3965-3983

Bernardi P (1999) Mitochondrial transport of cations: channels, exchangers, and permeability transition. Physiol Rev **79:** 1127-1155

Blanc G, Agarkova I, Grimwood J, Kuo A, Brueggeman A, Dunigan DD, Gurnon J, Ladunga I, Lindquist E, Lucas S, Pangilinan J, Proschold T, Salamov A, Schmutz J, Weeks D, Yamada T, Lomsadze A, Borodovsky M, Claverie JM, Grigoriev IV, Van Etten JL (2012) The genome of the polar eukaryotic microalga Coccomyxa subellipsoidea reveals traits of cold adaptation. Genome Biol **13:** R39

Bolter B, Mitterreiter MJ, Schwenkert S, Finkemeier I, Kunz HH (2020) The topology of plastid inner envelope potassium cation efflux antiporter KEA1 provides new insights into its regulatory features. Photosynth Res **145:** 43-54

Bouchnak I, Brugiere S, Moyet L, Le Gall S, Salvi D, Kuntz M, Tardif M, Rolland N (2019) Unraveling Hidden Components of the Chloroplast Envelope Proteome: Opportunities and Limits of Better MS Sensitivity. Mol Cell Proteomics **18:** 1285-1306

Bowman JL, Kohchi T, Yamato KT, Jenkins J, Shu S, Ishizaki K, Yamaoka S, Nishihama R, Nakamura Y, Berger F, Adam C, Aki SS, Althoff F, Araki T, Arteaga-Vazquez MA, Balasubrmanian S, Barry K, Bauer D, Boehm CR, Briginshaw L, Caballero-Perez J, Catarino B, Chen F, Chiyoda S, Chovatia M, Davies KM, Delmans M, Demura T, Dierschke T, Dolan L, Dorantes-Acosta AE, Eklund DM, Florent SN, Flores-Sandoval E, Fujiyama A, Fukuzawa H, Galik B, Grimanelli D, Grimwood J, Grossniklaus U, Hamada T, Haseloff J, Hetherington AJ, Higo A, Hirakawa Y, Hundley HN, Ikeda Y, Inoue K, Inoue SI, Ishida S, Jia Q, Kakita M, Kanazawa T, Kawai Y, Kawashima T, Kennedy M, Kinose K, Kinoshita T, Kohara Y, Koide E, Komatsu K, Kopischke S, Kubo M, Kyozuka J, Lagercrantz U, Lin SS, Lindquist E, Lipzen AM, Lu CW, De Luna E, Martienssen RA, Minamino N, Mizutani M, Mizutani M, Mochizuki N, Monte I, Mosher R, Nagasaki H, Nakagami H, Naramoto S, Nishitani K, Ohtani M, Okamoto T, Okumura M, Phillips J, Pollak B, Reinders A, Rovekamp M, Sano R, Sawa S, Schmid MW, Shirakawa M, Solano R, Spunde A, Suetsugu N, Sugano S, Sugiyama A, Sun R, Suzuki Y, Takenaka M, Takezawa D, Tomogane H, Tsuzuki M, Ueda T, Umeda M, Ward JM, Watanabe Y, Yazaki K, Yokoyama R, Yoshitake Y, Yotsui I, Zachgo S, Schmutz J (2017) Insights into Land Plant Evolution Garnered from the Marchantia polymorpha Genome. Cell **171:** 287-304 e215

Brautigam A, Hoffmann-Benning S, Weber AP (2008) Comparative proteomics of chloroplast envelopes from C3 and C4 plants reveals specific adaptations of the plastid envelope to C4 photosynthesis and candidate proteins required for maintaining C4 metabolite fluxes. Plant Physiol **148:** 568-579

Charpentier M, Bredemeier R, Wanner G, Takeda N, Schleiff E, Parniske M (2008) Lotus japonicus CASTOR and POLLUX are ion channels essential for perinuclear calcium spiking in legume root endosymbiosis. Plant Cell **20:** 3467-3479

Charpentier M, Sun J, Vaz Martins T, Radhakrishnan GV, Findlay K, Soumpourou E, Thouin J, Very AA, Sanders D, Morris RJ, Oldroyd GE (2016) Nuclear-localized cyclic nucleotide-gated channels mediate symbiotic calcium oscillations. Science **352:** 1102-1105

Cheng S, Xian W, Fu Y, Marin B, Keller J, Wu T, Sun W, Li X, Xu Y, Zhang Y, Wittek S, Reder T, Gunther G, Gontcharov A, Wang S, Li L, Liu X, Wang J, Yang H, Xu X, Delaux PM, Melkonian B, Wong GK, Melkonian M (2019) Genomes of Subaerial Zygnematophyceae Provide Insights into Land Plant Evolution. Cell **179:** 1057-1067 e1014

Clausen C, Ilkavets I, Thomson R, Philippar K, Vojta A, Mohlmann T, Neuhaus E, Fulgosi H, Soll J (2004) Intracellular localization of VDAC proteins in plants. Planta **220:** 30-37

Clough SJ, Bent AF (1998) Floral dip: a simplified method for Agrobacterium-mediated transformation of Arabidopsis thaliana. Plant J **16:** 735-743

De Clerck O, Kao SM, Bogaert KA, Blomme J, Foflonker F, Kwantes M, Vancaester E, Vanderstraeten L, Aydogdu E, Boesger J, Califano G, Charrier B, Clewes R, Del Cortona A, D'Hondt S, Fernandez-Pozo N, Gachon CM, Hanikenne M, Lattermann L, Leliaert F, Liu X, Maggs CA, Popper ZA, Raven JA, Van Bel M, Wilhelmsson PKI, Bhattacharya D, Coates JC, Rensing SA, Van Der Straeten D, Vardi A, Sterck L, Vandepoele K, Van de Peer Y, Wichard T, Bothwell JH (2018) Insights into the

Evolution of Multicellularity from the Sea Lettuce Genome. Curr Biol **28:** 2921-2933 e2925

de Vries J, Curtis BA, Gould SB, Archibald JM (2018) Embryophyte stress signaling evolved in the algal progenitors of land plants. Proc Natl Acad Sci U S A **115:** E3471-E3480

de Vries J, de Vries S, Curtis BA, Zhou H, Penny S, Feussner K, Pinto DM, Steinert M, Cohen AM, von Schwartzenberg K, Archibald JM (2020) Heat stress response in the closest algal relatives of land plants reveals conserved stress signaling circuits. Plant J **103:** 1025-1048

DeTar RA, Barahimipour R, Manavski N, Schwenkert S, Höhner R, Bölter B, Inaba T, Meurer J, Zoschke R, Kunz H-H (2021) Loss of inner-envelope K+/H+ exchangers impairs plastid rRNA maturation and gene expression. The Plant Cell

Dohm JC, Minoche AE, Holtgrawe D, Capella-Gutierrez S, Zakrzewski F, Tafer H, Rupp O, Sorensen TR, Stracke R, Reinhardt R, Goesmann A, Kraft T, Schulz B, Stadler PF, Schmidt T, Gabaldon T, Lehrach H, Weisshaar B, Himmelbauer H (2014) The genome of the recently domesticated crop plant sugar beet (Beta vulgaris). Nature **505:** 546-549

Eisenhut M, Hoecker N, Schmidt SB, Basgaran RM, Flachbart S, Jahns P, Eser T, Geimer S, Husted S, Weber APM, Leister D, Schneider A (2018) The Plastid Envelope CHLOROPLAST MANGANESE TRANSPORTER1 Is Essential for Manganese Homeostasis in Arabidopsis. Mol Plant **11:** 955-969

Flores-Perez U, Jarvis P (2017) Isolation and Suborganellar Fractionation of Arabidopsis Chloroplasts. Methods Mol Biol **1511:** 45-60

Frank J, Happeck R, Meier B, Hoang MTT, Stribny J, Hause G, Ding H, Morsomme P, Baginsky S, Peiter E (2019) Chloroplast-localized BICAT proteins shape stromal calcium signals and are required for efficient photosynthesis. New Phytol **221:** 866-880

Froehlich J (2011) Studying Arabidopsis envelope protein localization and topology using thermolysin and trypsin proteases. Methods Mol Biol **774:** 351-367

Furst-Jansen JMR, de Vries S, de Vries J (2020) Evo-physio: on stress responses and the earliest land plants. J Exp Bot **71:** 3254-3269

Gietz RD, Woods RA (2001) Genetic transformation of yeast. Biotechniques **30:** 816-820, 822-816, 828 passim

Gutierrez-Carbonell E, Takahashi D, Lattanzio G, Rodriguez-Celma J, Kehr J, Soll J, Philippar K, Uemura M, Abadia J, Lopez-Millan AF (2014) The distinct functional roles of the inner and outer chloroplast envelope of Pea (Pisum sativum) as revealed by proteomic approaches. J Proteome Res **13:** 2941-2953

Hoang DT, Chernomor O, von Haeseler A, Minh BQ, Vinh LS (2018) UFBoot2: Improving the Ultrafast Bootstrap Approximation. Mol Biol Evol **35:** 518-522

Höhner R, Day PM, Zimmermann SE, Lopez LS, Krämer M, Giavalisco P, Correa Galvis V, Armbruster U, Schöttler MA, Jahns P, Krueger S, Kunz H-H (2021) Stromal NADH supplied by PHOSPHOGLYCERATE DEHYDROGENASE3 is crucial for photosynthetic performance. Plant Physiology

Höhner R, Galvis VC, Strand DD, Völkner C, Kramer M, Messer M, Dinc F, Sjuts I, Bolter B, Kramer DM, Armbruster U, Kunz HH (2019) Photosynthesis in Arabidopsis Is Unaffected by the Function of the Vacuolar K(+) Channel TPK3. Plant Physiol **180:** 1322-1335

Höhner R, Tabatabaei S, Kunz H-H, Fittschen U (2016) A rapid total reflection X-ray fluorescence protocol for micro analyses of ion profiles in Arabidopsis thaliana. Spectrochimica Acta Part B: Atomic Spectroscopy **125:** 159-167

Hori K, Maruyama F, Fujisawa T, Togashi T, Yamamoto N, Seo M, Sato S, Yamada T, Mori H, Tajima N, Moriyama T, Ikeuchi M, Watanabe M, Wada H, Kobayashi K, Saito M, Masuda T, Sasaki-Sekimoto Y, Mashiguchi K, Awai K, Shimojima M, Masuda S, Iwai M, Nobusawa T, Narise T, Kondo S, Saito H, Sato R, Murakawa M, Ihara Y, Oshima-Yamada Y, Ohtaka K, Satoh M, Sonobe K, Ishii M, Ohtani R, Kanamori-Sato M, Honoki R, Miyazaki D, Mochizuki H, Umetsu J, Higashi K, Shibata D, Kamiya Y, Sato N, Nakamura Y, Tabata S, Ida S, Kurokawa K, Ohta H (2014) Klebsormidium flaccidum genome reveals primary factors for plant terrestrial adaptation. Nat Commun **5:** 3978

Hu TT, Pattyn P, Bakker EG, Cao J, Cheng JF, Clark RM, Fahlgren N, Fawcett JA, Grimwood J, Gundlach H, Haberer G, Hollister JD, Ossowski S, Ottilar RP, Salamov AA, Schneeberger K, Spannagl M, Wang X, Yang L, Nasrallah ME, Bergelson J, Carrington JC, Gaut BS, Schmutz J, Mayer KF, Van de Peer Y, Grigoriev IV, Nordborg M, Weigel D, Guo YL (2011) The Arabidopsis lyrata genome sequence and the basis of rapid genome size change. Nat Genet **43:** 476-481

Imaizumi-Anraku H, Takeda N, Charpentier M, Perry J, Miwa H, Umehara Y, Kouchi H, Murakami Y, Mulder L, Vickers K, Pike J, Downie JA, Wang T, Sato S, Asamizu E, Tabata S, Yoshikawa M, Murooka Y, Wu GJ, Kawaguchi M, Kawasaki S, Parniske M, Hayashi M (2005) Plastid proteins crucial for symbiotic fungal and bacterial entry into plant roots. Nature **433:** 527-531

International Brachypodium I (2010) Genome sequencing and analysis of the model grass Brachypodium distachyon. Nature **463:** 763-768

Jiao C, Sorensen I, Sun X, Sun H, Behar H, Alseekh S, Philippe G, Palacio Lopez K, Sun L, Reed R, Jeon S, Kiyonami R, Zhang S, Fernie AR, Brumer H, Domozych DS, Fei Z, Rose JKC (2020) The Penium margaritaceum Genome: Hallmarks of the Origins of Land Plants. Cell **181:** 1097-1111 e1012

Ju C, Van de Poel B, Cooper ED, Thierer JH, Gibbons TR, Delwiche CF, Chang C (2015) Conservation of ethylene as a plant hormone over 450 million years of evolution. Nat Plants **1:** 14004

Kalyaanamoorthy S, Minh BQ, Wong TKF, von Haeseler A, Jermiin LS (2017) ModelFinder: fast model selection for accurate phylogenetic estimates. Nat Methods **14:** 587-589

Katoh K, Standley DM (2013) MAFFT multiple sequence alignment software version 7: improvements in performance and usability. Mol Biol Evol **30:** 772-780

Kilian J, Whitehead D, Horak J, Wanke D, Weinl S, Batistic O, D'Angelo C, Bornberg-Bauer E, Kudla J, Harter K (2007) The AtGenExpress global stress expression data set: protocols, evaluation and model data analysis of UV-B light, drought and cold stress responses. Plant J **50:** 347-363

Kim S, Zeng W, Bernard S, Liao J, Venkateshwaran M, Ane JM, Jiang Y (2019) Ca(2+)-regulated Ca(2+) channels with an RCK gating ring control plant symbiotic associations. Nat Commun **10:** 3703

Knight H, Trewavas AJ, Knight MR (1996) Cold calcium signaling in Arabidopsis involves two cellular pools and a change in calcium signature after acclimation. Plant Cell **8:** 489-503

Kreplak J, Madoui MA, Capal P, Novak P, Labadie K, Aubert G, Bayer PE, Gali KK, Syme RA, Main D, Klein A, Berard A, Vrbova I, Fournier C, d'Agata L, Belser C, Berrabah W, Toegelova H, Milec Z, Vrana J, Lee H, Kougbeadjo A, Terezol M, Huneau C, Turo CJ, Mohellibi N, Neumann P, Falque M, Gallardo K, McGee R, Tar'an B, Bendahmane A, Aury JM, Batley J, Le Paslier MC, Ellis N, Warkentin TD, Coyne CJ, Salse J, Edwards D, Lichtenzveig J, Macas J, Dolezel J, Wincker P, Burstin J (2019) A reference genome for pea provides insight into legume genome evolution. Nat Genet **51:** 1411-1422

Kunz HH, Gierth M, Herdean A, Satoh-Cruz M, Kramer DM, Spetea C, Schroeder JI (2014) Plastidial transporters KEA1, -2, and -3 are essential for chloroplast osmoregulation, integrity, and pH regulation in Arabidopsis. Proc Natl Acad Sci U S A **111:** 7480-7485

Lamesch P, Berardini TZ, Li D, Swarbreck D, Wilks C, Sasidharan R, Muller R, Dreher K, Alexander DL, Garcia-Hernandez M, Karthikeyan AS, Lee CH, Nelson WD, Ploetz L, Singh S, Wensel A, Huala E (2012) The Arabidopsis Information Resource (TAIR): improved gene annotation and new tools. Nucleic Acids Res **40:** D1202-1210

Lang D, Ullrich KK, Murat F, Fuchs J, Jenkins J, Haas FB, Piednoel M, Gundlach H, Van Bel M, Meyberg R, Vives C, Morata J, Symeonidi A, Hiss M, Muchero W, Kamisugi Y, Saleh O, Blanc G, Decker EL, van Gessel N, Grimwood J, Hayes RD, Graham SW, Gunter LE, McDaniel SF, Hoernstein SNW, Larsson A, Li FW, Perroud PF, Phillips J, Ranjan P, Rokshar DS, Rothfels CJ, Schneider L, Shu S, Stevenson DW, Thummler F, Tillich M, Villarreal Aguilar JC, Widiez T, Wong GK, Wymore A, Zhang Y, Zimmer AD, Quatrano RS, Mayer KFX, Goodstein D, Casacuberta JM, Vandepoele K, Reski R, Cuming AC, Tuskan GA, Maumus F, Salse J, Schmutz J, Rensing SA (2018) The Physcomitrella patens chromosome-scale assembly reveals moss genome structure and evolution. Plant J **93:** 515-533

Le SQ, Gascuel O (2008) An improved general amino acid replacement matrix. Mol Biol Evol **25:** 1307-1320

Leitao N, Dangeville P, Carter R, Charpentier M (2019) Nuclear calcium signatures are associated with root development. Nat Commun **10:** 4865

Lenzoni G, Knight MR (2019) Increases in Absolute Temperature Stimulate Free Calcium Concentration Elevations in the Chloroplast. Plant Cell Physiol **60:** 538-548

Li FW, Nishiyama T, Waller M, Frangedakis E, Keller J, Li Z, Fernandez-Pozo N, Barker MS, Bennett T, Blazquez MA, Cheng S, Cuming AC, de Vries J, de Vries S, Delaux PM, Diop IS, Harrison CJ, Hauser D, Hernandez-Garcia J, Kirbis A, Meeks JC, Monte I, Mutte SK, Neubauer A, Quandt D, Robison T, Shimamura M, Rensing SA, Villarreal JC, Weijers D, Wicke S, Wong GK, Sakakibara K, Szovenyi P (2020) Anthoceros genomes illuminate the origin of land plants and the unique biology of hornworts. Nat Plants **6:** 259-272

Li H, Jiang F, Wu P, Wang K, Cao Y (2020) A High-Quality Genome Sequence of Model Legume Lotus japonicus (MG-20) Provides Insights into the Evolution of Root Nodule Symbiosis. Genes (Basel) **11**

Maresova L, Sychrova H (2005) Physiological characterization of Saccharomyces cerevisiae kha1 deletion mutants. Mol Microbiol **55:** 588-600

Marti Ruiz MC, Jung HJ, Webb AAR (2020) Circadian gating of dark-induced increases in chloroplast- and cytosolic-free calcium in Arabidopsis. New Phytol **225:** 1993-2005

Mehlmer N, Parvin N, Hurst CH, Knight MR, Teige M, Vothknecht UC (2012) A toolset of aequorin expression vectors for in planta studies of subcellular calcium concentrations in Arabidopsis thaliana. J Exp Bot **63:** 1751-1761

Merchant SS, Prochnik SE, Vallon O, Harris EH, Karpowicz SJ, Witman GB, Terry A, Salamov A, Fritz-Laylin LK, Marechal-Drouard L, Marshall WF, Qu LH, Nelson DR, Sanderfoot AA, Spalding MH, Kapitonov VV, Ren Q, Ferris P, Lindquist E, Shapiro H, Lucas SM, Grimwood J, Schmutz J, Cardol P, Cerutti H, Chanfreau G, Chen CL, Cognat V, Croft MT, Dent R, Dutcher S, Fernandez E, Fukuzawa H, Gonzalez-Ballester D, Gonzalez-Halphen D, Hallmann A, Hanikenne M, Hippler M, Inwood W, Jabbari K, Kalanon M, Kuras R, Lefebvre PA, Lemaire SD, Lobanov AV, Lohr M, Manuell A, Meier I, Mets L, Mittag M, Mittelmeier T, Moroney JV, Moseley J, Napoli C, Nedelcu AM, Niyogi K, Novoselov SV, Paulsen IT, Pazour G, Purton S, Ral JP, Riano-Pachon DM, Riekhof W, Rymarquis L, Schroda M, Stern D, Umen J, Willows R, Wilson N, Zimmer SL, Allmer J, Balk J, Bisova K, Chen CJ, Elias M, Gendler K, Hauser C, Lamb MR, Ledford H, Long JC, Minagawa J, Page MD, Pan J, Pootakham W, Roje S, Rose A, Stahlberg E, Terauchi AM, Yang P, Ball S, Bowler C, Dieckmann CL, Gladyshev VN, Green P, Jorgensen R, Mayfield S, Mueller-Roeber B, Rajamani S, Sayre RT, Brokstein P, Dubchak I, Goodstein D, Hornick L, Huang YW, Jhaveri J, Luo Y, Martinez D, Ngau WC, Otillar B, Poliakov A, Porter A, Szajkowski L, Werner G, Zhou K, Grigoriev IV, Rokhsar DS, Grossman AR (2007) The Chlamydomonas genome reveals the evolution of key animal and plant functions. Science **318:** 245-250

Mi F, Peters JS, Berkowitz GA (1994) Characterization of a chloroplast inner envelope K+ channel. Plant Physiol **105:** 955-964

Minh BQ, Schmidt HA, Chernomor O, Schrempf D, Woodhams MD, von Haeseler A, Lanfear R (2020) IQ-TREE 2: New Models and Efficient Methods for Phylogenetic Inference in the Genomic Era. Mol Biol Evol **37:** 1530-1534

Nickel C, Brylok T, Schwenkert S (2016) In Vivo Radiolabeling of Arabidopsis Chloroplast Proteins and Separation of Thylakoid Membrane Complexes by Blue Native PAGE. Methods Mol Biol **1450:** 233-245

Nishiyama T, Sakayama H, de Vries J, Buschmann H, Saint-Marcoux D, Ullrich KK, Haas FB, Vanderstraeten L, Becker D, Lang D, Vosolsobe S, Rombauts S, Wilhelmsson PKI, Janitza P, Kern R, Heyl A, Rumpler F, Villalobos L, Clay JM, Skokan R, Toyoda A, Suzuki Y, Kagoshima H, Schijlen E, Tajeshwar N, Catarino B, Hetherington AJ, Saltykova A, Bonnot C, Breuninger H, Symeonidi A, Radhakrishnan GV, Van Nieuwerburgh F, Deforce D, Chang C, Karol KG, Hedrich R, Ulvskov P, Glockner G, Delwiche CF, Petrasek J, Van de Peer Y, Friml J, Beilby M, Dolan L, Kohara Y, Sugano S, Fujiyama A, Delaux PM, Quint M, Theissen G, Hagemann M, Harholt J, Dunand C, Zachgo S, Langdale J, Maumus F, Van Der Straeten D, Gould SB, Rensing SA (2018) The Chara Genome: Secondary Complexity and Implications for Plant Terrestrialization. Cell **174:** 448-464 e424

Nomura H, Komori T, Uemura S, Kanda Y, Shimotani K, Nakai K, Furuichi T, Takebayashi K, Sugimoto T, Sano S, Suwastika IN, Fukusaki E, Yoshioka H, Nakahira Y, Shiina T (2012) Chloroplast-mediated activation of plant immune signalling in Arabidopsis. Nat Commun **3:** 926

Ouyang S, Zhu W, Hamilton J, Lin H, Campbell M, Childs K, Thibaud-Nissen F, Malek RL, Lee Y, Zheng L, Orvis J, Haas B, Wortman J, Buell CR (2007) The TIGR Rice Genome Annotation Resource: improvements and new features. Nucleic Acids Res **35:** D883-887

Porra RJ, Thompson WA, Kriedemann PE (1989) Determination of accurate extinction coefficients and simultaneous equations for assaying chlorophylls a and b extracted with four different solvents: verification of the concentration of chlorophyll standards by atomic absorption spectroscopy. Biochimica et Biophysica Acta (BBA) - Bioenergetics **975:** 384-394

Pottosin, II, Muniz J, Shabala S (2005) Fast-activating channel controls cation fluxes across the native chloroplast envelope. J Membr Biol **204:** 145-156

Pottosin I, Dobrovinskaya O (2015) Ion Channels in Native Chloroplast Membranes: Challenges and Potential for Direct Patch-Clamp Studies. Front Physiol **6:** 396

Pratt AI, Knoblauch J, Kunz HH (2020) An updated pGREEN-based vector suite for cost-effective cloning in plant molecular biology. MicroPubl Biol **2020**

Resentini F, Ruberti C, Grenzi M, Bonza MC, Costa A (2021) The signatures of organellar calcium. Plant Physiol

Roy A, Kucukural A, Zhang Y (2010) I-TASSER: a unified platform for automated protein structure and function prediction. Nat Protoc **5:** 725-738

Schwacke R, Schneider A, van der Graaff E, Fischer K, Catoni E, Desimone M, Frommer WB, Flugge UI, Kunze R (2003) ARAMEMNON, a novel database for Arabidopsis integral membrane proteins. Plant Physiol **131:** 16-26

Shikanai T, Muller-Moule P, Munekage Y, Niyogi KK, Pilon M (2003) PAA1, a P-type ATPase of Arabidopsis, functions in copper transport in chloroplasts. Plant Cell **15:** 1333-1346

Sohrt K, Soll J (2000) Toc64, a new component of the protein translocon of chloroplasts. J Cell Biol **148:** 1213-1221

Stahl T, Glockmann C, Soll J, Heins L (1999) Tic40, a new "old" subunit of the chloroplast protein import translocon. J Biol Chem **274:** 37467-37472

Sun Q, Zybailov B, Majeran W, Friso G, Olinares PD, van Wijk KJ (2009) PPDB, the Plant Proteomics Database at Cornell. Nucleic Acids Res **37:** D969-974

Tanaka K, Choi J, Stacey G (2013) Aequorin luminescence-based functional calcium assay for heterotrimeric G-proteins in Arabidopsis. Methods Mol Biol **1043:** 45-54

Teardo E, Carraretto L, Moscatiello R, Cortese E, Vicario M, Festa M, Maso L, De Bortoli S, Cali T, Vothknecht UC, Formentin E, Cendron L, Navazio L, Szabo I (2019) A chloroplast-localized mitochondrial calcium uniporter transduces osmotic stress in Arabidopsis. Nat Plants **5:** 581-588

Trentmann O, Muhlhaus T, Zimmer D, Sommer F, Schroda M, Haferkamp I, Keller I, Pommerrenig B, Neuhaus HE (2020) Identification of Chloroplast Envelope Proteins with Critical Importance for Cold Acclimation. Plant Physiol **182:** 1239-1255

Tsujii M, Kera K, Hamamoto S, Kuromori T, Shikanai T, Uozumi N (2019) Evidence for potassium transport activity of Arabidopsis KEA1-KEA6. Sci Rep **9:** 10040

Venkateshwaran M, Cosme A, Han L, Banba M, Satyshur KA, Schleiff E, Parniske M, Imaizumi-Anraku H, Ane JM (2012) The recent evolution of a symbiotic ion channel in the legume family altered ion conductance and improved functionality in calcium signaling. Plant Cell **24:** 2528-2545

Voinnet O, Rivas S, Mestre P, Baulcombe D (2003) An enhanced transient expression system in plants based on suppression of gene silencing by the p19 protein of tomato bushy stunt virus. Plant J **33:** 949-956

Waadt R, Schlucking K, Schroeder JI, Kudla J (2014) Protein fragment bimolecular fluorescence complementation analyses for the in vivo study of protein-protein interactions and cellular protein complex localizations. Methods Mol Biol **1062:** 629-658

Wallis JW, Chrebet G, Brodsky G, Rolfe M, Rothstein R (1989) A hyper-recombination mutation in S. cerevisiae identifies a novel eukaryotic topoisomerase. Cell **58:** 409-419

Wan T, Liu ZM, Li LF, Leitch AR, Leitch IJ, Lohaus R, Liu ZJ, Xin HP, Gong YB, Liu Y, Wang WC, Chen LY, Yang Y, Kelly LJ, Yang J, Huang JL, Li Z, Liu P, Zhang L, Liu HM, Wang H, Deng SH, Liu M, Li J, Ma L, Liu Y, Lei Y, Xu W, Wu LQ, Liu F, Ma Q, Yu XR, Jiang Z, Zhang GQ, Li SH, Li RQ, Zhang SZ, Wang QF, Van de Peer Y, Zhang JB, Wang XM (2018) A genome for gnetophytes and early evolution of seed plants. Nat Plants **4:** 82-89

Wang S, Li L, Li H, Sahu SK, Wang H, Xu Y, Xian W, Song B, Liang H, Cheng S, Chang Y, Song Y, Cebi Z, Wittek S, Reder T, Peterson M, Yang H, Wang J, Melkonian B, Van de Peer Y, Xu X, Wong GK, Melkonian M, Liu H, Liu X (2020) Genomes of early-diverging streptophyte algae shed light on plant terrestrialization. Nat Plants **6:** 95-106

Wang X, Berkowitz GA, Peters JS (1993) K+-conducting ion channel of the chloroplast inner envelope: functional reconstitution into liposomes. Proc Natl Acad Sci U S A **90:** 4981-4985

Weinl S, Held K, Schlucking K, Steinhorst L, Kuhlgert S, Hippler M, Kudla J (2008) A plastid protein crucial for Ca2+-regulated stomatal responses. New Phytol **179:** 675-686

Whelan S, Goldman N (2001) A general empirical model of protein evolution derived from multiple protein families using a maximum-likelihood approach. Mol Biol Evol **18:** 691-699

Worden AZ, Lee JH, Mock T, Rouze P, Simmons MP, Aerts AL, Allen AE, Cuvelier ML, Derelle E, Everett MV, Foulon E, Grimwood J, Gundlach H, Henrissat B, Napoli C, McDonald SM, Parker MS, Rombauts S, Salamov A, Von Dassow P, Badger JH, Coutinho PM, Demir E, Dubchak I, Gentemann C, Eikrem W, Gready JE, John U, Lanier W, Lindquist EA, Lucas S, Mayer KF, Moreau H, Not F, Otillar R, Panaud O, Pangilinan J, Paulsen I, Piegu B, Poliakov A, Robbens S, Schmutz J, Toulza E, Wyss T, Zelensky A, Zhou K, Armbrust EV, Bhattacharya D, Goodenough UW, Van de Peer Y, Grigoriev IV (2009) Green evolution and dynamic adaptations revealed by genomes of the marine picoeukaryotes Micromonas. Science **324:** 268-272

Wu W, Peters J, Berkowitz GA (1991) Surface Charge-Mediated Effects of Mg on K Flux across the Chloroplast Envelope Are Associated with Regulation of Stromal pH and Photosynthesis. Plant Physiol **97:** 580-587

Zhang B, Zhang C, Liu C, Jing Y, Wang Y, Jin L, Yang L, Fu A, Shi J, Zhao F, Lan W, Luan S (2018) Inner Envelope CHLOROPLAST MANGANESE TRANSPORTER 1 Supports Manganese Homeostasis and Phototrophic Growth in Arabidopsis. Mol Plant **11:** 943-954

Zhang H, Zhang F, Yu Y, Feng L, Jia J, Liu B, Li B, Guo H, Zhai J (2020) A Comprehensive Online Database for Exploring approximately 20,000 Public Arabidopsis RNA-Seq Libraries. Mol Plant **13:** 1231-1233

2.8 Addendum: Physiological context of PEC1/2

Connection of PEC proteins to jasmonic acid signaling

In our publication in *Plant Physiology* (Chapter 2, Völkner et al., 2021), we provided first characterization of PLASTID ENVELOPE ION CHANNEL1/2 (PEC1/2) proteins. We presented PEC1/2 plastid envelope localization in a multi-pronged approach and found evidence for K^+-permeability of the proteins in a heterologous system. Surprisingly, the two independent *pec1pec2* double mutants used in this study did not reveal any phenotypes when grown under standard long-day conditions or challenged by salt, osmotic, and cold stress. However, while the WT displayed a sharp increase in stromal Ca^{2+} after application of specific elicitors, *pec1pec2* mutants lacked such a response even though these triggers did not result in mutant-specific growth phenotypes. Therefore, the physiological role of PEC1/2 in the chloroplast envelope remains to be understood. Here, we update on recent, unpublished findings that may give context to PEC1/2 function and the generation of plastid Ca^{2+} signals.

In publicly available transcriptomics and co-expression studies, we noticed a strong *PEC1/2* gene expression induction in response to jasmonic acid (JA) treatments. Additionally, the Electronic Fluorescent Pictograph (eFP) browser revealed a substantial increase in *PEC1/2* expression after wounding (Add. Fig. 2.1A (Winter et al., 2007)). A co-expression analysis using atted.jp found a correlation of *PEC1* to wounding- and JA-induced genes *CORI1* (*CHLOROPHYLLASE1*), *LOX2* (*LIPOXYGENASE2*), *DDE2* (*ALLENE OXIDE SYNTHASE*) (Add. Fig. 2.1B, atted.jp, (Obayashi et al., 2018)). Intriguingly, LOX2 and AOS are directly involved in the plastid-localized biosynthesis of the JA precursor OPDA (Wasternack and Hause, 2013). Lastly, transcriptome analysis indicated that *CORONATINE-INSENSITIVE1 (coi1)* mutants could not initiate *PEC1* expression to the same degree WT controls can (Add. Fig. 2.1C,

(Hruz et al., 2008). *coi1* mutants are defective in the sensing of JA by the SCF^{COI1} ubiquitin-ligase due to the lack of the F-Box motif protein (Wasternack and Hause, 2013). In plants, the SCF^{COI1} complex ubiquitinates JASMONATE-ZIM-DOMAIN PROTEIN1 (JAZ1), a repressor of wounding induced gene transcription, after binding of JA, which is then degraded by the proteasome (Wasternack and Hause, 2013).

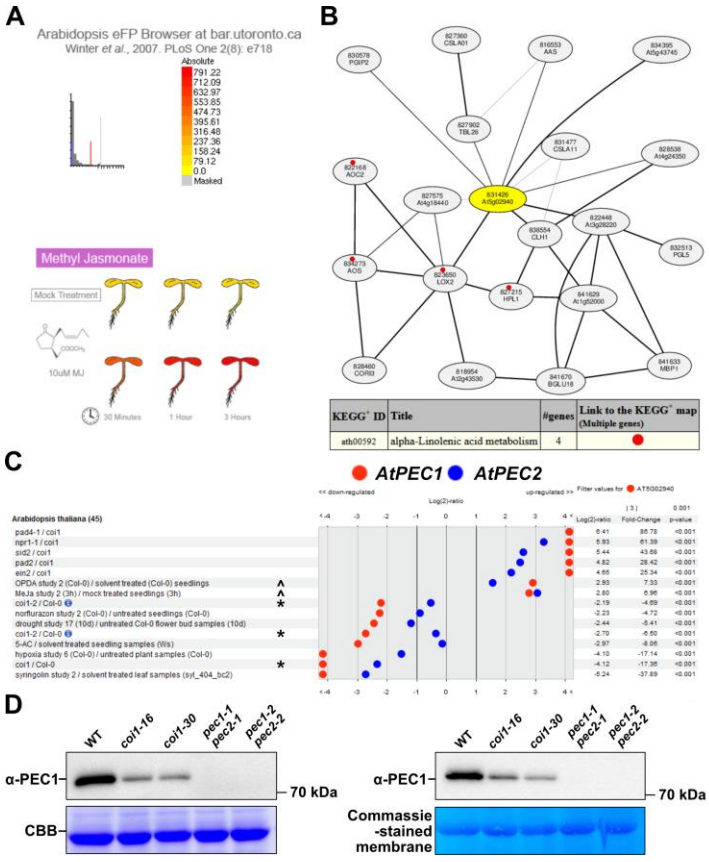

Addendum Figure 2.1 Expression analysis of *AtPEC1* and COI1-dependency. A) Co-expression network of *AtPEC1* (atted.jp, accessed October 20, 2021, Obayashi et al., 2018). *PEC1* in yellow is co-expressed with genes involved in the α-linolenic acid pathway *AOC2*, *AOS*, *LOX2*, and *HPL1* (AT4G15440). Noteworthy is co-expression with *CLH1* (AT1G19670, encoding CHLOROPHYLLASE1). B) Induction of *PEC1* expression according to eFP browser (accessed October 20, 2021, Winter et al., 2007). C) Analysis of *AtPEC1* (red dots) and *AtPEC2* (blue dots) expression in different mutant backgrounds or after treatment. Only highly significantly changed expression values are shown (accessed October 24, 2015, Hruz et al., 2008). Note the upregulation in salicylic acid-free free backgrounds (*pad4*, *npr1*, *sid2*, *pad2*) compared to *coi1* (first four rows), upregulation after JA/OPDA treatment (^), and downregulation in *coi1* background when compared to the Col-0 wild-type (*****). D) Immunoblotting of with α-PEC1 antibody reveals lower PEC1 protein levels in leaf tissue of 28-d-old *coi1* mutants compared to the WT. Two independent experiments are shown. CBB=commassie brilliant blue.

To investigate *PEC1/2* expression control by the SCF^{COI1} complex, we ordered two independent *coi1* mutant alleles, *coi1-16* and *coi1-30* (Ellis and Turner, 2002; Yang et al., 2012). We then extracted protein extracts of wild-type Col-0 (WT), *coi1-16, coi1-30,* and two *pec1pec2* double mutant lines. After adjusting protein concentration, we separated the proteins on an SDS-PAGE and transferred the proteins to a PVDF membrane which we probed with the α-PEC1 antibody (Völkner et al., 2021). While the WT tissue consistently gave a strong signal when treated with α-PEC1, the signal in extracts of both independent alleles of *coi1* was much fainter in comparison (Add. Fig. 2.1D). This result confirms the transcriptomics studies mentioned above on a protein level. Furthermore, as shown previously, the PEC1 signal was absent in both *pec1pec2* double mutants. Our finding points to expression control of *PEC1 via* the SCF^{COI1} complex, linking plastid K^+-flux and the generation of Ca^{2+} transients to JA signaling.

Indeed, the chloroplast has received increasing attention as a hub for detecting and fending off various plant stress factors (Littlejohn et al., 2021). Additionally, a link between cation flux and increased levels of JA has been described in the past. When screening a mutagenized seed pool for mutants with higher rates of LOX activity, a mutant labeled *fou2* (*fatty acid oxygenation upregulated2*) was identified (Bonaventure et al., 2007). Surprisingly, *fou2* possesses a point mutation (D454N) in the vacuole-localized cation channel TWO PORE CHANNEL1 (TPC1). This mutation renders the channel insensitive to vacuolar Ca^{2+}, leading to significantly increased vacuolar Ca^{2+} and decreased K^+ concentrations (Beyhl et al., 2009). Wound-induced systemic Ca^{2+} signals have been well characterized in the past (Glauser et al., 2008; Mousavi et al., 2013; Kiep et al., 2015). Intriguingly, cytosolic Ca^{2+} levels are decreased in *fou2* compared to the WT but display similar kinetics upon wounding, consistent with the suggested impermeability of TPC1 to Ca^{2+} (Lenglet et al., 2017). While *fou2* plants had slightly

increased levels of JA under normal conditions compared to the WT, wounding led to JA accumulation five times higher than the WT (Bonaventure et al., 2007). While it has been suggested that endomembrane cation fluxes might control JA pathway activity (Lenglet et al., 2017), the increase in basal and wound-induced accumulation of JA in *fou2* has not been fully understood thus far. PEC1 proteins might represent the missing link between endomembrane cation fluxes and increased JA biosynthesis.

Considering the localization of PEC, co-regulation, and COI1/JA dependency of *PEC1*, we propose a critical role of PEC1 in the generation of stromal Ca^{2+} transients, leading to biosynthesis of JA precursors with the involvement of LOX2.

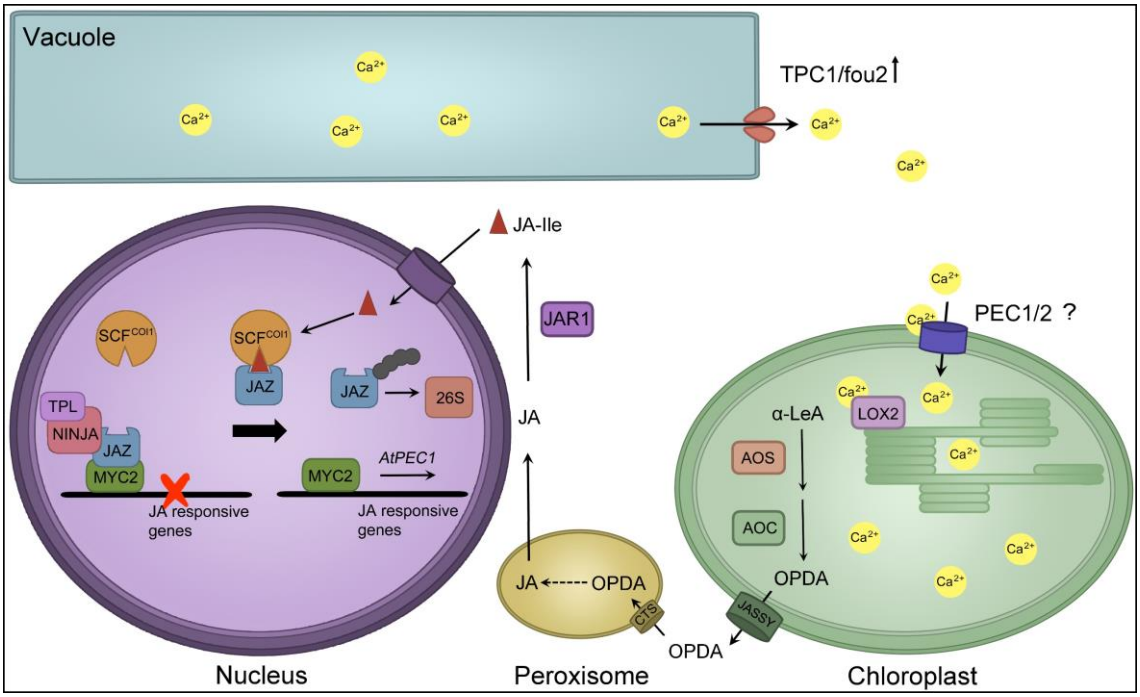

Addendum Figure 2.2 Model of the proposed function of *At*PEC in JA biosynthesis. After wounding, cytosolic Ca^{2+} levels are elevated, leading to increased activation of PEC proteins *via* the RCK domain and subsequent Ca^{2+} influx into the chloroplast. In the stroma, elevated Ca^{2+} may interact with and activate LOX2, leading to increased biosynthesis of α-linolenic acid (α-LeA), the JA precursor OPDA. Conversion of JA to JA-isoleucine (JA-Ile) by JAR1 leads to degradation JAZ proteins by the SCF^{COI1} complex in the nucleus and expression of JA responsive genes. *fou2* mutants display deregulated subcellular cation flux even when not wounded. This might lead to activation of PEC, elevated stromal Ca^{2+} concentration and increased OPDA biosynthesis, comparable to the wound-induced JA biosynthesis in the WT. Nuclear processes are presented with modifications from (Ruan et al., 2019).

Following this working model, in a *fou2* background, we suggest activation of PEC1 by increased subcellular cation/K^+ fluxes, leading to increased stromal Ca^{2+} (Add. Fig. 2.2). Homology modeling revealed the presence of a putative regulator of K^+ conductance (RCK) domain in PEC1/2, which is associated with Ca^{2+}-dependent gating of K^+-permeable channels (Kim et al., 2019, Völkner et al., 2021). In animals, LOXs interacted with Ca^{2+} *via* the C2 domain (Oldham et al., 2005). Intriguingly, *At*LOX2 also harbors a similar C2 domain (Bonaventure et al., 2007), and increased plastid Ca^{2+} could also affect the 'wounding lipoxygenase' LOX2. The increase in stromal Ca^{2+} would result in a higher concentration of α-linolenic acid and rates of OPDA synthesis. Therefore, the absence of PEC1/2 may diminish the *fou2* phenotype since our data point to the critical importance of PEC1/2 channel activity in generating plastid Ca^{2+} transients. More importantly, this mode of action would also provide insight into PEC1/2 in a WT background. Here, subcellular Ca^{2+} transients appear after wounding. These transients could similarly trigger PEC1/2, leading to LOX2 activation and the biosynthesis of JA. Additional Ca^{2+} transport proteins or other players might also be involved in the potential activation of LOX2.

References

Beyhl D, Hortensteiner S, Martinoia E, Farmer EE, Fromm J, Marten I, Hedrich R (2009) The fou2 mutation in the major vacuolar cation channel TPC1 confers tolerance to inhibitory luminal calcium. Plant J **58:** 715-723

Bonaventure G, Gfeller A, Proebsting WM, Hortensteiner S, Chetelat A, Martinoia E, Farmer EE (2007) A gain-of-function allele of TPC1 activates oxylipin biogenesis after leaf wounding in Arabidopsis. Plant J **49:** 889-898

Ellis C, Turner JG (2002) A conditionally fertile coi1 allele indicates cross-talk between plant hormone signalling pathways in Arabidopsis thaliana seeds and young seedlings. Planta **215:** 549-556

Glauser G, Grata E, Dubugnon L, Rudaz S, Farmer EE, Wolfender JL (2008) Spatial and temporal dynamics of jasmonate synthesis and accumulation in Arabidopsis in response to wounding. J Biol Chem **283:** 16400-16407

Hruz T, Laule O, Szabo G, Wessendorp F, Bleuler S, Oertle L, Widmayer P, Gruissem W, Zimmermann P (2008) Genevestigator v3: a reference expression database for the meta-analysis of transcriptomes. Adv Bioinformatics **2008:** 420747

Kiep V, Vadassery J, Lattke J, Maass JP, Boland W, Peiter E, Mithofer A (2015) Systemic cytosolic Ca(2+) elevation is activated upon wounding and herbivory in Arabidopsis. New Phytol **207:** 996-1004

Kim S, Zeng W, Bernard S, Liao J, Venkateshwaran M, Ane JM, Jiang Y (2019) Ca(2+)-regulated Ca(2+) channels with an RCK gating ring control plant symbiotic associations. Nat Commun **10:** 3703

Lenglet A, Jaslan D, Toyota M, Mueller M, Muller T, Schonknecht G, Marten I, Gilroy S, Hedrich R, Farmer EE (2017) Control of basal jasmonate signalling and defence through modulation of intracellular cation flux capacity. New Phytol **216:** 1161-1169

Littlejohn GR, Breen S, Smirnoff N, Grant M (2021) Chloroplast immunity illuminated. New Phytol **229**: 3088-310

Mousavi SA, Chauvin A, Pascaud F, Kellenberger S, Farmer EE (2013) GLUTAMATE RECEPTOR-LIKE genes mediate leaf-to-leaf wound signalling. Nature **500:** 422-426

Obayashi T, Aoki Y, Tadaka S, Kagaya Y, Kinoshita K (2018) ATTED-II in 2018: A Plant Coexpression Database Based on Investigation of the Statistical Property of the Mutual Rank Index. Plant Cell Physiol **59:** e3

Oldham ML, Brash AR, Newcomer ME (2005) Insights from the X-ray crystal structure of coral 8R-lipoxygenase: calcium activation via a C2-like domain and a structural basis of product chirality. J Biol Chem **280:** 39545-39552

Ruan J, Zhou Y, Zhou M, Yan J, Khurshid M, Weng W, Cheng J, Zhang K (2019) Jasmonic Acid Signaling Pathway in Plants. Int J Mol Sci **20**

Völkner C, Holzner LJ, Day PM, Ashok AD, Vries Jd, Bölter B, Kunz H-H (2021) Two plastid POLLUX ion channel-like proteins are required for stress-triggered stromal Ca2+ release. Plant Physiology

Wasternack C, Hause B (2013) Jasmonates: biosynthesis, perception, signal transduction and action in plant stress response, growth and development. An update to the 2007 review in Annals of Botany. Ann Bot **111:** 1021-1058

Winter D, Vinegar B, Nahal H, Ammar R, Wilson GV, Provart NJ (2007) An "Electronic Fluorescent Pictograph" browser for exploring and analyzing large-scale biological data sets. PLoS One **2:** e718

Yang DL, Yao J, Mei CS, Tong XH, Zeng LJ, Li Q, Xiao LT, Sun TP, Li J, Deng XW, Lee CM, Thomashow MF, Yang Y, He Z, He SY (2012) Plant hormone jasmonate prioritizes defense over growth by interfering with gibberellin signaling cascade. Proc Natl Acad Sci U S A **109:** E1192-1200

CHAPTER THREE: FUNCTIONAL OVERLAP OF INNER ENVELOPE KEA AND MSL PROTEINS IN CHLOROPLAST PHYSIOLOGY

This chapter was formatted in a style suitable for submission in *Journal of Experimental Botany* with co-authors Katinka Bünger and Hans-Henning Kunz.

3.1 Abstract

Metabolic and developmental activities inside living cells result in dynamic concentrations of solutes. These changes in osmotic pressure result in water flux across membranes, critical for plant growth and shape. However, our knowledge of how cells or organelles regulate and coordinate the response to dynamic osmotic conditions is limited. This is also true for plastids. Thus far, two different envelope protein families impacting plastid osmoregulation have been described in *Arabidopsis thaliana*: K^+-EFFLUX ANTIPORTER1 (KEA1) and KEA2, and MSCS-LIKE2 (MSL2) and MSL3. Interestingly, in both families, the plastid-localized members seem to be redundant under ideal growth conditions. Therefore, only the simultaneous loss of both copies in *kea1kea2* and *msl2msl3* double mutants affects chloroplast size and morphology. Additionally, *kea1kea2* mutant plants grow slower, displaying virescent leaves, delayed plastid development, and low rates of plastid gene expression. On the other hand, MSL2 and MSL3 are involved in chloroplast division. Mutants show reduced growth and different developmental defects in leaves. Even though a functional interaction between K^+-carriers KEA1/2 and ion channel proteins MSL2/3 within the same membrane seems logical, the genetic overlap of both protein families has not been investigated so far. In this work, we present the isolation of two independent *kea1msl2* mutants. These mutants display distinct phenotypic and photosynthetic abnormalities not observed in either *kea1* or *msl2* loss-of-function single mutant. Interestingly, *kea1msl2* phenotypes are partially recovered under external salt stress. Our

data suggest that KEA1 and MSL2 function in concert to maintain chloroplast osmoregulation and are needed for proper chloroplast development and organelle function.

3.2 Introduction

Due to their sessile nature, plants need to adapt to changing environmental conditions continuously. In order to grow and reproduce, plants need to fend off pathogens, pests, and herbivores, known as biotic stress factors—abiotic stress factors, such as varying temperatures, light conditions, and humidity further impact plant performance. Additionally, drought or sudden rain can lead to varying water availability and water use over a single day. As a result, plants have evolved to become champions of adaptation to these challenges.

Maintaining proper solute concentrations, *i.e.*, sugars, amino acids, and ions, is critical for plants, which rely on internal water pressure for cell shape and expansion (Verslues and Sharma, 2010). In nature, biotic or abiotic stress can challenge plant osmolyte content. Specifically, stress factors such as drought or soil salinity put a significant burden on global food production (Boyer, 1982). During these osmotic stress conditions, plants invest many resources into the biosynthesis of specialized metabolites such as proline, glycine betaine, or Myo-inositol (Yancey, 2005). These so-called compatible osmolytes do not interfere with other biological processes and can therefore accumulate in the cytoplasm to aid cellular function (Cushman, 2001). Subcellular adjustments are required as well, for example, in organelles that themselves produce high amounts of osmolytes and proteins, such as the chloroplast.

Chloroplasts are specialized plastids and represent the organelle in plant cells that harbor the photosynthetic apparatus. Besides assimilating atmospheric carbon into sugars, chloroplasts also aid in nitrogen fixation and synthesize fatty acids, amino acids, and precursors for several phytohormones. Furthermore, chloroplasts contain their own genome, DNA-replication and -

reparation, and protein synthesis mechanisms (Lopez-Juez and Pyke, 2005). These processes are highly dynamic and result in constantly changing osmotic potentials inside chloroplasts. Therefore, the chloroplast has to balance solute and water content to keep from bursting due to hypoosmotic shock (Veley et al., 2012). Membrane proteins like ion transport proteins have been assigned this function, mainly inferred by their mode of action in bacteria (Haswell and Meyerowitz, 2006; Hamilton et al., 2015).

In prokaryotes, a sudden increase in environmental osmotic potential can accelerate water influx, causing the cell to burst. In *Escherichia coli*, mechanosensitive channel of large conductance (MscL) and mechanosensitive channel of small conductance (MscS) work in concert to prevent cellular rupture (Levina et al., 1999). Mechanosensitive (MS) channels are gated (opened) by mechanical force (Hamilton et al., 2015). Recent crystal structures show that membrane lipids associate with transmembrane residues and block pore domains of the channel in a closed state, causing opening of the pore in response to membrane tension (Zhang et al., 2021). This way, MS channels transduce physical force into a chemical signal (Hamilton et al., 2015).

While MscL homologs are not found in the plant kingdom, the model plant *Arabidopsis thaliana* encodes ten different *MscS-LIKE* (*MSL*) genes, *MSL1-10* (Hamilton et al., 2015). Two of those genes, *MSL2* and *MSL3*, encode proteins that localize to the plastid inner envelope membrane (Haswell and Meyerowitz, 2006). Intriguingly, heterologously expressed MSL3 protein complements osmotic-shock defective *E. coli* mutants, implying a function as MS channel (Haswell and Meyerowitz, 2006). Complementation with MSL2 was not pursued due to the lethal effect of the transformation of MSL2 cDNA into *E. coli*. Nevertheless, it was inferred that MSL2 also acts as an MS channel since overall similarity to MSL3 on amino acid level is

high (50%), particularly in the pore region aligning to the bacterial MscS (91% identical to MSL3) (Haswell and Meyerowitz, 2006). The cargo substrates for MSL2 or MSL3 proteins have not been experimentally confirmed thus far (Szabo and Spetea, 2017). However, plasma membrane-localized homolog AtMSL10 has been measured using electrophysiology approaches, and a slight preference for anions over cations was determined (Maksaev and Haswell, 2012). At the same time, it was suggested that MSLs generally act as nonselective ion channels (Hamilton et al., 2015).

MSL2 and MSL3 were suggested to be involved in osmoregulation of the organelle based on phenotypes observed in *msl2msl3* double mutants. In *msl2msl3*, chloroplasts appear enlarged and thylakoid membranes misshaped (Haswell and Meyerowitz, 2006). Initially, only experiments on double mutants were attempted due to the lack of an *msl2* null mutant. Nevertheless, after isolation of the null allele *msl2-3*, it was observed that loss-of-function *msl2* mutants also carry defects in plastid morphology and plant growth, albeit much less pronounced than in the double mutant (Jensen and Haswell, 2012). While *msl2* mutants are slightly smaller than the wild-type (WT), they are homogenously green. The leaves, however, display rumpled edges, indicating developmental complications (Haswell and Meyerowitz, 2006; Jensen and Haswell, 2012). Still, no *msl3* null mutant has been identified thus far (Hamilton et al., 2015). Additionally, based on their distinct localization at plastid poles, both proteins have been implicated to be involved in plastid division (Wilson et al., 2011).

Another ion transport family connected to chloroplast osmoregulation are the family of K^+-EFFLUX ANTIPORTERS (KEA). *At*KEA1 and *At*KEA2 localize to the inner chloroplast envelope membrane and export K^+ from the stroma in exchange for H^+. *kea1* or *kea2* single loss-of-function mutants show no phenotypic differences from the WT, pointing to partially

redundant functions. However, loss of both proteins results in swollen chloroplasts, but otherwise, the phenotypes of the mutants are clearly different (Kunz et al., 2014; Aranda-Sicilia et al., 2016). While *msl2(msl3)* mutants are slightly smaller than the WT and green, *kea1kea2* mutants display a strong reduction in growth and a delayed-greening phenotype (Kunz et al., 2014). Furthermore, studying the leaf ionome of *kea1kea2* revealed that these younger leaves possess significantly increased K^+ (Höhner et al., 2016), explained by the lack of K^+-export from chloroplasts leading to disturbed K^+ homeostasis in the cell. More recent research noticed the virescent, delayed greening phenotype as a common feature of mutants compromised in plastid gene expression (PGE). The authors were able to show that loss of both KEA1 and KEA2 results in defects in ribosome assembly and activity, impaired PGE, and plastid development (DeTar et al., 2021). Intriguingly, both MSL2/MSL3 and KEA1/2 have been observed to localize to patchy spots in mature chloroplasts (Aranda-Sicilia et al., 2016). Since MSL2/3 also have a suggested role in plastid division, it was proposed that KEA1/KEA2 might share a similar localization in the inner plastid envelope and that both protein families work together in a pathway that links plastid division and osmoregulation (Aranda-Sicilia et al., 2016).

Still, studies researching the functional overlap between plastid KEA and MSL proteins are lacking. In this work, we present initial evidence for such partial functional overlap through the generation of *kea1msl2* loss-of-function double mutants. *kea1msl2* mutants display a patchy, chlorotic phenotype not observed in either *kea1* or *msl2* single mutant. In addition to reduced growth, a significant loss in chlorophyll content and disturbed leaf ion concentrations became apparent. Finally, we were able to show that these phenotypes can be partially recovered when seedlings are grown on salt-supplemented media.

3.3 Results

Isolation of kea1msl2 loss-of-function double mutants

Past research has focused on generating mutants lacking transport proteins in KEA or MSL protein families separately. However, no apparent phenotype is visible in *kea1* or *kea2* single mutants, which led to the assumption that these proteins function redundantly. While that may be the case, expression of *KEA1* is much higher (Suppl. Fig. S3.1 (Bolter et al., 2020; Zhang et al., 2020)), implying that the low amounts of KEA2 present in leaf plastids is sufficient for normal function under the tested growth conditions (Kunz et al., 2014; Bolter et al., 2020). Therefore, we chose two previously identified *kea1* loss-of-function mutant lines to investigate the interaction between both families (Fig. 3.1A).

In *A. thaliana*, the MSL protein family consists of ten members, two of which, MSL2 and MSL3, localize to plastids (Hamilton et al., 2015). Due to the absence of any phenotype in the tested *msl3* mutants, most research has been done using *msl2* loss-of-function mutants. In *msl2*, two mutant alleles have been identified thus far: *msl2-1* and *msl2-3* (Fig. 3.1B). While *msl2-1* is regarded only as a partial knock-down and does not have an obvious phenotype (Haswell and Meyerowitz, 2006), *msl2-3* appears different from WT plants (Wilson et al., 2011). Loss-of-function *msl2*-3 mutants are smaller than the WT and possess wrinkled leaves with obvious deformations (Jensen and Haswell, 2012). Here, we present the successful isolation of another *msl2* loss-of-function T-DNA insertion line, *msl2-4* (Fig. 3.1B, SALK_058329). Because the loss of MSL3 does not seem to affect plant growth, we focused on the interaction of highly-expressed *KEA1* and *MSL2* in this work.

Both KEA and MSL proteins have previously been suggested to aid in chloroplast osmoregulation (Codjoe et al., 2021). Therefore, we aimed to gain insight into possible functional overlap through creating loss-of-function double mutants. After isolating the novel

msl2-4 allele, we introgressed *kea1-1* and *kea1-2* mutants into *msl2-4* and *msl2-3*, respectively. As expected, F_1 plant individuals appeared WT-like (not shown). After confirming T-DNA borders in both genes in the F_1, the F_2 generation was screened by PCR genotyping on genomic DNA (gDNA) extracts. We were able to confirm homozygous *kea1-1msl2-4* (Fig. 3.1C) and *kea1-2msl2-3* (Fig. 3.1D) loss-of-function mutants using oligonucleotide combinations indicated in Fig. 3.1A-B and Suppl. Tables S3.1, S3.2. Additionally, through immunoblotting (Bolter et al., 2020), we further confirmed the absence of KEA1 on protein level (Suppl. Fig. 3.2).

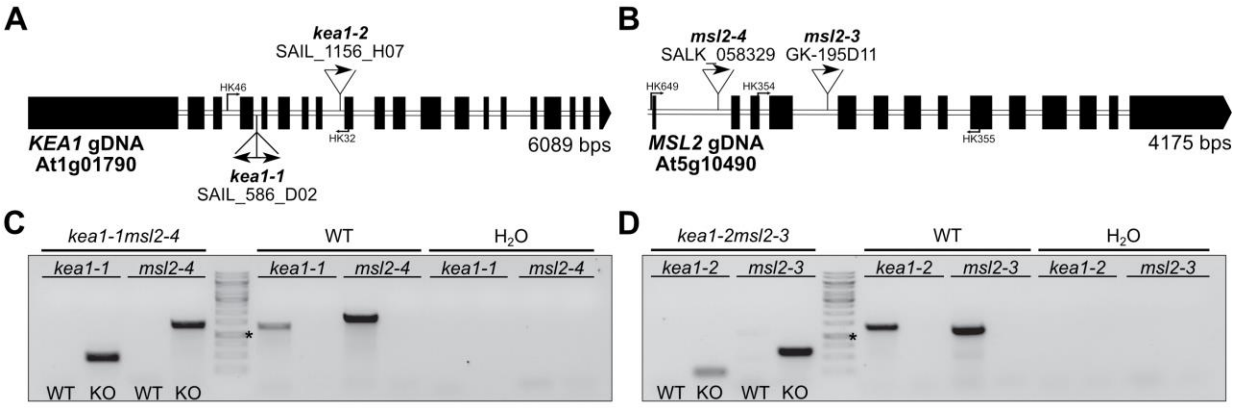

Figure 3.1 Locus of *AtKEA1, AtMSL2,* and isolation of insertion lines used in this work. A) Locus of *AtKEA*1, modified from (Kunz et al., 2014). B) Locus of *AtMSL2*, including newly isolated T-DNA insertion line *msl2-4*. Primers used for amplifications of products (Suppl. Table S3.1) are indicated at their respective positions. C-D) Genotyping of homozygous loss-of-function double mutants *kea1-1msl2-4* (C) and *kea1-2msl2-3* (D). Oligonucleotide combinations can be accessed from Suppl. Table S3.2. Pipetting scheme indicated for the first four wells continued for the entirety of the gel. * indicates the 1 kb band of the DNA ladder.

Mutants lacking both KEA1 and MSL2 reveal distinct phenotypes

Homozygous *kea1msl2* were fertile and produced seeds that were used to grow seedlings for further experiments. To our surprise, plants lacking both KEA1 and MSL2 proteins were smaller than both respective *kea1* and *msl2* single mutant controls. Furthermore, *kea1msl2* mutants displayed deformed leaves reminiscent of *msl2* single mutants, if less strongly pronounced. Interestingly, we also observed phenotypes exclusive to the loss-of-function double

mutants. *kea1msl2* plants were much brighter in color with chlorotic leaves, most prominent in younger tissues and on the edges of older leaves (Fig. 3.2A).

In order to analyze photosynthetic parameters in *kea1msl2* mutants, we subjected 28-d-old 12 h/12 h-grown plants to pulse-amplitude modulation (PAM) fluorometry measurements. As reported previously, the maximum quantum efficiency of PS II (F_v/F_m) of *kea1* mutants was not different from WT controls (Kunz et al., 2014). Surprisingly, we recorded altered chlorophyll fluorescence parameters in *msl2* mutants (Fig. 3.2B), which had not been studied in the past. Here, a slight but significant reduction in F_v/F_m became obvious. More importantly, deficiencies of *kea1msl2* revealed even more drastic differences than the independent *kea1* and *msl2* single mutants. A significant drop in F_v/F_m was observed in both *kea1-1msl2-4* and *kea1-2msl2-3*. (Fig. 3.2B-D). In our analysis, it became apparent that the brighter leaves also displayed the lowest F_v/F_m.

Non-photochemical quenching (NPQ) describes the regulated dissipation of a surplus in excitation energy as heat (Klughammer and Schreiber, 2008). *Arabidopsis* mutants defective in H^+ homeostasis, like *kea1kea2*, can exhibit drastically altered NPQ due to a disturbance in ΔpH across the thylakoid membrane. However, deficiency in other plastid ion transporter proteins can also affect NPQ. One example is the chloroplast envelope Ca^{2+}/Mn^{2+} carrier BIVALENT CATION TRANSPORTER2 (BICAT2). *bicat2* loss-of-function mutants display elevated NPQ, pronounced at high-light (Frank et al., 2019).

Transient NPQ of WT is represented as the sharp, initial rise in NPQ after exposure to ambient light (Fig. 3.2C-D, ~40-120 s). The following decrease in NPQ in WT plants correlates to activation of the ATPase which consumes protons on the lumenal side, diminishing ΔpH (Kalituho et al., 2007). Consistently, *kea1msl2* mutants display the highest and *kea1* mutants the

lowest NPQ throughout the course of the measurement. Interestingly, *kea1* and *msl2* display WT-like steady-state NPQ. In *kea1msl2* mutants, on the other hand, the prolonged transient NPQ never reaches steady-state WT levels. As mentioned earlier, NPQ is a protective mechanism, which prevents oxidative damage in plants. Therefore, less energy is being used for photochemical purposes and may result in generation of fewer reducing equivalents.

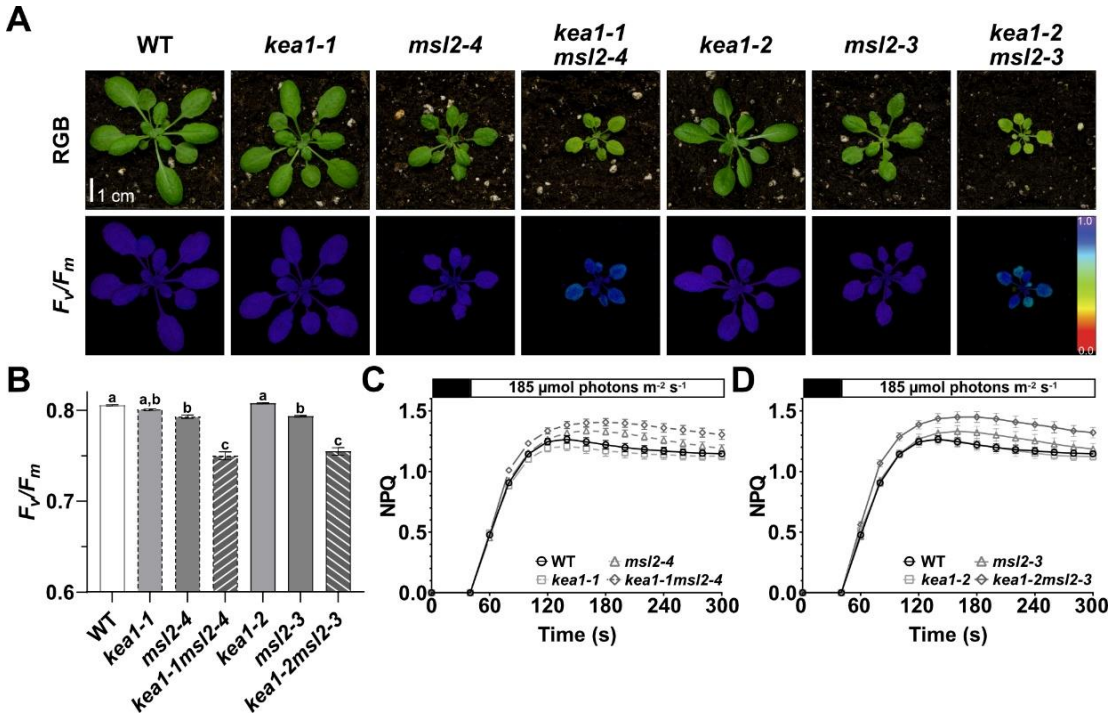

Figure 3.2 Cumulative loss of KEA1 and MSL2 leads to phenotypic and photosynthetic abnormalities. A) Representative RGB and F_v/F_m images of 28-d-old plants grown in 12 h light/12 h darkness. Both images reveal distinct growth phenotypes in *kea1msl2* mutants. B-D) PAM analysis reveals drop in photosynthetic parameters in *kea1msl2*. Shown are F_v/F_m (B) and NPQ (C+D). NPQ graphs have been split between the independent mutant lines out of spatial reasons. A representative result of three independent experiments is shown. Data are presented as mean ± standard error of the mean (SEM), n=20. In B), different letters indicate different levels of significance (p<0.05) as determined by one-way analysis of variance (ANOVA) and Tukey's multiple comparisons test.

Determination of chlorophyll levels reflects the chlorotic phenotype of kea1msl2

Next up, we wanted to investigate the chlorotic phenotype in a quantifiable way. To that end, we extracted chlorophyll from tissue and analyzed pigments with a spectrophotometer. So far, pigments have not been analyzed for any of the loss-of-function lines. As expected, both

kea1 mutants did not show differences in chlorophylls *a* or *b*, nor in total chlorophyll content compared to the WT. Surpisingly, chlorophyll *a* content in *msl2* mutants was significantly reduced without the presence of chlorotic anomalies in the plants. At the same time, *kea1msl2* mutants display chlorotic younger leaves and pronounced bright green spots in older tissue. While *kea1msl2* has significantly lower chlorophyll amounts than WT and *kea1*, statistical analysis between *msl2* and *kea1msl2* did not reveal a significant difference among the independent mutants (Fig. 3.3A-B).

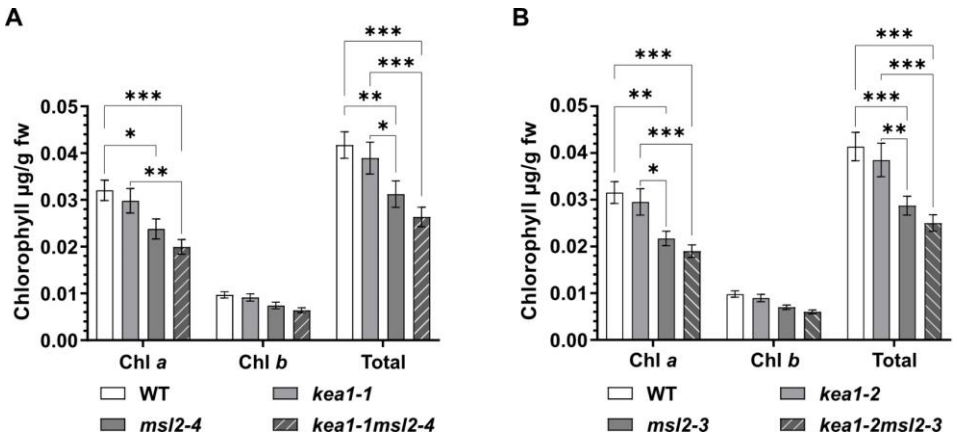

Figure 3.3 Chlorophyll analysis reflects phenotypic deficiencies in *kea1msl2*. Chlorophyll analysis in *kea1-1msl2-4* and controls (A), and *kea1-2msl2-3* and controls (B). Chlorophyll was extracted with 80% (v/v) acetone and calculated according to (Porra et al., 1989). Data are presented as mean ± SEM, *n*=9. Experiment was repeated three times with similar results. Statistical analysis was determined by ANOVA followed by Tukey's multiple comparisons test (p*<0.05, p**<0.01, p***<0.001).

The leaf ionome is disturbed in kea1msl2 mutants

Mutations in ion transport proteins can result in leaf ionome changes, giving insights into potential substrates. In order to study the leaf ionome, we harvested whole rosettes which were dried and digested with nitric acid (HNO_3). We employed total x-ray reflection fluorescence (TXRF) for analysis, a highly sensitive method used for accurate quantification of selected leaf elements in *A. thaliana* (Höhner et al., 2016).

In general, mutants in this study that are disturbed in growth also reflect defects in their respective leaf ionome. Consequently, loss-of-function *kea1* mutants again appeared WT-like while *msl2* and *kea1msl2* mutants displayed abnormalities in some leaf ions (Table 3.1). Intriguingly, the loss of *msl2-3* or *msl2-4* led to significantly lower leaf K^+ amounts. This trend was observed in both *kea1msl2* loss-of-function double mutants as well. However, in contrast to the chlorotic phenotype present after loss of both MSL2 and KEA1, this phenotype was not exacerbated by the additional loss of KEA1. Furthermore, *kea1-2msl2-3* portrayed a low-Ca^{2+} phenotype which was not present in any other tested mutant. Surprisingly, Cl^- levels were increased in *msl2-3* compared to WT and other single mutants but not compared to *kea1-2msl2-3*. This might point towards a specific effect of the *msl2-3* allele (Table 3.1).

Table 3.1 Leaf-level concentrations of elements (mg*g DW^{-1}). Mean leaf concentration of indicated elements from 28-d-old plants normalized to dry weight (mg* g DW^{-1}) (mean ± SEM, n=12). Data are averaged across three independent experiments. Different letters indicate different levels of significance (p<0.05) as determined by ANOVA and Tukey's multiple comparisons test.

	K		Ca		Cl	
Genotype	Mean	SEM	Mean	SEM	Mean	SEM
WT	51.183 ^{a}	1.144	36.954 ^{a}	1.708	0.663 ^{ab}	0.085
kea1-1	49.94 ^{ab}	1.329	37.876 ^{ab}	2.558	0.486 ^{ab}	0.057
msl2-4	42.13 ^{bc}	2.125	34.538 ^{ab}	2.983	0.797 ^{ab}	0.08
kea1-1msl2-4	43.069 ^{bc}	1.617	37.526 ^{ab}	2.235	0.694 ^{ab}	0.06
kea1-2	50.538 ^{a}	1.38	37.252 ^{a}	1.824	0.496 ^{ab}	0.053
msl2-3	38.781 ^{c}	0.721	34.122 ^{ab}	1.281	1.486 ^{c}	0.128
kea1-2msl2-3	43.424 ^{bc}	1.427	29.302 ^{bc}	0.805	1.074 ^{bc}	0.194

Partial recovery of kea1msl2 mutant phenotypes by exogenously applied salt

MSL2 belongs to a family of MS channels. In *E. coli*, MscS, closest homolog to plant MSL2, promotes survival of cells after exposure to hypoosmotic shock (Levina et al., 1999). During a sudden rise in environmental osmotic potential, MscS channels open in response to the swelling of cells because of water influx. With this mechanism, solutes can exit cells and reduce

tension on the membrane by subsequent water efflux (Booth and Louis, 1999; Levina et al., 1999). In plastids, similar mechanisms exist. Indeed, loss of MSL2/3 or KEA1/2 resulted in swollen chloroplasts in loss-of-function double mutants (Haswell and Meyerowitz, 2006; Kunz et al., 2014, Aranda-Sicilia et al., 2016). Interestingly, these phenotypes were complemented independently by the addition of external osmolytes. In *kea1kea2*, for example, growing seedlings in the presence of 75 mM NaCl partially restored growth and plastid morphology (Kunz et al., 2014), while *msl2msl3* mutants saw a reversion of the swollen chloroplasts after growth on 82 mM NaCl (Veley et al., 2012; Wilson et al., 2014).

To test whether exogenously applied salt would affect the growth of *kea1msl2* mutants, we grew seedlings on agar plates and transferred 7-d-old seedlings onto media containing or lacking exogenous salt. On 1/2 MS media, both *kea1msl2* mutants again displayed the typical bright, chlorotic leaves and stunted growth (Fig. 3.4A) as previously overserved on soil (Fig. 3.2A). In contrast to growth on soil, both *msl2* mutant alleles were also very strongly affected in growth under these conditions. However, no obvious penalty to color became apparent even though F_v/F_m was decreased similarly to growth on soil. *kea1-1* and *kea1-2* again were no different from WT controls (Fig. 3.4A). Astonishingly, *kea1msl2* mutants lost their chlorotic phenotype on media supplied with either NaCl or KCl (Fig. 3.4B-C). The overall plant size was still impacted, *i.e.*, *kea1msl2* mutants were much smaller than WT and *kea1* loss-of-function mutants. Nevertheless, loss-of-function double mutants resembled *msl2* single mutants in size and color when grown on 75 mM NaCl (Fig. 3.4B). When grown on 75 mM KCl, WT and *kea1* mutants suffered growth penalties as well. Again, *kea1msl2* mutants displayed recovered leaf color and growth (Fig. 3.4C).

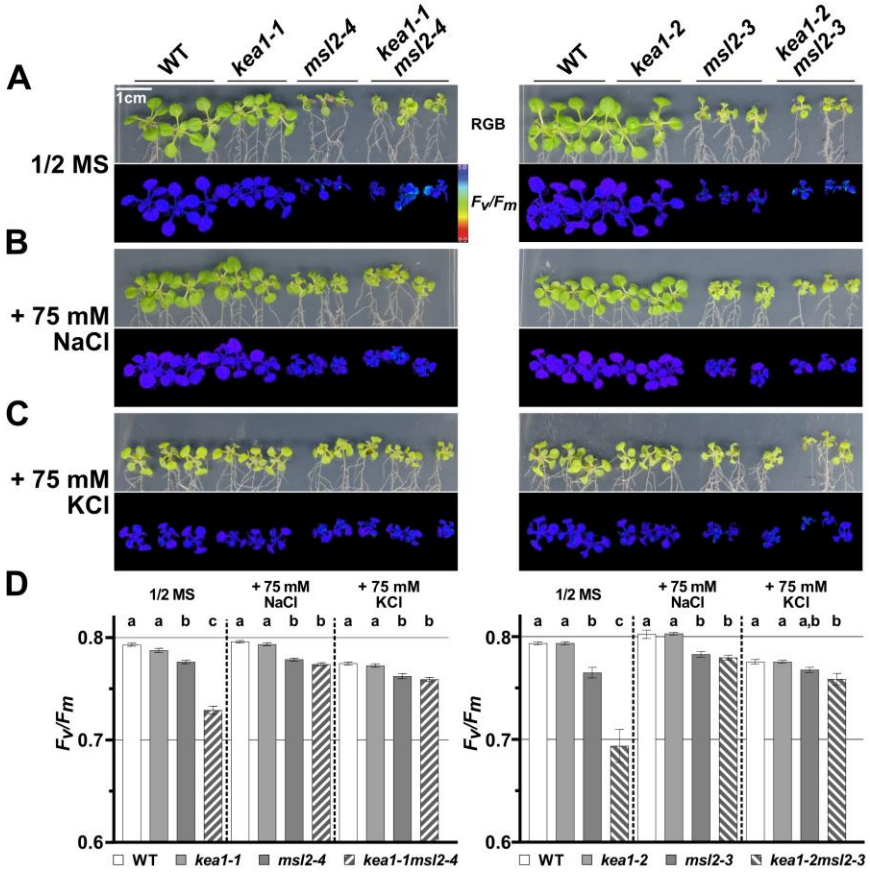

Figure 3.4 Growth on exogenous salt leads to partial recovery of phenotypes in *kea1msl2*. 7-d-old seedlings were transferred onto solid 1/2 MS (A) or 1/2 MS supplemented with either NaCl (B) or KCl (C). RGB images and PAM measurements were taken 7 d later. Representative plates are shown D) Statistical analysis of F_v/F_m in all lines tested. Different letters indicate different levels of significance by treatment ($p<0.05$) as determined by ANOVA and Tukey's multiple comparisons test. Values are presented as mean ± SEM, $n=9$. Experiment was repeated three times with similar results.

The strong photosynthetic defects of the *kea1msl2* loss-of-function double mutant became more apparent in a statistical analysis of F_v/F_m values. On, 1/2 MS media, F_v/F_m of *kea1msl2* was significantly lower than *msl2*. It is noteworthy that loss of MSL2 alone had a measurable negative effect on photosynthetic performance. Interestingly, F_v/F_m of *kea1msl2* recovered to *msl2*-like values after supplementation of NaCl and KCl, regardless of the cation. Nevertheless, F_v/F_m of double mutants were still significantly lower than WT or *kea1* (Fig. 3.4D). On KCl plates, WT or *kea1* mutants both displayed visual growth deficits along with a

reduction in F_v/F_m, while the growth of *kea1msl2* recovered even though to a lesser degree than on NaCl. The *msl2-3* mutants no longer exhibited a significantly reduced F_v/F_m compared to the WT and *kea1* mutants on KCl, which was still observed in *msl2-4* (Fig. 3.4D).

MSL proteins have been suggested to transport anions and cations non-selectively (Hamilton et al., 2015). Therefore, we wanted to test whether the increased Cl^- concentrations in NaCl- or KCl-supplemented media impacted F_v/F_m. To this end, we also transferred seedlings to plates containing either 75 mM sodium gluconate or 75 mM potassium gluconate. Surprisingly, we did not find significant differences between any of the mutants or the WT (Suppl. Fig. S3.3). At the same time, overall F_v/F_m values and growth were decreased across all lines compared to 1/2 MS or NaCl-supplemented media.

3.4 Discussion

The focus of this study was investigating functional overlap in plastid homeostasis between two plastid ion transport protein families, KEA and MSL. While both families have previously been connected to plastid osmohomeostasis, a connection has not been established thus far. Based on the newly observed phenotypes described in this study, we present evidence for a possible interaction using independent *kea1msl2* loss-of-function double mutants. We characterized chlorophyll and ion content, in addition to in-depth chlorophyll fluorescence measurements of plants grown on regular and salt-supplemented media, showcasing the importance of KEA1 and MSL2 on plastid homeostasis.

We started by isolating an independent *msl2* allele since *msl2-3* was the only loss-of-function line available at the time (Wilson et al., 2011; Jensen and Haswell, 2012). We confirmed homozygous T-DNA insertions in *msl2-4* individuals, accompanied by phenotypic

deficiencies typical for loss-of-function of MSL2. Compared to WT plants, *msl2* displays smaller growth and rumpled leaf edges, visible in both *msl2-3* and *msl2-4* (Fig. 3.1A).

Next up, we crossed both *msl2* loss-of-function lines into *kea1* single mutants. Surprisingly, in both independent *kea1xmsl2* crosses, the F_2 pool gave rise to individuals with a unique phenotype. We identified homozygous *kea1msl2* double mutants (Fig. 3.1C-D, Suppl. Fig. S3.2). When grown on soil, these individuals were much smaller than either *kea1* or *msl2* single mutants with wrinkled, patchy yellow leaves (Fig. 3.2A). The discoloration of *kea1msl2* leaves was accompanied by a reduction in the maximum quantum efficiency of PS II, F_v/F_m. This phenotype became particularly visible in F_v/F_m false-color images from PAM measurements in the edges of leaves of older tissue. Overall, F_v/F_m of both independent *kea1msl2* mutants was significantly compared to *kea1* or *msl2* loss-of-function single mutants. This indicates that KEA1 and MSL2 proteins functionally interact, maintaining chloroplast plasticity and photosynthetic performance.

In contrast to previous assumptions that KEA1/2 and MSL2/3 function redundantly (Haswell and Meyerowitz, 2006; Kunz et al., 2014), we find that the presence of KEA2 and MSL3 cannot compensate for the loss of KEA1 and MSL2, respectively. Indeed, MSL2 was shown to interact with itself and MSL3, while MSL3 could not form homomers and strictly interacted with MSL2 (Lee et al., 2019). It follows that plastid MSLs are multimeric channels, indicating distinct functions of MSL2 and MSL3. Further evidence for non-redundancy between MSL2 and MSL3 came from chlorophyll fluorescence studies. Here, F_v/F_m was significantly reduced in *msl2-3* and *msl2-4* compared to the WT, which could explain the chloroplast morphology phenotypes observed previously, *i.e.*, misshaped thylakoids and swollen chloroplasts resulting in plastid osmotic stress (Wilson et al., 2014).

In addition to decreased F_v/F_m, *kea1msl2* mutants displayed altered non-photochemical quenching. Both *kea1msl2* mutants displayed prolonged transient NPQ that did not reach WT-like steady-state levels, even towards the end of our 5-minute measurement (Fig. 3.2C-D). Prolonged transient NPQ may indicate decreased activity of the Calvin-Benson-Bassham cycle (CBBC). Under ambient light, as is the case in our measurements, the initiation of CO_2 fixation consumes ATP. This allows for ATP production *via* the ATP-synthase, which helps in diminishing ΔpH and NPQ (Kalituho et al., 2007; Höhner et al., 2021). The inability of *kea1msl2* to reduce NPQ may stem from delayed CBBC activity initiation and CO_2 fixation, which could contribute to the growth deficits in mutants. Comparing CO_2 assimilation of *kea1msl2* to WT plants would provide much needed insight into the CBBC activity.

Next up, we wanted to quantify the chlorotic, patchy yellow leaf phenotype. After chlorophyll extraction, we identified significantly decreased chlorophyll *a*, but not chlorophyll *b*, in both *kea1-1msl2-4* and *kea1-2msl2-3*. Surprisingly, chlorophyll *a* was also significantly decreased in *msl2-3* and *msl2-4* loss-of-function mutants. Even though only *kea1msl2* double mutants display the chlorotic phenotype, *msl2* single mutants seem disturbed in chlorophyll content even when KEA1 is present (Fig. 3.3A-B). Extended investigations using high-performance liquid chromatography (HPLC) might give insight into the profiles of xanthophylls and b-carotenes, which are altered in *kea1kea2* (Aranda-Sicilia et al., 2016).

The chlorotic, virescent phenotype of *kea1kea2* double mutants correlates with an increased K^+ content possibly originating from disturbed plastid osmoregulation (Kunz et al., 2014; Höhner et al., 2016). Mutants lacking MSL2, on the other hand, trended towards lowered K^+ content (Table 3.1). In the two *msl2* single and *kea1msl2* double mutants, we noticed a decrease in K^+, possibly due to disturbed plastid osmohomeostasis. This ties into the

photosynthetic deficiencies observed with chlorophyll fluorescence measurements, showcasing the importance of the K^+ ion in photosynthetic tissue. Unfortunately, the TXRF method cannot quantify Na^+ content. Further information into the makeup of the mutant's ion profile could come from inductively coupled plasma (ICP)-mass spectrometry (MS) studies (Baxter et al., 2007). Additionally, measurements of the osmoticum proline, which was significantly increased in *msl2-3* mutants (Wilson et al., 2014), will be needed to resolve possible osmoregulation deficiencies in *kea1msl2*.

Finally, we wanted to investigate the effect of external osmolytes on *msl2* single and *kea1msl2* double mutants. In studies employing *msl2msl3* mutants, previous research has demonstrated that decreasing the osmotic potential of the growth substrate and potentially the cytoplasm can ameliorate the enlarged-plastid phenotype by drawing water from plastids (Veley et al., 2012; Wilson et al., 2014). This may overcome the need for a molecular valve in the form of MSL proteins. A similar recovery is observed in *kea1kea2* mutants, which harbor populations of enlarged plastids under normal conditions (Aranda-Sicilia et al., 2016). However, when grown on media with 75 mM NaCl, plastid size shrinks, and mutants gain chlorophyll and fresh weight (Kunz et al., 2014).

Even though the phenotype of *kea1msl2* mutants differs from that of *msl2msl3* and *kea1kea2*, we wanted to investigate if the same mechanism can recover photosynthetic deficiencies or size. First, we analyzed growth on 1/2 MS media and found that *msl2* mutants had stronger growth deficits than observed from soil growth (Fig. 3.4A). Still, F_v/F_m was similarly disturbed in *msl2* single mutants and *kea1msl2* double mutants. The addition of 75 mM NaCl (Fig. 3.4B) or 75 mM KCl (Fig. 3.4C) reduced growth in WT and *kea1* seedlings while slightly increasing growth of *kea1msl2*. Growth of *msl2* mutants was improved in the presence of

osmotic support as well, confirming data from Wilson and colleagues (Wilson et al., 2014). More importantly, deficits in F_v/F_m of *kea1msl2* mutants recovered and reached *msl2*-like values, which still were significantly lower than both WT and *kea1*. This indicates additional developmental problems in *msl2* that the addition of osmolytes cannot recover. Intriguingly, F_v/F_m values of *kea1msl2* mutants did not deviate from any other tested line when grown on Na-gluconate or K-gluconate. This rescue of photosynthetic efficiency in these mutants implies that Cl^- ions are not the main ionic player and points towards recovery by either cation, the osmotic support, or a combination of both factors. Even so, the growth defects observed in *kea1msl2* may stem from altered plastid development. Germinating seedlings in the presence of osmolytes could give further insight into this phenomenon.

As mentioned, the involvement of both MSL2/3 and KEA1/2 in plastid development has been suggested previously (Wilson et al., 2011; Aranda-Sicilia et al., 2016). The developmental defects might have independent origins; MSL2/3 are needed for correct z-ring placement and aid in the division of chloroplasts, while KEA1/2 are critical for plastid gene expression and chloroplast-to-nucleus signaling, leading to disturbed plastid development and delayed leaf greening. Interestingly, the *kea1msl2* phenotype differs from the *kea1kea2* phenotype, even though both display disturbed plastid osmoregulation. This could be explained by the presence of KEA2 being sufficient for partially functional chloroplast gene expression.

It is intriguing why *kea1kea2* mutants are disturbed in plastid osmohomeostasis even with MSL2 and MSL3 intact. Therefore, it is plausible that MSL2 could support KEA1 function, and *vice versa*, under control conditions. On media with osmotic support, the osmotic valve MSL2 is no longer needed, yet defects in plastid division might persist. If both proteins are absent, KEA2 and MSL3 can only partially cover for KEA1 and MSL2, respectively, resulting in the *kea1msl2*

phenotypic abnormalities. Likewise, in *msl2msl3* mutants, disturbed osmoregulation could also lead to the malfunction of KEA1/2, impacting K^+/H^+ transport or RNA-binding capabilities.

Our studies add new insight into plastid osmoregulation and ion homeostasis. We show that the absence of KEA1 in an *msl2* mutant background impairs photosynthetic performance, even when supposedly redundant proteins KEA2 and MSL3 are present. The partial photosynthetic recovery of *kea1msl2* mutants on salt-supplemented media points toward disturbed osmoregulation under normal conditions associated with a disturbed leaf ionome. Our experiments indicate a concerted functional interaction of KEA1 and MSL2 in maintaining plastid osmoregulation and development.

3.5 Materials and Methods

Plant growth conditions

For plant growth, seeds were sown directly onto soil. The pots were stratified in a humid environment at 4°C in the dark for 3d. Then, pots were placed directly into growth chambers and grown at 150 µmol photons m^{-2} s^{-1} in a 12 h light/12 h darkness regime. After 7 d, seedlings were separated into individual pots. 28-d-old plants were used for characterization unless otherwise indicated.

gDNA extraction and genotyping

Isolation of gDNA was performed by grinding leaf material in extraction buffer (200 mM Tris pH 7.5, 250 mM NaCl, 25 mM EDTA, and 0.5% SDS (w/v). If not indicated otherwise, all consumables were ordered from Roth, Carl Roth, Karlsruhe, Germany). In order to remove cell debris, the suspension was centrifuged for 5 minutes (min) at 15000*g*. Next, DNA was pelleted by rigorous mixing of the supernatant with isopropanol followed by centrifugation at 20000*g* for 10 minutes (min). The pellet was washed with 70% (v/v) EtOH and pelleted again by

centrifugation. Then, the supernatant was discarded, and the pellet was dried at RT for 30 min. DNA was rehydrated in H_2O and used for polymerase chain reactions (PCR). Primers used in genotyping reactions are listed in Suppl. Table S3.1. PCR products were generated using primer combinations from Suppl. Table S3.2.

Chlorophyll fluorescence measurements

Chlorophyll fluorescence was determined with pulse amplitude modulation (PAM) fluorometry using a WALZ IMAG K7 MAXI (WALZ, Walz, Effeltrich, Germany). After dark-adaption of at least 20 min, plants were placed onto the imaging platform, and the built-in induction curve program was run with a photosynthetically active radiation intensity of 185 µmol photons m^{-2} s^{-1}. Maximum quantum efficiency of photosystem II F_v/F_m was calculated at the start of each measurement.

Immunoblotting

9 mm diameter leaf stamps were ground in 100 µl protein extraction buffer (200 mM dithiothreitol (DTT, added fresh), 100 mM Tris/HCl pH 8.5, 2% (w/v) sodium dodecyl sulfate (SDS) with plant protease inhibitor (PPI, self-made)) and centrifuged for 10 min at 4°C and 15000 *g*. Then, the supernatant was mixed with 6x SDS loading dye and heated at 80°C for 8 min. Protein extracts were adjusted to total protein and loaded alongside prestained protein ladder (Thermo Scientific, Waltham, USA) on a 10 % SDS gel in SDS running buffer (25 mM Tris, 384 mM glycine, 0.1 % (w/v) SDS) in a Bio-Rad Mini-PROTEAN system (Bio-Rad, Hercules, USA). 120 V was applied until the samples reached the separating gel, after which 150 V was applied until the loading dye front ran off the gel. Proteins were transferred in a wet-blot system (BioRad) onto a PVDF membrane (0.45 µm pore size) for 1 h at 100 V. After transfer, the membrane was blocked in blocking buffer containing tris-buffered saline (50 mM Tris pH 7.6, 150 mM NaCl with 0.05% tween (TBS-T)) and 5% skim milk for 1 h at room temperature (RT). Then, the membrane was

gently shaken overnight at 4°C in α-KEA1(2) (Bolter et al., 2020) diluted 1:1.000 in blocking buffer. The next day, the membrane was washed three times for 10 min in TBS-T, followed by incubation in secondary antibody (goat-anti-rabbit, Proteintech Cat# SA00001-2, Proteintech, Rosemont, USA)) diluted 1:10.000 in blocking buffer at RT for 1 h. Membranes were washed three times for 10 minutes and then incubated for up to 5 min in Bio-Rad clarity ECL substrates (Cat#1705060). Signal was detected using an ImageQuant LAS 4000 (GE Healthcare, Chalfont St Giles, UK) with the precision setting and automatic exposure.

Chlorophyll extraction and determination

For chlorophyll determination, tissue was ground in liquid N_2 and extracted using 80% (v/v) acetone. Samples were kept at -20°C in the dark overnight, interrupted by multiple rounds of rigorous vortexing. Then, tubes were spun down for 15 min at 20000*g* and 4°C, and absorption of the supernatant was measured on a spectrophotometer (Thermo Scientific GENESYS UV-Vis, Thermo Fisher). Chlorophyll amounts were calculated according to (Porra et al., 1989).

Leaf ion determination

Leaf ion levels were determined according to (Höhner et al., 2016). In short, 28-d-old rosettes were harvested and dried out completely. The tissue was ground using a zirconium mortar and pestle to avoid contamination (Stanford Advanced Materials, Lake Forest, USA). 5-10 mg were weighed and completely digested with ultra-pure 70% (v/v) HNO_3 (Merck, Darmstadt, Germany). Samples were diluted 10-fold with deionized water and mixed with internal standards Scandium and Gallium to a final concentration of 50 parts per million (ppm) and 1 ppm, respectively. Then, samples were spotted on silicone-coated blanked quartz carriers and dried. Carriers were measured in a Bruker S4 T-STAR TXRF spectrometer (Bruker, Billerica, United States).

Sterile growth of seedlings on saline media

For complementation assays with salts, seeds were surface-sterilized with two rounds of 70% (v/v) ethanol (EtOH), followed by a round of 95% (v/v) EtOH. Seeds were then pipetted onto autoclaved paper and dried before sowing onto 1/2-strength Murashige & Skoog (1/2 MS, (Murashige and Skoog, 1962) and 0.5 g/L 2-(N-morpholino) ethanesulfonic acid (MES) pH5.7) media containing 0.8% Phyto agar (Duchefa, Haarlem, Netherlands). Plates were stratified for 3 d at 4°C wrapped in tinfoil. Then, plates were placed upright into a plate growth chamber and grown at 150 μmol photons m^{-2} s^{-1} in a 16 h/8 h light regime. After 7 d, seedlings were carefully transferred onto effector plates under sterile conditions. Effector plates were prepared like regular 1/2 MS plates, except salts were added before autoclaving. The pH of the media was controlled again after the addition of salts.

Accession numbers

The WT used was Col-0 (CS70000, ordered from the Arabidopsis Biological Resource Center (ABRC)). Other lines used were *msl2-3* (CS69611, kind gift of E. Haswell, Washington University in St. Louis), *msl2-4* (SALK_058329), *kea1-1* (CS875131), *kea1-2* (CS842660). loss-of-function Double mutants *kea1-1msl2-4* and *kea1-2msl2-3* were created in this work.

3.6 Supplemental Material

Supplemental Tables

Supplemental Table S3.1 List of oligonucleotides used in this study. Binding sites of bolded primers are shown in Fig. 3.1.

Oligonucleotide Name	**Sequence**	**Used in**
HK46 kea1 s1	ccctcaaactcctacaatttctatg	Genotyping
HK32 kea1 as5	gcaattattgcagtaatagccactgc	Genotyping
HK649 msl2 fwd 1	ggtttcgtctggttttcatgagg	Genotyping
HK354 msl2(a) fwd + BamHI	ggatccaaaatggccctttatggtacattgc	Genotyping
HK355 msl2(d)	aacatggtacgtaccactcttcttcc	Genotyping
HK10 Sail LB3	tagcatctgaatttcataaccaatctcgatacac	Genotyping Sail lines
HK366 Salk LBb1.3	attttgccgatttcggaac	Genotyping Salk line
HK69 GABI-LB	cccatttggacgtgaatgt	Genotyping *msl2-3*

Supplemental Table S3.2 Accessions and oligonucleotide combinations used in genotyping PCRs in this study.

Line name:	Stock nr.:	WT PCR primers	WT product size	KO PCR primers	~KO product size
kea1-1	SAIL_586_D02	HK46/HK32	1290	HK46/HK10	400
kea1-2	SAIL_1156_H07	HK46/HK32	1290	HK10/HK32	200
msl2-3	GK-195D11	HK354/HK355	1094	HK69/HK355	600
msl2-4	SALK_058329	HK649/HK355	1656	HK366/HK355	1300

Supplemental Figures

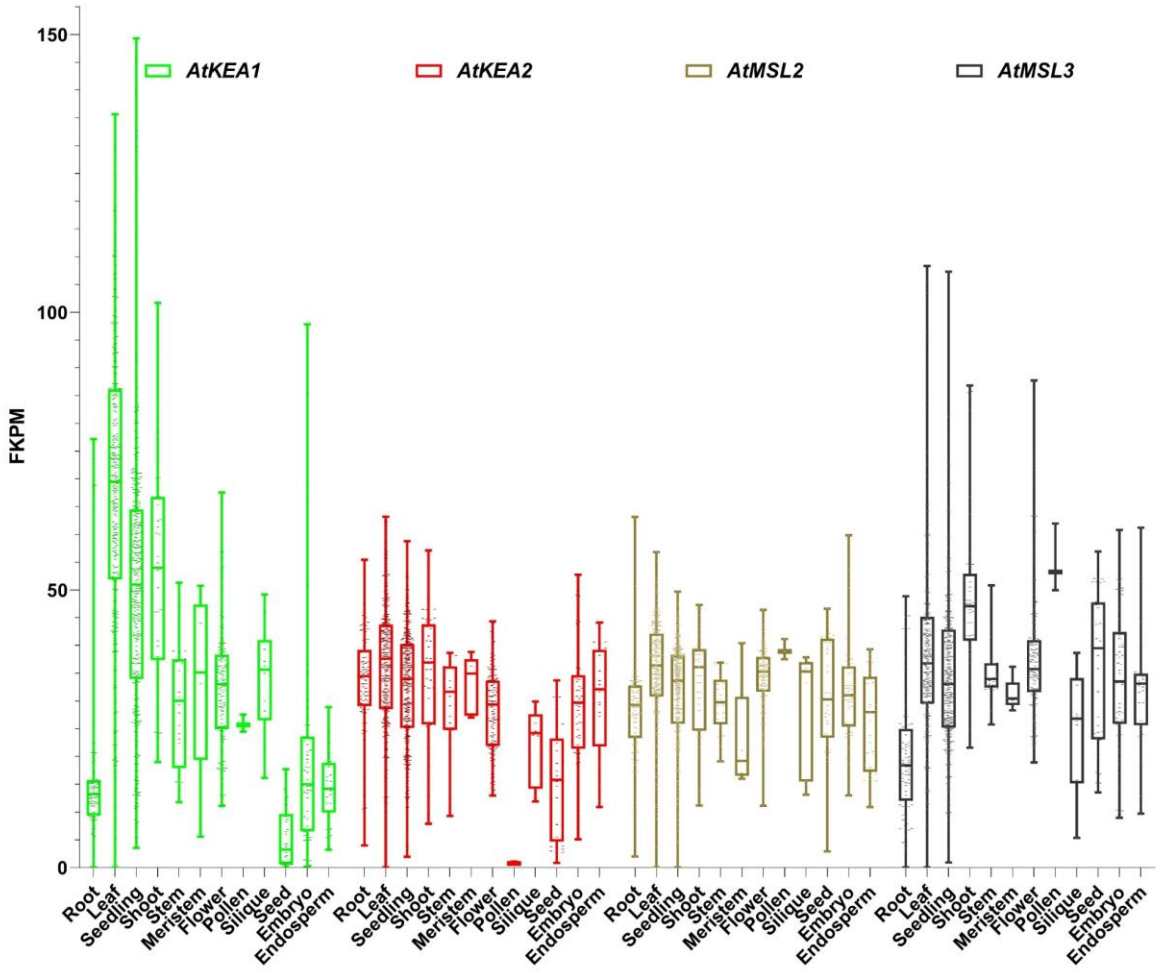

Supplemental Figure S3.1 Tissue-dependent expression profiles of plastid localized members of *KEA* and *MSL* families. Shown are *AtKEA1* (At1g01790, green), *AtKEA2* (At4g00630, red), *AtMSL2* (At5g10490, light brown), and *AtMSL3* (At1g58200, black. Data were taken from (Zhang et al., 2020). Ticks represent individual RNA-seq experiments.

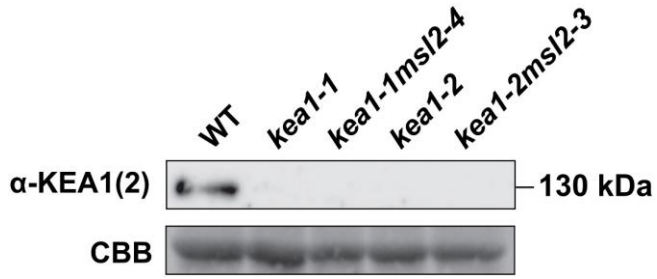

Supplemental Figure S3.2. Immunoblot confirming the absence of KEA1 in *kea1* single and *kea1msl2* loss-of-function double mutants. Total protein of leaf tissue was extracted, ran on an SDS-PAGE, and transferred to a PVDF membrane. The membrane was then blocked and probed with the α-KEA1(2) antibody (Bolter et al., 2020). Commassie brilliant blue (CBB) stained SDS-PAGE is presented as loading control. A representative result of three independent experiments is shown.

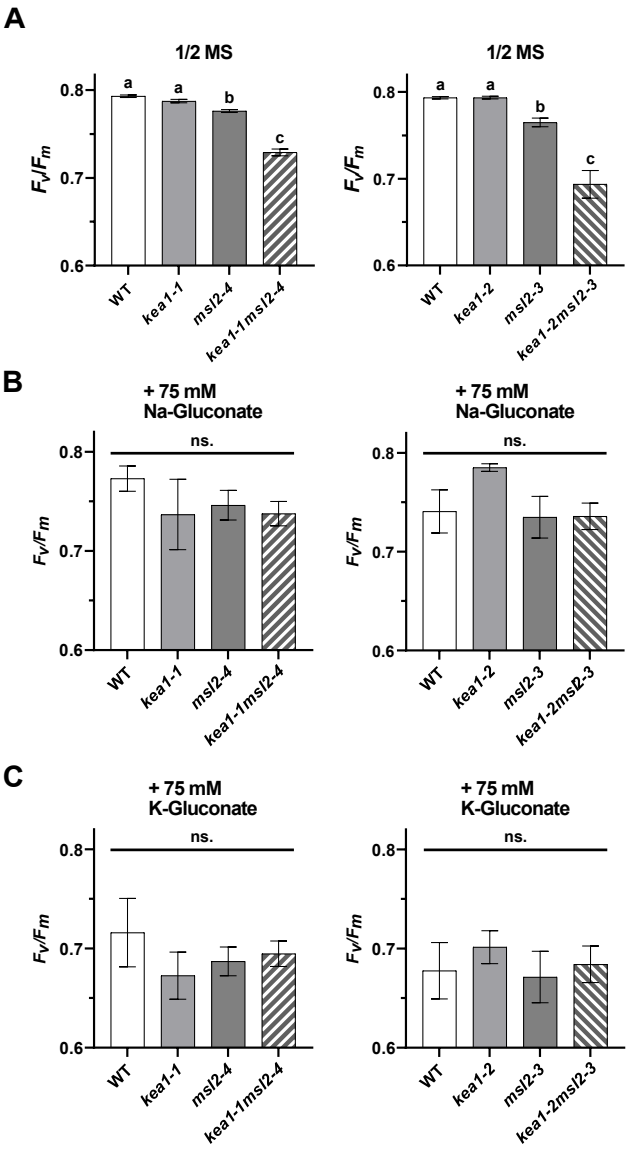

Supplemental Figure S3.3. Recovery of the photosynthetic efficiency of *kea1msl2* loss-of-function double mutants does not require Cl^-. 7-d-old seedlings were transferred to control plates (A, from Fig 3.4D) or plates supplemented with 75 mM Na-gluconate (B) or 75 mM K-Gluconate (C). Values are presented as mean ± SEM, n=9. Different letters indicate different levels of significance (p<0.05) as determined by ANOVA and Tukey's multiple comparisons test. No significance (ns.) between the genotypes was determined in Na-Gluconate or K-Gluconate treatments. Experiment was repeated three times with similar results.

3.7 References

Aranda-Sicilia MN, Aboukila A, Armbruster U, Cagnac O, Schumann T, Kunz HH, Jahns P, Rodriguez-Rosales MP, Sze H, Venema K (2016) Envelope K+/H+ Antiporters AtKEA1 and AtKEA2 Function in Plastid Development. Plant Physiol **172:** 441-449

Baxter I, Ouzzani M, Orcun S, Kennedy B, Jandhyala SS, Salt DE (2007) Purdue Ionomics Information Management System. An integrated functional genomics platform. Plant Physiology **143:** 600-611

Bolter B, Mitterreiter MJ, Schwenkert S, Finkemeier I, Kunz HH (2020) The topology of plastid inner envelope potassium cation efflux antiporter KEA1 provides new insights into its regulatory features. Photosynth Res **145:** 43-54

Booth IR, Louis P (1999) Managing hypoosmotic stress: aquaporins and mechanosensitive channels in Escherichia coli. Curr Opin Microbiol **2:** 166-169

Boyer JS (1982) Plant productivity and environment. Science **218:** 443-448

Codjoe JM, Miller K, Haswell ES (2021) Plant Cell Mechanobiology: Greater Than the Sum of Its Parts. Plant Cell

Cushman JC (2001) Osmoregulation in plants: Implications for agriculture. American Zoologist **41:** 758-769

DeTar RA, Barahimipour R, Manavski N, Schwenkert S, Höhner R, Bölter B, Inaba T, Meurer J, Zoschke R, Kunz H-H (2021) Loss of inner-envelope K+/H+ exchangers impairs plastid rRNA maturation and gene expression. The Plant Cell

Frank J, Happeck R, Meier B, Hoang MTT, Stribny J, Hause G, Ding H, Morsomme P, Baginsky S, Peiter E (2019) Chloroplast-localized BICAT proteins shape stromal calcium signals and are required for efficient photosynthesis. New Phytol **221:** 866-880

Hamilton ES, Schlegel AM, Haswell ES (2015) United in diversity: mechanosensitive ion channels in plants. Annu Rev Plant Biol **66:** 113-137

Haswell ES, Meyerowitz EM (2006) MscS-like proteins control plastid size and shape in Arabidopsis thaliana. Curr Biol **16:** 1-11

Höhner R, Day PM, Zimmermann SE, Lopez LS, Krämer M, Giavalisco P, Correa Galvis V, Armbruster U, Schöttler MA, Jahns P, Krueger S, Kunz H-H (2021) Stromal NADH supplied by PHOSPHOGLYCERATE DEHYDROGENASE3 is crucial for photosynthetic performance. Plant Physiology

Höhner R, Tabatabaei S, Kunz H-H, Fittschen U (2016) A rapid total reflection X-ray fluorescence protocol for micro analyses of ion profiles in Arabidopsis thaliana. Spectrochimica Acta Part B: Atomic Spectroscopy **125:** 159-167

Jensen GS, Haswell ES (2012) Functional analysis of conserved motifs in the mechanosensitive channel homolog MscS-Like2 from Arabidopsis thaliana. PLoS One **7:** e40336

Kalituho L, Beran KC, Jahns P (2007) The transiently generated nonphotochemical quenching of excitation energy in Arabidopsis leaves is modulated by zeaxanthin. Plant Physiol **143:** 1861-1870

Klughammer C, Schreiber U (2008) Complementary PS II quantum yields calculated from simple fluorescence parameters measured by PAM fluorometry and the Saturation Pulse method. PAM application notes **1:** 201-247

Kunz HH, Gierth M, Herdean A, Satoh-Cruz M, Kramer DM, Spetea C, Schroeder JI (2014) Plastidial transporters KEA1, -2, and -3 are essential for chloroplast osmoregulation, integrity, and pH regulation in Arabidopsis. Proc Natl Acad Sci U S A **111:** 7480-7485

Lee JS, Wilson ME, Richardson RA, Haswell ES (2019) Genetic and physical interactions between the organellar mechanosensitive ion channel homologs MSL1, MSL2, and MSL3 reveal a role for inter-organellar communication in plant development. Plant Direct **3:** e00124

Levina N, Totemeyer S, Stokes NR, Louis P, Jones MA, Booth IR (1999) Protection of Escherichia coli cells against extreme turgor by activation of MscS and MscL mechanosensitive channels: identification of genes required for MscS activity. EMBO J **18:** 1730-1737

Lopez-Juez E, Pyke KA (2005) Plastids unleashed: their development and their integration in plant development. International Journal of Developmental Biology **49:** 557-577

Maksaev G, Haswell ES (2012) MscS-Like10 is a stretch-activated ion channel from Arabidopsis thaliana with a preference for anions. Proc Natl Acad Sci U S A **109:** 19015-19020

Murashige T, Skoog F (1962) A Revised Medium for Rapid Growth and Bio Assays with Tobacco Tissue Cultures. Physiologia Plantarum **15:** 473-497

Porra RJ, Thompson WA, Kriedemann PE (1989) Determination of accurate extinction coefficients and simultaneous equations for assaying chlorophylls a and b extracted with four different solvents: verification of the concentration of chlorophyll standards by atomic absorption spectroscopy. Biochimica et Biophysica Acta (BBA) - Bioenergetics **975:** 384-394

Szabo I, Spetea C (2017) Impact of the ion transportome of chloroplasts on the optimization of photosynthesis. J Exp Bot **68:** 3115-3128

Veley KM, Marshburn S, Clure CE, Haswell ES (2012) Mechanosensitive channels protect plastids from hypoosmotic stress during normal plant growth. Curr Biol **22:** 408-413

Verslues PE, Sharma S (2010) Proline metabolism and its implications for plant-environment interaction. Arabidopsis Book **8:** e0140

Wilson ME, Basu MR, Bhaskara GB, Verslues PE, Haswell ES (2014) Plastid osmotic stress activates cellular stress responses in Arabidopsis. Plant Physiol **165:** 119-128

Wilson ME, Jensen GS, Haswell ES (2011) Two mechanosensitive channel homologs influence division ring placement in Arabidopsis chloroplasts. Plant Cell **23:** 2939-2949

Yancey PH (2005) Organic osmolytes as compatible, metabolic and counteracting cytoprotectants in high osmolarity and other stresses. Journal of Experimental Biology **208:** 2819-2830

Zhang H, Zhang F, Yu Y, Feng L, Jia J, Liu B, Li B, Guo H, Zhai J (2020) A Comprehensive Online Database for Exploring approximately 20,000 Public Arabidopsis RNA-Seq Libraries. Mol Plant **13:** 1231-1233

Zhang YX, Daday C, Gu RX, Cox CD, Martinac B, de Groot BL, Walz T (2021) Visualization of the mechanosensitive ion channel MscS under membrane tension. Nature **590:** 509-514

CHAPTER FOUR: THE ION TRANSPORT PROTEIN NHD1 IS CRITICAL FOR PLANT ACCLIMATION TO FLUCTUATING LIGHT

This chapter was formatted in a style suitable for submission in *Plant Physiology* with co-authors Dunia Velazquez, Bettina Bölter, Ute Armbruster, David M Kramer, and Hans-Henning.

4.1 Abstract

Under natural light, plants need to precisely adjust photosynthetic energy absorption and dissipation mechanisms to maximize growth. In *Arabidopsis thaliana*, several ion transport proteins embedded in the thylakoid membrane aid in such a function. VCCN1 and CLCe, for example, are responsible for thylakoid Cl^- uptake in the light to balance the positively charged lumen. Simultaneously, H^+-export is realized in exchange with K^+ ions by the carrier KEA3. Altogether, transporters are crucial for efficient photosynthesis under fluctuating light (FL). Additional mechanisms of K^+-transport in the thylakoid membrane are expected. Here, we present evidence for the localization of AtNHD1 in thylakoid membranes using fluorescence microscopy and immunoblotting studies. NHD1, as a member of the NHaD family, had been linked to $K^+(Na^+):H^+$ antiport previously. We show that heterologously expressed NHD1 is capable of complementing K^+-defective *Escherichia coli* mutants. Therefore, K^+-transport via NHD1 might be linked to proton motive force (*pmf*) regulation in dynamic light. Indeed, *nhd1* loss-of-function mutants show severe growth deficits when exposed to FL. Chlorophyll fluorescence measurements reveal progressing photosystem II (PS II) damage and decreased transient non-photochemical quenching (NPQ) after continued exposure. Complementary experiments in a dynamic environmental photosynthetic imaging (DEPI) chamber show additional NPQ phenotypes in *nhd1* mutants. After the shift to FL, seedlings display increased

NPQ component qE but interestingly reduced photoinhibition component qI. This study settles the previous localization uncertainty of NHD1 and thereby adds another ion transport protein to the thylakoid ion transportome capable of modifying the *pmf* and impacting energy conversion.

4.2 Introduction

On the largest scale imaginable, plants in temperate climates seem to only adapt throughout the different seasons. Spring annuals, for example, need to germinate, grow, and flower over the course of the warmer months (Preston and Sandve, 2013). On the other hand, deciduous trees shed their leaves over the fall and winter months and grow new ones the following spring (Taiz et al., 2015). While these changes appear over months, much faster adaptations take place inside of the photosynthetic apparatus. This is because the quality and quantity of light used to drive the electron transport chain (ETC) can change drastically within fractions of seconds (Mullineaux et al., 1994). Reasons for such a change can be cloud movement in front of the sun, shading of the canopy, or movement of leaves in the wind. Under these dynamic light conditions, irradiance can change up to 100-fold, creating so-called sunflecks (Pearcy, 1990; Reinhardt et al., 2010). Such is the reality for most outdoor plants. Therefore, understanding the plants' molecular adjustment mechanisms is highly important to maximize crop yield (Kaiser et al., 2018).

On one side, plants will try to use every photon available to drive photosynthetic electron transport (PET) (Demmig-Adams et al., 2012). On the other side, a surplus in excitation will result in reactive oxygen species (ROS) formation. Accordingly, plants need to precisely fine-tune responses to fluctuating light (FL) conditions to minimize photodamage, *i.e.*, damage in their photosynthetic apparatus. Under high-light stress, accumulation of ROS can lead to oxidative photodamage and, eventually, photoinhibition (Demmig-Adams et al., 2012). Indeed,

plants have evolved mechanisms to adapt to challenging conditions and maintain ideal performance.

A prevalent short-term mechanism for the dissipation of excess energy is called non-photochemical quenching (NPQ). The primary and fastest component of NPQ is feedback-deexcitation, also called high-energy state quenching qE (Muller et al., 2001; Li et al., 2002), activated by a high concentration of H^+ in the lumen. Besides a low lumenal pH, qE requires the action of VIOLAXANTHIN DE-EPOXIDASE (VDE) and involves protonation of photosystem II (PS II) subunit S (PsbS) (Pascal et al., 2005). VDE realizes the conversion of violaxanthin to zeaxanthin in the xanthophyll cycle, which acts as an alternative acceptor site for excitons. Protonation of PsbS induces conformational changes in LHCII, leading to increased rates of quenching and dissipation as heat (Gjindali et al., 2021). These quenching mechanisms take place on a timescale of seconds to minutes. Meanwhile, NPQ relaxation can take much longer and has been identified as a potentially critical target in optimizing photosynthesis (Zhu et al., 2004). After a switch from high to low light, the sluggish qE turnoff kinetics lower photosynthetic efficiency. Indeed, biotechnological approaches to improve NPQ kinetics showed promising results towards boosting crop yield in the field (Kromdijk et al., 2016).

An exciting target for protein modifications that result in enhanced photosynthetic efficiency are ion transport proteins. For example, the thylakoid-localized K^+-EFFLUX ANTIPORTER3 (KEA3) was implicated in NPQ relaxation (Armbruster et al., 2014). Ion transporters and channels can modulate the proton motive force (*pmf*), which drives ATP synthesis at the ATP synthase (Armbruster et al., 2017). *pmf* consists primarily of a ΔpH component and the electric field component $\Delta\Psi$ (Mitchell, 1966), generated over the thylakoid membrane. KEA3 is responsible for the electroneutral export of H^+, which provides a H^+ valve

lowering ΔpH to allow for faster NPQ relaxation (Armbruster et al., 2014). The simultaneous import of K^+ into the lumen supports *pmf* and ATP synthesis, which can also be driven by ΔΨ (Cruz et al., 2001). Loss-of-function *kea3* plants display slight growth deficits when grown under fluctuating light conditions, showcasing the importance of this mechanism on plant health (Armbruster et al., 2016).

In addition, thylakoid cation and anion channels have been implicated in charge balancing for the light-driven H^+ transport into the lumen (Schonknecht et al., 1988; Tester and Blatt, 1989). Several gene candidates have been investigated in this context in the last years. *Arabidopsis* mutants overexpressing the thylakoid-localized VOLTAGE-DEPENDENT CHLORIDE CHANNEL1 (VCCN1) display altered *pmf* partitioning, supposedly due to dissipation of ΔΨ (Herdean et al., 2016). The authors argued that the increased influx of Cl^- anions into the lumen was involved in this process. Accordingly, *vccn1* loss-of-function mutants displayed a lower NPQ after transfer to high light, consistent with a smaller ΔpH portion of the *pmf* (Herdean et al., 2016). In addition, the Cl^- CHANNEL/TRANSPORTER (CLCe) may work in maintaining Cl^- homeostasis and re-establishing ΔpH after a shift to high light (Herdean et al., 2016; Dukic et al., 2019). However, the overall contribution of CLCe seems to be minor or not well understood (Li et al., 2021).

In addition to the VCCN1-mediated uptake of Cl^- anions, a countermovement of K^+ cations from the lumen can likewise balance H^+ uptake into the lumen and similarly fine-tune photosynthesis (Pottosin and Shabala, 2016). Indeed, K^+-movement across the thylakoid membrane has been measured independently in the past (Hind et al., 1974; Tester and Blatt, 1989). The TWO-PORE-DOMAIN K^+ CHANNEL3 (TPK3) was suggested to fulfill the long-sought K^+-conductance (Carraretto et al., 2013). In immunoblotting and fluorescence microscopy

studies, TPK3 was found to localize to the thylakoid membrane. Additionally, photosynthetic measurements obtained from RNAi knock-down lines indicated a higher $\Delta\Psi$ fraction and lowered NPQ (Carraretto et al., 2013), reminiscent of *vccn1* loss-of-function mutants. However, extensive localization studies using immunoblotting, fluorescence microscopy, and chloroplast import studies performed in our group and others could not confirm TPK3 localization to chloroplast or thylakoids (Höhner et al., 2019). Furthermore, loss of function *tpk3* T-DNA insertion lines did not replicate findings from the previously analyzed *TPK3RNAi* line concerning the impact of TPK3 on photosynthesis (Höhner et al., 2019). In summary, our results agree with a previously reported localization of TPK3 in vacuoles (Voelker et al., 2006) which was further confirmed by two other studies (Jaslan et al., 2019; Tang et al., 2020). It follows that the molecular identity of the thylakoid-localized K^+-transport protein remains unknown.

To reveal a candidate K^+-transport protein in thylakoid membranes, we pursued in-depth studies on the previously published inner envelope Na^+/H^+ carrier. We found evidence for a thylakoid localization of *At*NHD1, a member of the NHaD family. Like other carrier proteins of this family, NHD1 complemented K^+-defective *Escherichia coli* mutants. Additionally, we were able to confirm the presence of NHD1 in thylakoids of different organisms employing different microscopy and biochemical approaches. Moreover, loss-of-function *nhd1* mutants display a severe growth deficit and progressing PS II damage when grown under fluctuating light conditions. Interestingly, the additional loss of KEA3 did not seem to impact plant performance in the *nhd1* background indicating a possible overlap in function between the two thylakoid-localized K^+-transporters or very distinct protein regulation. This functional overlap needs to be dissected in the future.

4.3 Results

NHD1 is K^+-permeable in a heterologous system.

Highly similar proteins compared to NHD1 are present in *Physcomitrella patens*, *Pp*NHAD1, and *Pp*NHAD2, with 84.5% and 85% protein similarity, respectively. Members of the NHaD family are permeable to both Na^+ and K^+ (Barrero-Gil et al., 2007; Ruiz-Lau et al., 2017). Truncated versions of the *Pp*NHAD1/2 proteins lacking the putative chloroplast transit peptide complemented Na^+- and K^+-transport defective *E. coli* mutants EP432 (*melBLid, nhaA1, nhaB1, lacZY, thr1* (Pinner et al., 1993)) and TKW4205 (*thi rha lacZ nagA recA Sr::Tn10 kdpABC5 trkA405 Kup1* (Schleyer and Bakker, 1993)), respectively. Furthermore, K^+-substrate specificity was predominant at a low pH, pointing towards some form of proton dependency in this system (Ruiz-Lau et al., 2017).

In order to study the possible substrates of NHD1, we performed rescue assays on the K^+-defective *E. coli* strain LB2003 (F-, *thi*, *lacz*, *gal*, *rha*, Δ*kdpFABC5*, *trkD1*, Δ*trkA*, (Schlosser et al., 1995)). The same mutant strain was successfully employed recently to confirm K^+-transport activities for all six *Arabidopsis* members of the KEA carrier family (Tsujii et al., 2019). Consequently, we included the thylakoid localized KEA3 carrier as a positive control, which we cloned side by side using Gibson assembly (Gibson et al., 2009). Since uncontrolled expression of ion transport proteins can be toxic to bacterial cells (Wilson and Haswell, 2012), we employed pBAD expression vectors that allow for tight expression induction by feeding the sugar arabinose. At the same time, glucose can repress the expression (Guzman et al., 1995).

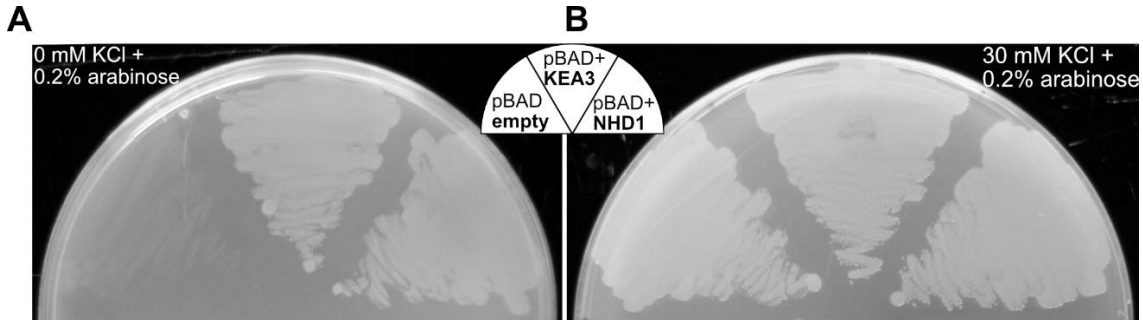

Figure 4.1 Complementation of the K^+-transport defective *E. coli* mutant LB2003 with *At*NHD1 cDNA. LB2003 strains transformed with either the empty pBAD vector, or *At*NHD1 or *At*KEA3 cDNA were washed, and adjusted to an OD600 of 0.125. 5 ul of each strain were streaked onto selective plates. A) Agar plates with minimal medium containing 0.2% arabinose without supplemented KCl. B) Same plate recipe but supplemented with 30 mM KCl. Pictures were taken after 24h at 37°C.

As shown in the past, *E. coli* mutant strain LB2003 displayed growth deficiencies on minimal medium without supplemented K^+ transformed with empty vector only (Fig 4.1A). Confirming results from Tsujii et al., 2019, KEA3 cDNA-transformed cells showed robust growth recovery on low K^+. Intriguingly, the NHD1 cDNA construct-transformed cells grew well without K^+ addition, similar to the KEA3 control (Fig. 4.1A). At the same time, the growth of empty vector-transformed strain was indistinguishable from KEA3 and NHD1 on plates supplemented with 30 mM KCl (Fig. 4.1B). Additionally, we were able to confirm plate growth with overnight growth curves in a liquid system. Here, the recovery of NHD1-transformed cells was more robust than that of KEA3, and cells reached the exponential phase faster than the KEA3 transformed strain (Suppl. Fig. S4.1). In conclusion, the growth recovery phenotypes indicate that *At*NHD1 also possesses K^+-permeability, as found for KEA3.

Localization of AtNHD1 to thylakoid membranes in N. benthamiana and A. thaliana

Next up, we revisited the suborganellar localization for AtNHD1. Previous publications claiming a chloroplast envelope membrane localization relied only on microscopy approaches (Cosentino et al., 2010; Muller et al., 2014) Interestingly, proteomics studies from The Plant

Proteome Database (PPDB, Cornell, (Sun et al., 2009)), in addition to a study analyzing thylakoid sub-compartment fractions, indicated NHD1 could also or exclusively be present in the thylakoid membrane (Tomizioli et al., 2014). To follow up on the proteomics studies, we chose different approaches: First, we generated stable overexpressor (ox) lines of NHD1-YFP (yellow fluorescent protein) constructs to study the localization of NHD1 in *A. thaliana*. Since wild-type (WT) transformations failed, we transformed flowers of *rdr6-11* mutants to enhance transgene expression of our construct. Loss-of-function mutants of RNA-DEPENDENT POLYMERASE6 (RDR6) are deficient in post-transcriptional RNA silencing (Peragine et al., 2004) and have been employed successfully in the past (Liu et al., 2020). Additionally, we investigated the localization through transiently expressing NHD1-YFP constructs in *Nicotiana benthamiana* leaves. Due to the complexity of studying suborganellar localization using confocal laser scanning microscopy (CLSM) images, we employed a variety of established chloroplast membrane controls in co-injections:

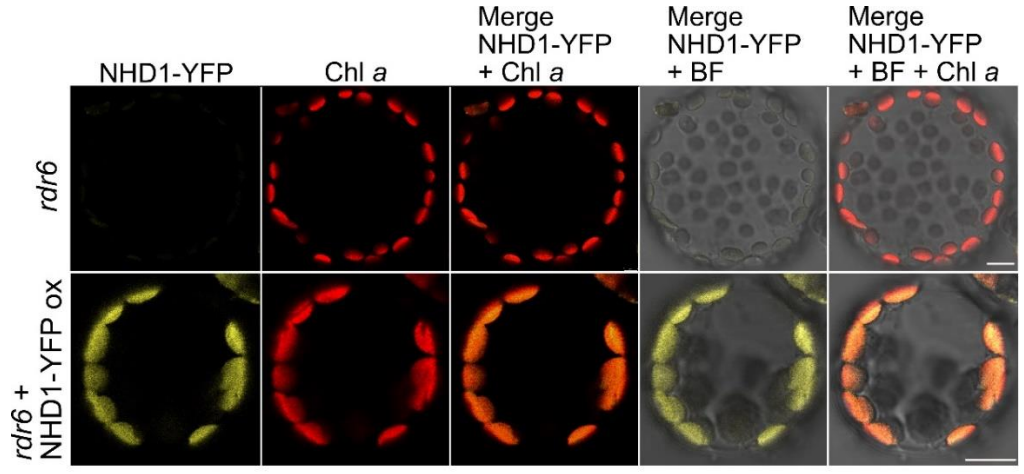

Figure 4.2 Protoplasts of *rdr*6 loss-of-function and stable *rdr6*+NHD1-YFP ox lines. Protoplasts of *rdr6* loss-of-function mutants *rdr6*+NHD1-YFP overexpressor were isolated and imaged with confocal microscopy at 100x magnification. Chl a = Chlorophyll *a* autofluorescence, BF= bright field. Scale bars are 5 µm.

TRANSLOCON AT THE INNER ENVELOPE MEMBRANE OF CHLOROPLASTS40 (TIC40)-RFP (red fluorescent protein) fusions in the inner chloroplast envelope membrane (Stahl et al., 1999), and CALCIUM SENSING RECEPTOR (CAS)-RFP fusions (Vainonen et al., 2008; Weinl et al., 2008), as well as chlorophyll (Chl) *a* autofluorescence as thylakoid controls. In order to minimize background signal, we isolated protoplasts of infiltrated leaves and subjected the protoplasts to in-depth CLSM studies.

In the *A. thaliana rdr6* background, as expected, no unspecific YFP signal or background noise could be detected. However, in stably transformed *rdr6*+NHD1-YFP overexpressors, YFP signal was easily detectable. Furthermore, merged images show the overlap between Chl *a* fluorescence and YFP, indicating co-localization of the two signals (Fig. 4.2). Confirming our initial results, we made similar observations in isolated protoplasts of transiently transformed *N. benthamiana* leaves. Here, co-injected controls TIC40-RFP and CAS-RFP provided further insights into the localization of NHD1. While protoplasts from uninfiltrated tissue did not give an unspecific signal in the RFP or YFP channels, NHD1-YFP localized to spots colocalizing with Chl *a* signal (Suppl. Fig. S4.2A). In addition, TIC40-RFP formed round signals around Chl *a* fluorescence, indicative of localization in the chloroplast envelope. In contrast to the TIC40-RFP signal, NHD1-YFP again localized to locations inside the circular chloroplast boundary (Fig. 4.3, Suppl. Fig. S4.2B). CAS-RFP, on the other hand, showed similar, spot-like localization overlapping with Chl *a* fluorescence. Moreover, RFP and YFP signals seem to overlap in a merged image, indicating a similar sub-organellar localization (Fig. 4.3). These results suggest that NHD1 localizes to the thylakoid membrane. Nevertheless, microscopy studies employing protein-fluorophore fusions cannot exclude a dual-localization of proteins.

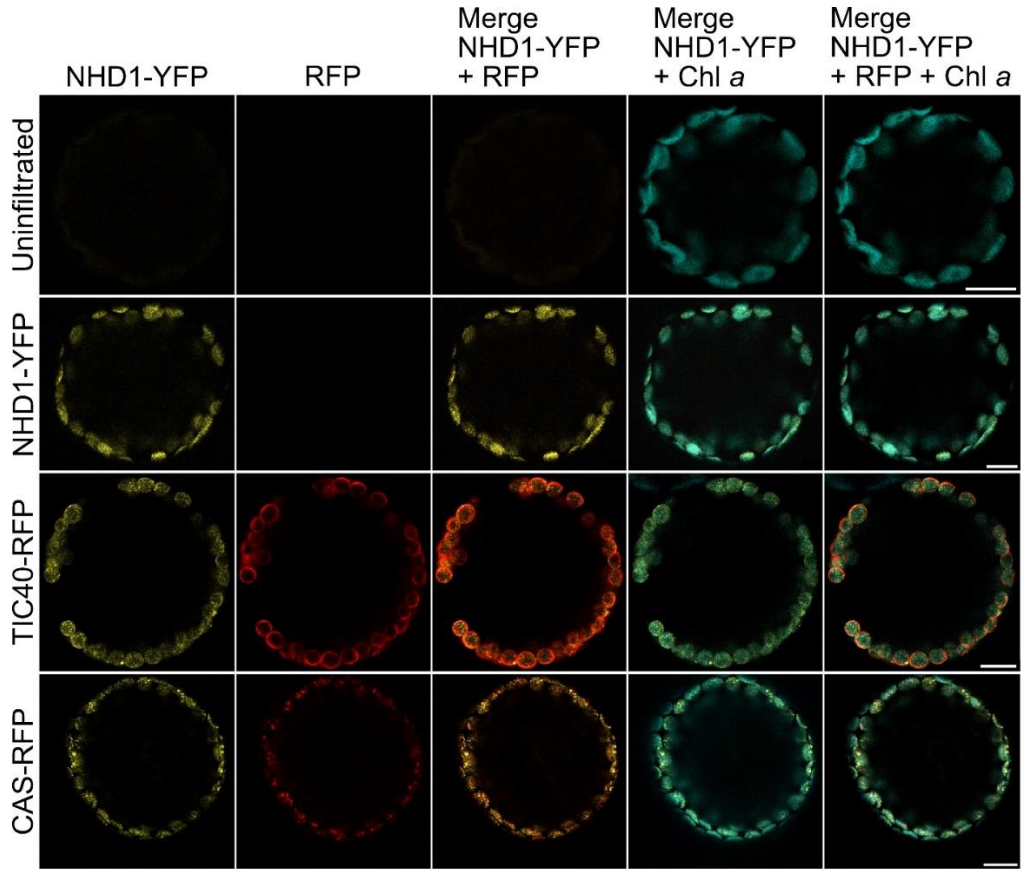

Figure 4.3 Isolated protoplasts of transiently transformed *N. benthamiana* leaves. Aside from uninfiltrated leaves, all other leaves were co-infiltrated with the NHD1-YFP construct. YFP, RFP, and merged channels are shown of each image. Scale bars are 5 µm.

Subfractionation of chloroplasts supports an exclusive localization of NHD1 in thylakoids

In addition to CSLM studies, we wanted to study the suborganellar localization of NHD1-YFP using immunoblotting of transiently transformed tissues. To that end, we isolated chloroplasts and subjected these to subfractionation using sucrose gradients (Bolter et al., 2020). Subsequently, we employed an α-GFP antibody (Roche, Switzerland) to detect YFP attached to NHD1. To probe the purity of the collected membrane fractions, we included controls probing against KEA1/2 in the inner envelope and LIGHT-HARVESTING CHLOROPHYLL A/B PROTEINS (LHCP) in the thylakoid membrane. As expected and in line with previous experiments, the α-KEA1/(2) antibody gave distinct signal only in the envelope fraction (Fig.

4.4) (Bolter et al., 2020; Völkner et al., 2021) while probing with the α-LHCP antibody confirmed the purity of our thylakoid fractions. Nevertheless, weak LHCP signal was also detected in the envelope fraction of both uninfiltrated and infiltrated tissue. The α-GFP antibody gave no signal in the uninfiltrated tissue. Interestingly, on top of a band in the fraction for the entire chloroplast, we detected a specific signal with the α-GFP antibody in the thylakoid membrane, but not in the envelope or stroma fractions (Fig. 4.4).

In conclusion, our CSLM studies and immunoblotting of chloroplast subfractions strongly suggest a thylakoid membrane localization for *At*NHD1.

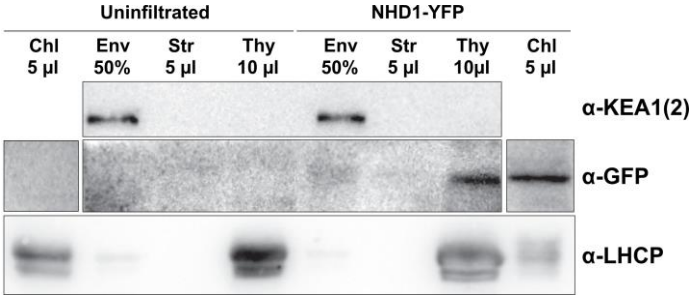

Figure 4.4 Immunoblotting of subfractioned chloroplasts. Chloroplasts of transiently transformed *N. benthamiana* were isolated and subfractioned. Samples for entire chloroplast (Chl), envelope membranes (Env), stroma (Str), and thylakoid (Thy) were loaded, adjusted to total protein. Chloroplast lanes were cut off before exposure to adjust for differing intensity of signal.

Isolation of new nhd1 loss-of-function mutant alleles

Thus far, previous studies on *nhd1* loss-of-function lines have only been realized in one T-DNA line thus far: *nhd1-1* (SALK008491) (Kunz et al., 2014; Muller et al., 2014). However, a follow-up study in our lab found that *nhd1-1* carries a 16 kilobase pair (kb) deletion starting in the 8th exon of *NHD1* (Fig. 4.5A, Lopez et al., in prep.). This deletion spans six reading frames in total, including that of chloroplast localized protein PHOSPHOGLYCERATE DEHYDROGENASE3 (PGDH3). Recently, PGDH3 was shown to be critical in balancing

chloroplast redox state and maintaining proper photosystem I (PS I) acceptor side oxidation. Consequently, *pgdh3* loss-of-function mutants are impaired in photosynthetic processes (Höhner et al., 2021). Therefore, photosynthetic defects in homozygous *nhd1-1* lines reported earlier (Muller et al., 2014) cannot be solely accredited to loss-of-function of NHD1 but a cumulative loss of five genes on chromosome 3, most importantly *PGDH3*. Thankfully, efforts at the Max-Planck Institute in Cologne made an independent *nhd1* loss-of-function line available to us (kindly donated by Imre E. Somssich). Subsequent allele-designated genotyping and backcrossing in our lab confirmed an insertion in exon four (Fig. 4.5A-B) that segregated like a recessive mutation. Under normal medium-day (12 h light/12 h darkness) conditions, the homozygous *nhd1-MPI* individuals were indistinguishable from WT plants (Fig. 4.5C).

Next up, we were interested in studying the possible functional link between NHD1 and KEA3 as our results indicate that both are transport proteins localized to the thylakoid membrane and may function in K^+-transport. *kea3* loss-of-function mutants have been extensively studied due to their well-characterized response to fluctuating light (Armbruster et al., 2014; Kunz et al., 2014; Armbruster et al., 2016; Correa Galvis et al., 2020; Uflewski et al., 2021). Due to the lack of lumenal proton export in *kea3*, mutants show prolonged transient NPQ and delayed NPQ deactivation after light exposure. Therefore, we crossed *nhd1-MPI* with *kea3-1* mutants and isolated homozygous F_2 individuals for propagation. Genotyping confirmed the loss of *nhd1* and *kea3* in loss-of-function single and double mutants (Fig. 4.5A). Under control conditions, mutants did not display a visible phenotype, appearing WT-like in size and maximum efficiency of PS II (F_v/F_m) values (Fig. 4.5C). The elevated transient NPQ phenotype of KEA3 loss was visible in both *kea3* and *kea3nhd1-MPI* mutants (Fig. 4.5D).

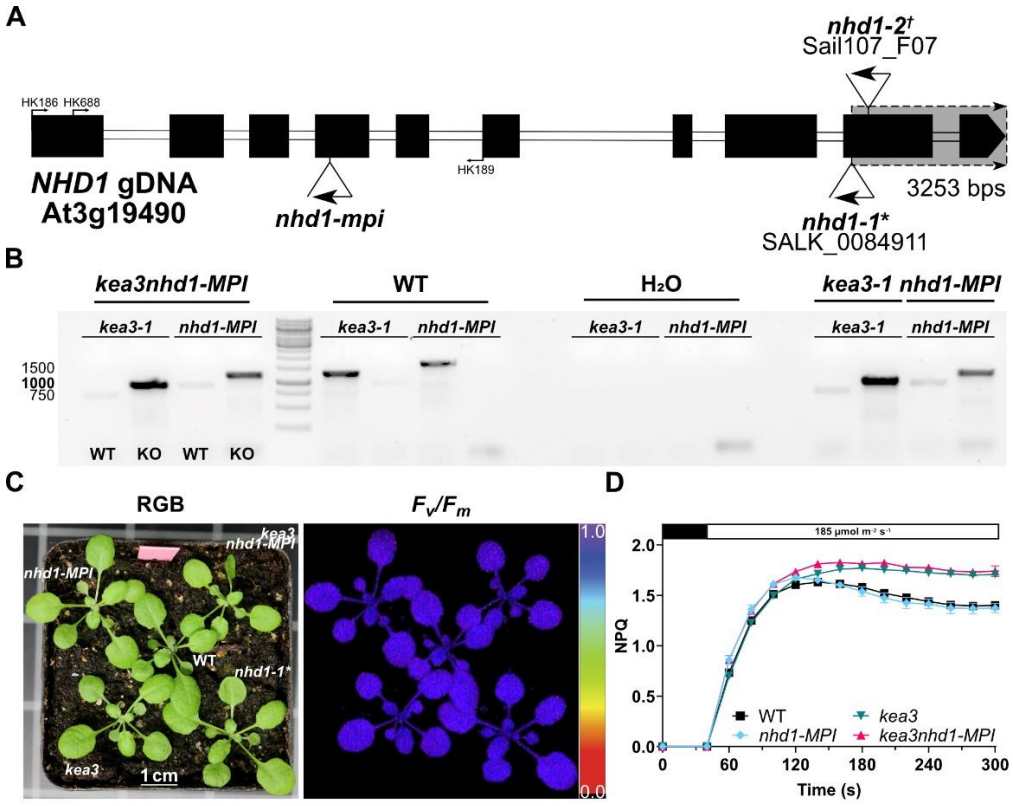

Figure 4.5 Isolation of a novel *nhd1* loss-of-function allele reveals no phenotype under control conditions. A) Locus information of *AtNHD1* (At3g19490). Black boxes represent exons and lines represent introns. Shown are left borders of T-DNA insertions used or mentioned in this work. **nhd1-1* is a large deletion line, beginning at the indicated T-DNA insertion and shaded box, spanning 16 kb in total. †*nhd1-2* is homozygous lethal (Muller et al., 2014). B) Genotyping of *nhd1-MPI* and *kea3nhd1-MPI* mutants. The indicated pipetting scheme from the *kea3nhd1-MPI* line continues through the entire gel. Thermo Fischer Gene Ruler 1kb ladder was used. Ghost bands appear in the double as well as in single mutants, which indicates contamination in the DNA C) *nhd1-MPI* and *kea3nhd1-MPI* do not display growth penalties or PS II damage (F_v/F_m) under control conditions. D) NPQ kinetics of 21-d-old plants. The transient NPQ phenotype is visible under control conditions in *kea3* and *kea3nhd1*, while *nhd1* has WT-like NPQ. Values are presented as mean ± SEM, *n*=6.

NHD1 is required for photoacclimation to fluctuating light conditions

In order to study fluctuating light responses in *nhd1* mutants, we built a commercially available 2000 W LED panel into a Percival growth chamber. Plants were grown at 50 µmol photons m^{-2} s^{-1} in a 12 h light/12 h darkness cycle. The LED panel was controlled by an Arduino microcontroller which activates every five minutes (min) during the light cycle to illuminate the plants with an additional 1000 µmol photons m^{-2} s^{-1} for one min (Schneider et al., 2019). Control

plants were grown in the same Percival chamber on a higher shelf so that growth conditions besides the fluctuating light were comparable. After growing seedlings for one week in control (C) light, seedlings were transplanted, combining all genotypes into the same pot and split into C and fluctuating light (FL) groups. We measured the plants twice per week for two weeks to study photosynthetic fluorescence parameters using pulse amplitude modulation (PAM) fluorometry (WALZ, MAXI IMAGING-PAM Walz, Effeltrich, Germany).

PAM measurements record fluorescence emitted from chlorophyll molecules located in closed PS II reaction centers after excitation. After a dark incubation of at least 15 min, all reaction centers of healthy, unstressed plants are open. In addition, no ΔpH and thus NPQ is present at this timepoint. A saturating light pulse allows measuring the maximum quantum efficiency of PS II, F_v/F_m, which can reach values of up to 0.83 in healthy plants (Bjorkman and Demmig, 1987). Under control light, none of the phenotypes recorded any changes in growth or F_v/F_m over 14 days of treatment (Fig. 4.6A, solid lines). In stark contrast, all genotypes recorded a substantial drop in F_v/F_m after four days of fluctuating light conditions. Interestingly, while the WT and *kea3* mutants displayed an F_v/F_m of ~0.7, *nhd1-MPI* and *kea3nhd1-MPI* showed a more pronounced drop in PS II capacity. All genotypes acclimated to the conditions to some degree and displayed higher F_v/F_m values after seven days of treatment.

Strikingly, the two mutant lines lacking NHD1 never caught up to WT values, and all showed significantly lower F_v/F_m than control plants after 14 days of treatment (Fig. 4.6B). In line with this observation, plant growth was heavily affected in *nhd1-MPI* single and double mutants (Fig. 4.6D). Furthermore, it seems as though the additional loss of *nhd1-MPI* in a *kea3* background overwrote the *kea3* phenotype. The dominance of the loss NHD1 of under continued fluctuating light became apparent not only in lowered F_v/F_m values of plants under FL but also in

NPQ kinetics (Fig. 4.6C). Here, *kea3nhd1-MPI* mutants did not show the characteristic prolonged transient NPQ, which has been reported before for *kea3* and is visible under control light (Fig. 4.5D). *kea3nhd1-MPI* resemble *nhd1-MPI* mutants with lowered NPQ after illumination.

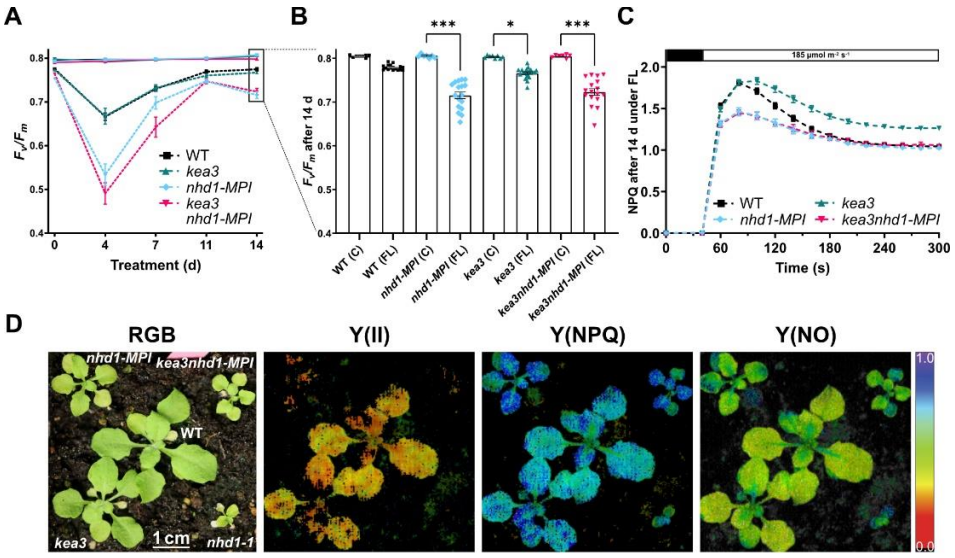

Figure 4.6 Chlorophyll fluorescence parameters under fluctuating light conditions. A) F_v/F_m was measured twice weekly after start of treatment. Dotted and solid lines refer to plants grown under fluctuating or control light conditions, respectively. B) Plot of F_v/F_m values after 14 d of treatment under control (C) or fluctuating light (FL) conditions. Statistical significance was tested using analysis of variance followed by Tukey's multiple comparisons test (*$p < 0.05$, ***$p < 0.001$). C) NPQ of FL-treated plants at day 14 of treatment. Shown in all graphs is mean ± SEM. At day 0, only 1 representative value was recorded, after which $n = 7/15$, for C/FL, respectively. D) RBG image and false color panel of a representative pot. Shown are quantum yields in PS II of: photosynthetic energy conversion (Y(II)), regulated non-photochemical energy loss (Y(NPQ)), and non-regulated non-photochemical energy loss (Y(NO)) at the 80s time point from Fig. 4.6C. *Even though *nhd1-1* was included in the pot, it was not included in data evaluations due to genetic complexities discussed earlier, and is focus of Lopez et al., in prep.

Quantum yields (Y) of PS II can be broken down into the individual parameters Y(II), Y(NPQ), and Y(NO). Y(II) describes the quantum yield of photochemical energy conversion in PS II, equivalent to the electron transfer rate (ETR). At the same time, Y(NPQ) and Y(NO) depict the quantum yields of regulated and unregulated non-photochemical energy loss in PS II, respectively. In sum, these values will equal 1 (Kramer et al., 2004; Klughammer and Schreiber,

2008). Loss-of-function mutants lacking NHD1 appear to be deficient in initiating photosynthetic energy conversion in PS II (Y(II)) after continued FL treatment, as the false-color images only show black spots in place of leaves (Fig. 4.6D). Accordingly, the regulated (Y(NPQ) but especially non-regulated (Y(NO)) energy loss appeared to be higher compared to WT or *kea3*.

Dynamic measurements reveal accumulation of photosynthetic defects

The ability of plants to modulate *pmf* is crucial for proper photosynthesis in plants under dynamic light conditions. Using the dynamic environmental photosynthetic imaging (DEPI) platform (Cruz et al., 2016), this has recently been demonstrated, among others, in loss-of-function mutants *kea3* and *vccn1* (Höhner et al., 2019). DEPI successfully reveals phenotypes of mutants defective in fluctuating light acclimation due to continuous monitoring of photosynthetic performance under dynamic conditions (Dutta et al., 2017). In an earlier study, we were able to show that *vccn1* mutants showed decreased capability of induction of qE/NPQ during higher light intensities (Höhner et al., 2019). These results were confirmed in a self-made fluctuating light imitation growth rack (Schneider et al., 2019).

In order to study the effects of the loss of *nhd1* in a DEPI chamber, we sent *nhd1-MPI* and F_1 seeds of an *nhd1-1nhd1-2* mutant cross to MSU. The *nhd1-1nhd1-2* line is heterozygous for the 16 kb deletion of *nhd1-1* but has lost *NHD1* entirely (Muller et al., 2014). Although this is not an ideal mutant allele, it was the closest independent line available at the time since *nhd1-2* is homozygous lethal (Fig. 4.5A, (Muller et al., 2014)). When exposed to constant light of 150 µmoles m^{-2} s^{-1}, the mutants did not differ from WT, indicated by black-colored bars. However, under sinusoidal or sinusoidal plus superimposed high light fluctuations, *nhd1* mutant lines, but not *kea3*, show a drop in F_v/F_m (Suppl. Fig. S4.3A).

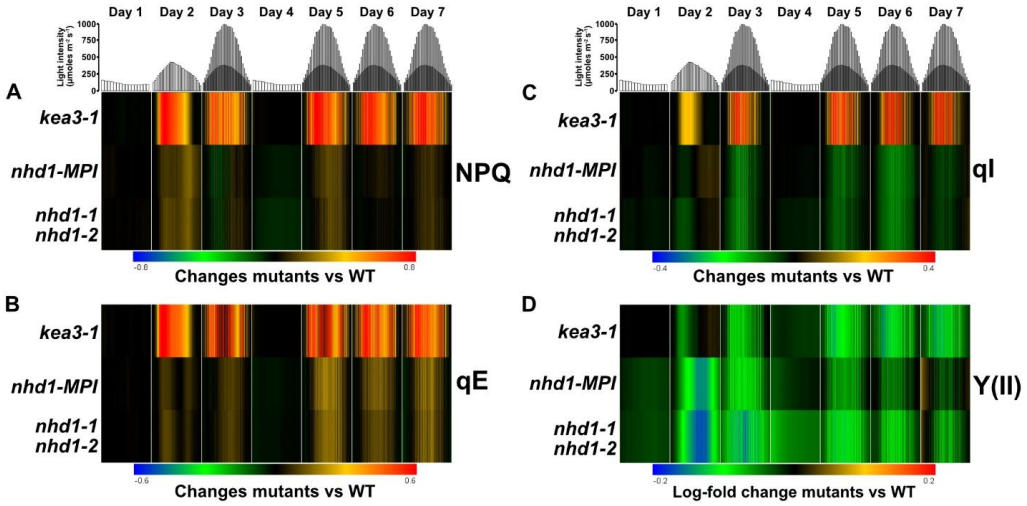

Figure 4.7 Heatmaps of photosynthetic parameters from DEPI measurements. Bars at the top represent light regime during the indicated day of measurement. Shown are NPQ (A), ΔpH component qE (B), photoinhibitory component qI (C), and photosynthetic efficiency Y(II) (D). Data from A-C are presented in changes from the WT, black areas indicate no change, while D) is presented as log-fold changes from the WT.

Nevertheless, these results partially reflect the data of the fluctuating light treatment in our Percival (Fig. 4.6). Furthermore, DEPI re-confirmed the increase in NPQ in *kea3* mutants that we saw under steady-state conditions (Fig. 4.6C, after 240s). In *nhd1* mutants, on the other hand, NPQ was lower only on the first day of high light phases, after which the mutants acclimated and showed a slight increase in NPQ (Fig. 4.7A). qE, as the fastest part of NPQ, seemed to behave similarly in *nhd1*. These effects seemed to accumulate and were prominent in the latter days of high light fluctuations (Days 5-7) but more pronounced in *kea3* (Fig. 4.7B). Interestingly, photoinhibitory component qI behaved oppositely. qI refers to long-term photoinhibition of PS II, partially due to D1 protein damage through high light (Bjorkman and Demmig, 1987). In *kea3*, qI is greatly increased, specifically during high light periods. Both *nhd1* loss-of-function mutants, on the other hand, show reduced qI during those periods (Fig. 4.7C). Still, the decrease of qI in *nhd1* does not positively affect the quantum yield of PS II Y(II), which is decreased across all mutants compared to the WT (Fig. 4.7D).

4.4 Discussion

This study focused on investigating a potential link between transport protein NHD1 and photosynthetic processes at the thylakoid membrane. To that end, we employed a variety of approaches to study substrate specificity, suborganellar localization, and photosynthesis studies in loss-of-function mutants. Our results indicate that NHD1 also accepts K^+ as a substrate, localizes to thylakoid membranes, and may work in balancing the $\Delta\Psi$ component of *pmf* during fluctuating light conditions.

NHD1 belongs to the family of NHaD transporters, initially described as Na^+:H^+ antiporters in bacteria (Dibrov, 2005). In *Vibrio cholerae*, for example, Vc-NHaD mediates efflux of Na^+ and Li^+ (Dzioba et al., 2002; Habibian et al., 2005). In previous studies, closely related NHaD proteins from *P. patens* were able to rescue Na^+- and K^+-defective *E. coli* mutant strains EP432 and TKW4205, respectively (Barrero-Gil et al., 2007; Ruiz-Lau et al., 2017). Identifying possible substrates is crucial in order to draw conclusions for the physiological context of *At*NHD1. In our studies employing the routinely used *E. coli* strain LB2003 (Schlosser et al., 1995; Tanudjaja et al., 2017), we confirmed the previously reported recovery of the growth penalty with KEA3 under low K^+ conditions (Tsujii et al., 2019). Using the thylakoid localized K^+:H^+ antiporter KEA3 as a positive control, we saw that transformation with NHD1 cDNA similarly rescued the growth penalty at low K^+ media concentration (Fig. 4.1A, Suppl. Fig. S4.1A). In an earlier study, reconstitution of his-tagged NHD1 into liposomes pointed towards Na^+-transport of NHD1 while being unable to transport K^+ in the same system. An explanation for this could be that our groups employed different systems. However, comparing the growth of KEA3-transformed LB2003 to the NHD1-transformed strain seemed to produce similar results in our hands, leading us to the conclusion that NHD1 can also accept K^+ as substrate *in vivo*.

Moreover, Na^+:H^+ antiporters of the NHX family have previously displayed a similar lack of substrate specificity, using either substrate depending on the circumstance (Barragan et al., 2012).

After substrate analysis, we explored the suborganellar localization of NHD1 since NHD1 could be critical for photosynthetic processes, including PET, if localized to the thylakoid membrane. While previous studies (Barrero-Gil et al., 2007; Cosentino et al., 2010; Muller et al., 2014) suggested a chloroplast envelope localization for *At*NHD1 and homologs from *Mesembryanthemum crystallinum* and *P. patens*, other proteomics studies point to a thylakoid membrane localization (Sun et al., 2009; Tomizioli et al., 2014). In order to study this, we first transformed NHD1-YFP into *A. thaliana.* After isolating protoplasts of plants of the T_2 generation, we were able to identify YFP signal from distinct spots inside the chloroplast. This signal was absent in untransformed control plants and overlapped with Chl *a* fluorescence (Fig. 4.2), indicating a thylakoid localization. Furthermore, we transiently injected the same construct alongside controls into *N. benthamiana* leaves. Using both microscopy on isolated protoplasts and immunoblotting against the fluorophore, we determined that NHD1-YFP localizes to the thylakoid membrane (Figs. 4.3-4.4, Suppl. Fig. S4.2). While the TIC40-RFP control localized to the envelope membrane in a ring-like structure (Fig. 4.3, Suppl. Fig. S4.2), investigation of CAS-RFP revealed a spotty pattern reminiscent of NHD1-YFP (Fig. 4.3, Suppl. Fig. S4.2A). Consistently, NHD1-YFP overlapped with Chl *a* fluorescence and CAS-RFP (arrows in Suppl. Fig. S4.2A). Employing YFP and RFP has distinct advantages over other fluorophores. Since we recorded YFP at wavelengths lower than the excitation wavelength of RFP (< 555 nm) and excited RFP at > 560 nm, crosstalk was abolished. This combination of fluorophores allows us to conclude that distinctly overlapping signals between CAS-RFP and NHD1-YFP stem from their

respective fluorophores. Our immunoblotting approaches confirmed these CSLM observations. No YFP signal could be detected in chloroplast envelope membrane fractions, whereas clear bands were found only in thylakoid fractions. These results are in accord with the proteomics studies mentioned above and lead us to the conclusion that NHD1 is localized to the thylakoid lumen.

Correct localization of NHD1 is critical because, depending on localization, the availability of substrates can drastically vary *in vivo*. A previous study presented a model connecting the Na^+:H^+ exchange of NHD1 to pyruvate uptake across the chloroplast envelope in C_4 plants (Furumoto et al., 2011). However, in C_4 plants, a Na^+ valve is necessary for establishing a gradient for the Na-driven uptake of pyruvate through BILE ACID:SODIUM SYMPORTER FAMILY PROTEIN (BASS) 2. Nevertheless, the C_3 plant *A. thaliana* uses a proton gradient for pyruvate uptake, established by light-driven H^+ uptake from the stroma through the plastoquinone (PQ) pool or envelope localized H^+ exporters like KEA1/2, among other players (Furumoto et al., 2011). Since NHD1 localizes to thylakoids, the primary transport substrate *in vivo* is likely the more abundant K^+ ion (Demmig and Gimmler, 1983; Robinson and Downton, 1984), similar to KEA3 using K^+ to modulate *pmf* via K^+:H^+ exchange. Therefore, K^+ deserves strong consideration for its role in charge balancing across chloroplast membranes and as a substrate of NHD1. Either way, the possible K^+(Na^+) export implies the involvement of NHD1 in the partitioning of *pmf*.

Studying the impact of NHD1 on thylakoid processes was, therefore, the main focus of this study. After isolation of *nhd1* and *kea3nhd1* mutants (Fig. 4.4), we set out to measure chlorophyll fluorescence parameters that would allow us to find out more about photosynthetic performance and thylakoid processes. Since all mutants were indistinguishable from the WT

under control light, we investigated the impact of fluctuating light on *nhd1* mutants. As recent research has shown, mutant plants lacking specific thylakoid ion transport proteins are defective in *pmf* composition and display distinct phenotypes in regards to photosynthesis and growth under fluctuating light conditions (Carraretto et al., 2013; Armbruster et al., 2016; Herdean et al., 2016; Armbruster et al., 2017). Indeed, both *nhd1* and *kea3nhd1* mutants revealed severe defects in maximum quantum efficiency, F_v/F_m, and were drastically smaller (Fig. 4.6). Although KEA3 and NHD1 proteins likely use the same substrate (K^+) *in vivo*, NPQ kinetics of *kea3* and *nhd1* mutants are shifted in different directions. As reported previously, *kea3* mutants display increased transient NPQ due to their inability to export H^+ (Fig. 4.6C). At the same time, initiation of NPQ is lower than that of the WT after two weeks of exposure to FL.

These results were partially confirmed by data from large-scale phenotyping in DEPI chambers. Here, photosynthetic parameters are continuously measured over multiple days during dynamic light conditions. In contrast to our continuous FL treatment, NPQ in *nhd1* was decreased only during the first sinusoidal plus superimposed high light day (Fig. 4.7B). Re-exposure to high light after a day of low light-triggered qE alongside NPQ. At this point, these differences can be explained by different setups: While we exposed seedlings as young as 7 d to FL conditions for up to two weeks, DEPI measurements are taken on healthy adult plants grown under long-day conditions (16 h light/8 h darkness). Therefore, measurements in our self-made setup plants differ from DEPI due to the sustained damage of the treatment. Astonishingly, *nhd1* mutants displayed decreased inhibitory NPQ, expressed as qI. These values are in stark contrast to the substantial increase of qI in *kea3*, which we could replicate from a previous study (Höhner et al., 2019). Considering the growth impairment and significantly reduced F_v/F_m of *nhd1* in growth under FL, this comes as a surprise and warrants further research. Since qI is a slower

component of photoinhibition, D1 protein turnover studies should give further insight into the decreased qI values in *nhd1*.

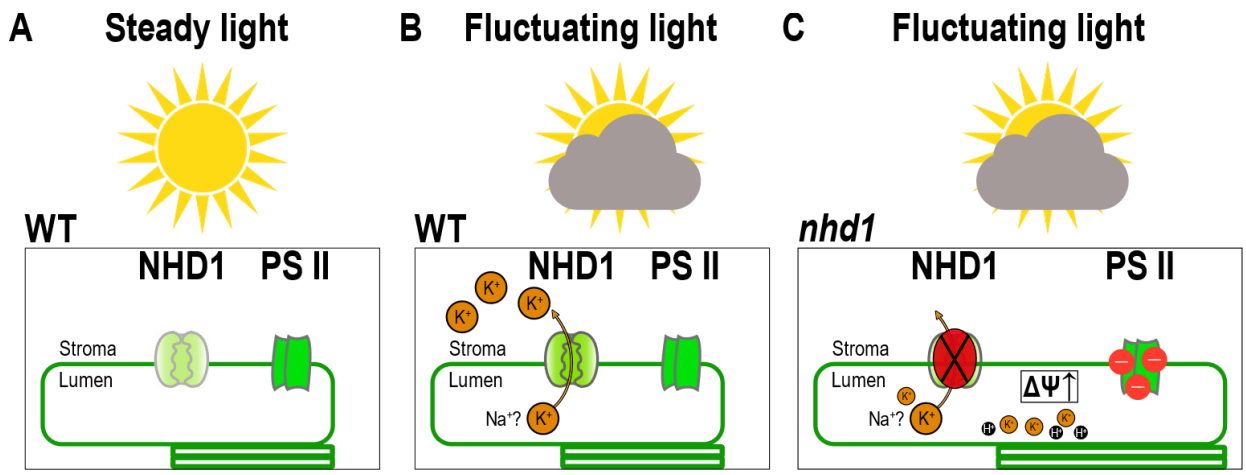

Figure 4.8 Model of the proposed function of *At*NHD1 in acclimation to fluctuating light. A) Our data on *nhd1* mutants grown under steady light points towards a minimal impact of NHD1 on photosynthesis and photosystem II (PS II). B) Under fluctuating light, accumulation of positive charges inside of the lumen can be alleviated by NHD1-mediated export of K^+ (or Na^+) into the stroma and support PS II function. C) In *nhd1* loss-of-function mutants, fluctuating light can have detrimental effects on PS II function due to the lack of a ΔΨ dissipation mechanism. The elevated ΔΨ results in increased charge recombination within PS II, leading to photodamage and inhibition of photosynthetic processes at the thylakoid membrane.

Taken together, NHD1 might function as a dissipation mechanism of ΔΨ, exporting K^+ out of the lumen and thereby dissipating ΔΨ (Fig. 4.8), a mechanism proposed by (Pottosin and Shabala, 2016). Excess ΔΨ results in increased rates of charge recombination within PS II, damaging photosystems in the process (Davis et al., 2016). Accumulation of damage to PS II could result in the phenotypes we observe in *nhd1* mutants, including low PS II quantum yield (Y(II)) and F_v/F_m, leading to severe growth penalties under fluctuating light (Fig. 4.8). A similar regulation of *pmf* can be observed in mutants of the thylakoid Cl^- channel VCCN1 (Herdean et al., 2016). VCCN1 reduces ΔΨ through the influx of Cl^- anions into the positively charged lumen, allowing for increased ΔpH. This shift leads to decreased activation of qE, resulting in

lowered NPQ. Loss-of-function mutants lacking VCCN1 display NPQ kinetics similar to *nhd1*, and both proteins might function similarly. In wild-type plants, NHD1 reduces ΔΨ by efflux of lumenal cations, while VCCN1 is responsible for the reduction of ΔΨ through influx of anions in the form of Cl^-. However, *vccn1* displays a slight increase in qI (Höhner et al., 2019) while it is decreased in *nhd1*. An *nhd1vccn1* loss-of-function double mutant should give more insight into the overlap of both proteins in establishing ΔΨ and protection of PS II. Studying growth under fluctuating light conditions and more precise measurements of *pmf* by electrochromic shift (ECS) will give much-needed insight into the regulatory function of NHD1.

4.5 Materials and Methods

Plasmid creation and E. coli complementation assays

If not otherwise indicated, consumables used were purchased from Roth (Carl Roth, Karlsruhe, Germany). TOP10 cells (Invitrogen, Waltham, USA) were routinely used for the propagation of plasmids. Information about constructs used in this study can be found in Supplemental Table S1. pBAD vectors were transformed into LB2003 (kindly provided by Nobuyuki Uozumi, Tohoku University) using the electroporation method at 2.5 kV. Selection took place overnight on lysogeny broth (LB) agar plates containing 25µg/mL chloramphenicol. Complementation of LB2003 was performed according to (Sato et al., 2014). In short, cells were shaken overnight in LBK medium (LB containing 100 mM KCl instead of NaCl) at 37°C. The following day, the culture was spun down and washed twice in modified M9 medium (46 mM Na_2HPO_4, 23 mM NaH_2PO_4, 8 mM $(NH_4)_2SO_4$, 0.4 mM $MgSO_4$, 0.6 µM $FeSO_4$, 0.1 mM $CaCl_2$). OD_{600} was adjusted to 0.125 in modified M9 medium, and 5 µl of the cell suspension was streaked on LB agarose plates with or without KCl and containing either 0.2% (w/v) arabinose or 0.2% (w/v) glucose. Alternatively, cells were added to liquid LB in a 48-well plate. The plates

were shaken every 5 min for 1 min in a TECAN (Tecan, Männedorf, Switzerland) plate reader to keep cells from settling, and OD_{600} was determined every 20 min. Experiments were repeated multiple times with similar results.

Generation of stable NHD1-YFP overexpressor lines

In order to reduce transgene silencing, flowers of *rdr6* mutants were dipped with *Agrobacterium tumefaciens* strains carrying the UBQ10::NHD1-YFP construct. Floral dip was performed according to (Clough and Bent, 1998). T_1 transformants were selected on Hygromycin at 50µg/mL, followed by confirmation of the fluorophore by fluorescence microscopy. In T_2, the strongest expressors were selected. Experiments were performed on T_3 individuals.

Protoplast isolation

For isolation of *A. thaliana* protoplasts, the 'Tape-Arabidopsis Sandwich' method was chosen (Wu et al., 2009). The protocol was followed and produced great results. In the case of *N. benthamiana*, leaves were cut into 1cm*1cm pieces. Outside of this, the protocol was not changed. Macerozyme R-10 and cellulase were purchased from Serva (Serva, Heidelberg, Germany).

Transient N. benthamiana infiltration and confocal microscopy for protein localization studies

Transient transformation of *N. benthamiana* was realized according to (Waadt et al., 2014). *Agrobacterium tumefaciens* strains carrying the respective vectors (Suppl. Table S4.1) were co-injected with the anti-silencing strain p19 (Voinnet et al., 2003). 28-d-old *N. benthamiana* were placed into a humid environment 2 h before infiltration. Then, bottom sides of leaves were infiltrated, and *N. benthamiana* were placed into a greenhouse for 3-5 days before imaging. Images were acquired using a Leica SP5 confocal microscope (Leica, Wetzlar, Germany). Fluorophores were excited using a white light laser (WLL) and recorded with hybrid

photodetectors (HyD). YFP was excited at 514 nm and recorded at 522-555 nm. RFP was excited at 561 nm and recorded at 579-629 nm. Chlorophyll *a* was excited with a UV laser at 405 nm and recorded at 714-750nm. Images were processed with LAS X (Leica) and Affinity Designer (serif) software.

Chloroplast subfractionation

Initial chloroplast isolation was performed according to (Bolter et al., 2020). Subfractionation of isolated chloroplasts was performed as described in (Flores-Perez and Jarvis, 2017) with slight modifications. Chloroplasts were incubated in lysis buffer (10 mM HEPES/KOH, 5 mM $MgCl_2$), and complete protease inhibitor (cpi, Roche, Basel, Switzerland) was added at a concentration of 1mg/ml chlorophyll. The suspension was placed on ice for 30 min followed by rupturing of 50 strokes in a Dounce homogenizer. The resulting homogenate was loaded onto a step sucrose gradient (0.46 M, 1.0 M, 1.2 M sucrose in lysis buffer) and centrifuged for 2 h at 58,000*g* and 4°C. The stroma was pipetted off the top and processed for sodium dodecyl sulfate–polyacrylamide gel electrophoresis (SDS-PAGE). The envelope fraction was collected from the interface between 0.46 M and 1.0 M sucrose. After 1:4 dilution with lysis buffer, this fraction was centrifuged at 256.000*g* for 30 min and 4 °C. The resulting pellet was resuspended in loading buffer containing a final conc. of 4% (w/v) SDS, 20% (w/v) glycerin, 0.004% bromophenol blue, and 125 mM Tris-HCl. Dithiothreitol (DTT) was added freshly to a final conc. of 20 mM. Thylakoids recovered from the pellet of the sucrose gradient were washed five times in lysis buffer. Loading of samples was adjusted to total protein.

Immunoblotting and SDS-PAGE

Chloroplast subfractions were run on a 10% SDS-PAGE in a Bio-Rad Mini-PROTEAN (Bio-Rad, Hercules, USA). The gel was run at 120 V until proteins reached the resolving gel and

then run at 150 V until the loading dye front ran out of the gel. The gel was rinsed and blotted onto a PVDF membrane (0.45 µm pore size) in Towbin buffer (25 mM Tris pH 8.3, 192 mM glycine, 1% (w/v) SDS, 20% (v/v) methanol) in a wet blot apparatus (Bio-Rad). The membrane was blocked in tris-buffered saline containing 50 mM Tris pH 7.6, 150 mM NaCl with 0.05% tween (TBS-T), and 5% skim milk for 30 min at room temperature (RT). Then, the membrane was then incubated with specific antibodies in 1:1.000 dilution in TBS-T overnight at 4 °C. Primary antibodies used were α-KEA1(2) (Bolter et al., 2020), α-LHCP (Clausen et al., 2004), and a commercial α-GFP antibody (Roche). Secondary horseradish peroxidase (HRP) coupled antibodies against α-KEA1(2), and α-LHCP were goat-anti-rabbit (Proteintech Cat# SA00001-2) or goat-anti-mouse in case of anti-GFP. After washing three times with TBS-T, secondary antibodies were diluted 1:10.000 in TBS-T + 5% skim milk and incubated with membranes for 1 h at RT. Membranes were washed thrice with TBS-T and then incubated with Agrisera ECL Bright solutions (Agrisera, Vännäs, SWEDEN). Finally, signal was detected with an ImageQuant LAS 4000 (GE Healthcare Bio-Sciences AB, Uppsala, Sweden).

Genotyping

Genomic DNA (gDNA) was isolated by grinding leaf material in extraction buffer (200 mM Tris/HCl pH 7.5, 250 mM NaCl, 25 mM EDTA, and 0.5% SDS (w/v)). Cell debris was removed by centrifuging for 5 min at 15000*g*. The supernatant was mixed with isopropanol, and DNA was pelleted by centrifugation at 20000*g* for 10 minutes. The pellet was washed with 70% (v/v) EtOH and pelleted again before drying at RT for 30 minutes. DNA was resuspended in H_2O and used for polymerase chain reactions (PCR). Primers used in genotyping reactions are listed in Suppl. Table S4.3.

Plant growth conditions

For fluctuating light experiments, *A. thaliana* seeds were sown on soil and stratified for 2 days at 4°C in the dark. Then, the pots were placed into the Percival growth chamber (Percival Scientific, Perry, USA) set to 12 h light at 100 µmol photons m^{-2} s^{-1}/12 h darkness, 23°C, and 50% relative humidity. 7-d-old seedlings were separated and placed under a 2000 W LED panel (Phlizon, Guangdong, China) or on a shelf above for control conditions. The panel was controlled by an Arduino microcontroller, turned on for one min every five minutes, and added 1000 µmol photons m^{-2} s^{-1} according to (Schneider et al., 2019). Pots were shuffled daily underneath the LED panel to ensure even exposure.

DEPI experiments

For DEPI experiments, Col-0 WT, *nhd1-MPI*, and *nhd1-1nhd1-2* (*n*=15 per genotype) were grown under a regime of 16 h light at 100 µmoles m^{-2} s^{-1}/8 h darkness and 21°C. After three weeks, plants were placed into a DEPI chamber and treated as described in (Cruz et al., 2016).

Accession numbers

Col-0 (WT, CS70000), *nhd1-MPI* (AT3G19490, kindly provided by Imre E. Somssich MPIZ Cologne), *kea3-1* (AT4G04850, SAIL_556_E12 (Kunz et al., 2014)), *kea3nhd1-mpi* (AT4G04850 AT3G19490, created during this work), *nhd1-1* (AT3G19490, AT3G19480, AT3G19470, AT3G19460, AT3G19450, AT3G19440, SALK_0084911), *rdr6* (AT3G49500).

4.6 Supplemental Material

Supplemental Tables

Supplemental Table S4.1. Constructs used in this study and their origin.

Name	**Source**
LB2003 ((F-, *thi*, *lacz*, *gal*, *rha*, Δ*kdpFABC5*, *trkD1*, Δ*trkA* (Schlosser et al., 1995))	Kind donation from Nobuyuki Uozumi, Tohoku University
Kea3 cDNA -Stop + pBAD_His	This work
Nhd1 cDNA -Stop + pBAD-His	This work
p19	(Voinnet et al., 2003)
KEA3.1 + pB7FWG2 GFP c-term	(Armbruster et al., 2014)
KEA3.3 + p B7FWG2 GFP c-term	(Armbruster et al., 2014)
Nhd1cDNA+Stop + pHygIIUT clone 1 via SpeI/XmaI	Lab stock
AtNhd1 cDNA - Stop + pHygIIUT-Venus via SpeI/XmaI	Lab stock
Tic40cDNA + pBARIIUT-mCherry-Cterm	Lab stock
Cas cDNA -Stop + BamHI/XmaI overhangs pBAR-mCherry cterm	Lab stock
pGGZ-RW104 - pGGZ003-pUBQ10-NTRC-mNectarine_ATG-GSL-mTurquoise-tHSP18.2M-hygR	Kind donation of Rainer Waadt, WWU Münster

Supplemental Table S4.2. Accessions used in this study.

Name	**Locus**	**Origin/Source**
Arabidopsis thaliana	-	WT accession CS70000, Lab stock
nhd1-mpi	AT3G19490	Kindly provided by Imre E. Somssich (MPIZ Cologne)
nhd1-4	AT3G19490	SALK_118891
kea3-1	AT4G04850	SAIL_556_E12 (Kunz et al., 2014)
kea3nhd1-mpi	AT4G04850 AT3G19490	Created during this work
doi	AT3G19490 AT3G19480 AT3G19470 AT3G19460 AT3G19450 AT3G19440	Formerly *nhd1-1* (SALK_0084911) Kindly provided by Laura Lopez
Rdr6-nhd1-YFP	AT3G49500, AT3G19490	Created during preliminary lab work
Nicotiana benthamiana	-	Lab stock

Supplemental Table S4.3. List of oligonucleotides used in this study. Bolded oligonucleotides are marked in Fig. 4.5A.

Oligonucleotide Name	**Sequence**	**Used in**
Sail LB3	tagcatctgaatttcataaccaatctcgatacac	Genotyping sail line
HK102 Kea3 s 1	caccatggcaattagtactatgttagg	Genotyping
HK103 Kea3 as 5	caggccttgaatgaaagaggaattc	Genotyping
HK186 Nhd1 cDNA s + SpeI	actagtaaaatggcggtgtttcctatcgg	Genotyping
HK189 Nhd1 as5	cactaccacacctcctagaagt	Genotyping
HK366 Salk LB1.3	attttgccgatttcggaac	Genotyping Salk line
HK688 FISH2 (nhd1-MPI LB))	cagtcatagccgaatagcctctcca	Genotyping MPI line
HK689 NHD1-143s	ctcgacgaggttatccaaacatggtg	Genotyping

Supplemental Figures

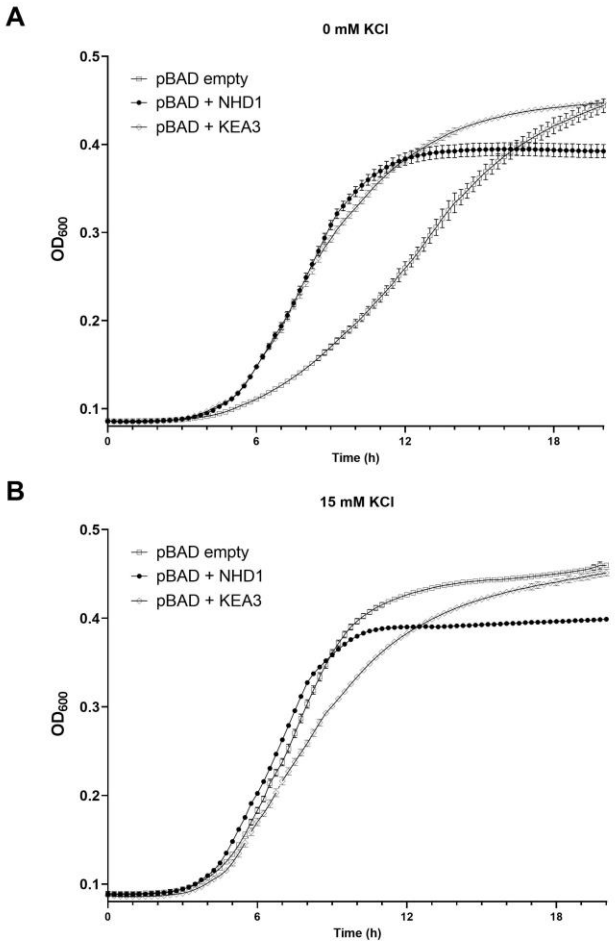

Supplemental Figure S4.1 Growth recovery of the K^+-transport deficient *E. coli* mutant LB2003 in liquid culture. A) Cells transformed with KEA3 or NHD1 cDNA, but not with empty vector pBAD alone, show a clear growth recovery in medium without supplemented KCl . B) The growth deficiency of LB2003 is restored in medium supplied with 15 mM KCl.

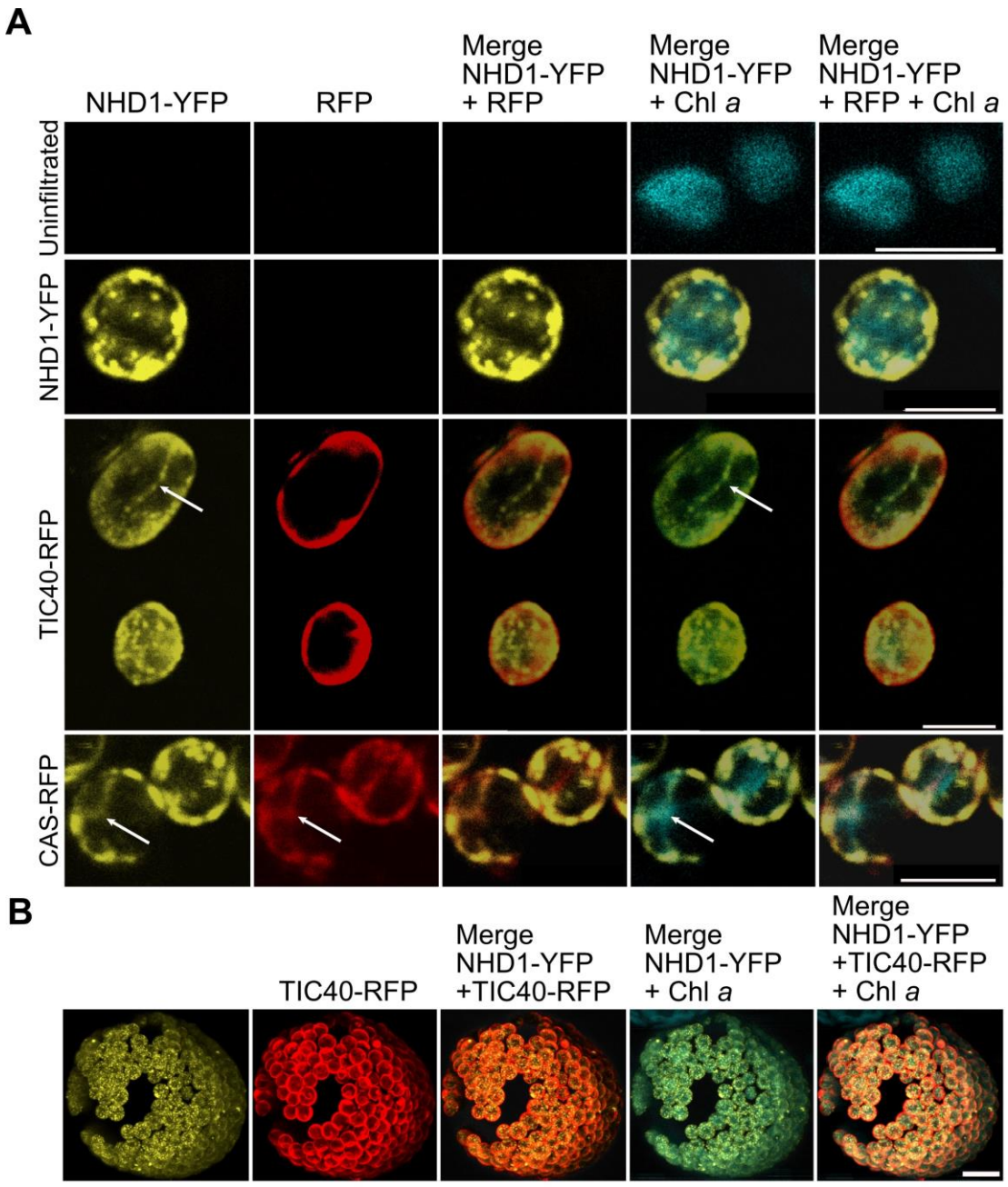

Supplemental Figure S4.2 Localization of NHD1 and controls in transiently transformed *N. benthamiana* leaves. A)Shown are single NHD1-YFP infiltrated leaves and co-injections with chloroplast inner envelope protein TIC40-RFP and thylakoid localized CAS-RFP construct. Arrows point to distinct overlaps in signal between thylakoid membrane localized Chl a autofluorescence or CAS-mCherry signal. B) MAX projection of a z-stack (stack size 1 µm) of a protoplast. Scale bars are 5 µm.

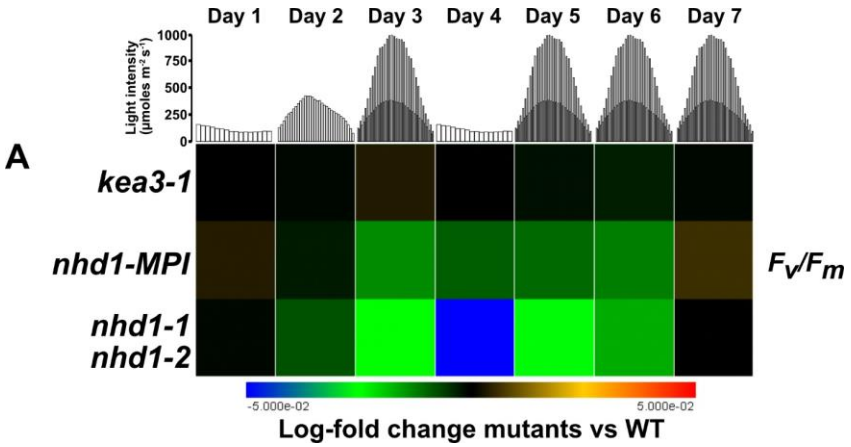

Supplemental Figure S4.3 F_v/F_m measured in DEPI at the beginning of each day. Bars at the top represent light regime during the indicated day of measurement. Data are presented in log-fold changes from the WT, black areas indicate no change. A representative result from three experiments is shown.

4.7 References

Armbruster U, Carrillo LR, Venema K, Pavlovic L, Schmidtmann E, Kornfeld A, Jahns P, Berry JA, Kramer DM, Jonikas MC (2014) Ion antiport accelerates photosynthetic acclimation in fluctuating light environments. Nat Commun **5:** 5439

Armbruster U, Correa Galvis V, Kunz HH, Strand DD (2017) The regulation of the chloroplast proton motive force plays a key role for photosynthesis in fluctuating light. Curr Opin Plant Biol **37:** 56-62

Armbruster U, Leonelli L, Galvis VC, Strand D, Quinn EH, Jonikas MC, Niyogi KK (2016) Regulation and Levels of the Thylakoid K+/H+ Antiporter KEA3 Shape the Dynamic Response of Photosynthesis in Fluctuating Light. Plant and Cell Physiology **57:** 1557-1567

Barragan V, Leidi EO, Andres Z, Rubio L, De Luca A, Fernandez JA, Cubero B, Pardo JM (2012) Ion exchangers NHX1 and NHX2 mediate active potassium uptake into vacuoles to regulate cell turgor and stomatal function in Arabidopsis. Plant Cell **24:** 1127-1142

Barrero-Gil J, Rodriguez-Navarro A, Benito B (2007) Cloning of the PpNHAD1 transporter of Physcomitrella patens, a chloroplast transporter highly conserved in photosynthetic eukaryotic organisms. J Exp Bot **58:** 2839-2849

Bjorkman O, Demmig B (1987) Photon yield of O2 evolution and chlorophyll fluorescence characteristics at 77 K among vascular plants of diverse origins. Planta **170:** 489-504

Bolter B, Mitterreiter MJ, Schwenkert S, Finkemeier I, Kunz HH (2020) The topology of plastid inner envelope potassium cation efflux antiporter KEA1 provides new insights into its regulatory features. Photosynth Res **145:** 43-54

Carraretto L, Formentin E, Teardo E, Checchetto V, Tomizioli M, Morosinotto T, Giacometti GM, Finazzi G, Szabó I (2013) A thylakoid-located two-pore K+ channel controls photosynthetic light utilization in plants. Science **342:** 114-118

Clausen C, Ilkavets I, Thomson R, Philippar K, Vojta A, Mohlmann T, Neuhaus E, Fulgosi H, Soll J (2004) Intracellular localization of VDAC proteins in plants. Planta **220:** 30-37

Clough SJ, Bent AF (1998) Floral dip: a simplified method for Agrobacterium-mediated transformation of Arabidopsis thaliana. Plant J **16:** 735-743

Correa Galvis V, Strand DD, Messer M, Thiele W, Bethmann S, Hübner D, Uflewski M, Kaiser E, Siemiatkowska B, Morris BA, Tóth SZ, Watanabe M, Brückner F, Höfgen R, Jahns P, Schöttler MA, Armbruster U (2020) H(+) Transport by K(+) EXCHANGE ANTIPORTER3 Promotes Photosynthesis and Growth in Chloroplast ATP Synthase Mutants. Plant Physiol **182:** 2126-2142

Cosentino C, Fischer-Schliebs E, Bertl A, Thiel G, Homann U (2010) Na+/H+ antiporters are differentially regulated in response to NaCl stress in leaves and roots of Mesembryanthemum crystallinum. New Phytol **186:** 669-680

Cruz JA, Sacksteder CA, Kanazawa A, Kramer DM (2001) Contribution of electric field (Delta psi) to steady-state transthylakoid proton motive force (pmf) in vitro and in vivo. control of pmf parsing into Delta psi and Delta pH by ionic strength. Biochemistry **40:** 1226-1237

Cruz JA, Savage LJ, Zegarac R, Hall CC, Satoh-Cruz M, Davis GA, Kovac WK, Chen J, Kramer DM (2016) Dynamic Environmental Photosynthetic Imaging Reveals Emergent Phenotypes. Cell Syst **2:** 365-377

Davis GA, Kanazawa A, Schöttler MA, Kohzuma K, Froehlich JE, Rutherford AW, Satoh-Cruz M, Minhas D, Tietz S, Dhingra A, Kramer DM (2016) Limitations to photosynthesis by proton motive force-induced photosystem II photodamage. Elife **5**

Demmig-Adams B, Cohu CM, Muller O, Adams WW, 3rd (2012) Modulation of photosynthetic energy conversion efficiency in nature: from seconds to seasons. Photosynth Res **113:** 75-88

Demmig B, Gimmler H (1983) Properties of the Isolated Intact Chloroplast at Cytoplasmic K Concentrations : I. Light-Induced Cation Uptake into Intact Chloroplasts is Driven by an Electrical Potential Difference. Plant Physiol **73:** 169-174

Dibrov P (2005) The sodium cycle in vibrio cholerae: riddles in the dark. Biochemistry (Mosc) **70:** 150-153

Dukic E, Herdean A, Cheregi O, Sharma A, Nziengui H, Dmitruk D, Solymosi K, Pribil M, Spetea C (2019) K(+) and Cl(-) channels/transporters independently fine-tune photosynthesis in plants. Sci Rep **9:** 8639

Dutta S, Cruz JA, Imran SM, Chen J, Kramer DM, Osteryoung KW (2017) Variations in chloroplast movement and chlorophyll fluorescence among chloroplast division mutants under light stress. J Exp Bot **68:** 3541-3555

Dzioba J, Ostroumov E, Winogrodzki A, Dibrov P (2002) Cloning, functional expression in Escherichia coli and primary characterization of a new Na+/H+ antiporter, NhaD, of Vibrio cholerae. Mol Cell Biochem **229:** 119-124

Flores-Perez U, Jarvis P (2017) Isolation and Suborganellar Fractionation of Arabidopsis Chloroplasts. Methods Mol Biol **1511:** 45-60

Furumoto T, Yamaguchi T, Ohshima-Ichie Y, Nakamura M, Tsuchida-Iwata Y, Shimamura M, Ohnishi J, Hata S, Gowik U, Westhoff P, Brautigam A, Weber APM, Izui K (2011) A plastidial sodium-dependent pyruvate transporter. Nature **478:** 274-274

Gibson DG, Young L, Chuang RY, Venter JC, Hutchison CA, 3rd, Smith HO (2009) Enzymatic assembly of DNA molecules up to several hundred kilobases. Nat Methods **6:** 343-345

Gjindali A, Herrmann HA, Schwartz JM, Johnson GN, Calzadilla PI (2021) A Holistic Approach to Study Photosynthetic Acclimation Responses of Plants to Fluctuating Light. Front Plant Sci **12:** 668512

Guzman LM, Belin D, Carson MJ, Beckwith J (1995) Tight regulation, modulation, and high-level expression by vectors containing the arabinose PBAD promoter. J Bacteriol **177:** 4121-4130

Habibian R, Dzioba J, Barrett J, Galperin MY, Loewen PC, Dibrov P (2005) Functional analysis of conserved polar residues in Vc-NhaD, Na+/H+ antiporter of Vibrio cholerae. J Biol Chem **280:** 39637-39643

Herdean A, Nziengui H, Zsiros O, Solymosi K, Garab G, Lundin B, Spetea C (2016) The Arabidopsis Thylakoid Chloride Channel AtCLCe Functions in Chloride Homeostasis and Regulation of Photosynthetic Electron Transport. Front Plant Sci **7:** 115

Herdean A, Teardo E, Nilsson AK, Pfeil BE, Johansson ON, Unnep R, Nagy G, Zsiros O, Dana S, Solymosi K, Garab G, Szabo I, Spetea C, Lundin B (2016) A voltage-dependent chloride channel fine-tunes photosynthesis in plants. Nat Commun **7:** 11654

Hind G, Nakatani HY, Izawa S (1974) Light-dependent redistribution of ions in suspensions of chloroplast thylakoid membranes. Proc Natl Acad Sci U S A **71:** 1484-1488

Höhner R, Day PM, Zimmermann SE, Lopez LS, Krämer M, Giavalisco P, Correa Galvis V, Armbruster U, Schöttler MA, Jahns P, Krueger S, Kunz H-H (2021) Stromal NADH supplied by PHOSPHOGLYCERATE DEHYDROGENASE3 is crucial for photosynthetic performance. Plant Physiology

Höhner R, Galvis VC, Strand DD, Völkner C, Kramer M, Messer M, Dinc F, Sjuts I, Bolter B, Kramer DM, Armbruster U, Kunz HH (2019) Photosynthesis in Arabidopsis Is Unaffected by the Function of the Vacuolar K(+) Channel TPK3. Plant Physiol **180:** 1322-1335

Jaslan D, Dreyer I, Lu J, O'Malley R, Dindas J, Marten I, Hedrich R (2019) Voltage-dependent gating of SV channel TPC1 confers vacuole excitability. Nat Commun **10:** 2659

Kaiser E, Morales A, Harbinson J (2018) Fluctuating Light Takes Crop Photosynthesis on a Rollercoaster Ride. Plant Physiol **176:** 977-989

Klughammer C, Schreiber U (2008) Complementary PS II quantum yields calculated from simple fluorescence parameters measured by PAM fluorometry and the Saturation Pulse method. PAM application notes **1:** 201-247

Kramer DM, Johnson G, Kiirats O, Edwards GE (2004) New Fluorescence Parameters for the Determination of QA Redox State and Excitation Energy Fluxes. Photosynth Res **79:** 209

Kromdijk J, Glowacka K, Leonelli L, Gabilly ST, Iwai M, Niyogi KK, Long SP (2016) Improving photosynthesis and crop productivity by accelerating recovery from photoprotection. Science **354:** 857-861

Kunz HH, Gierth M, Herdean A, Satoh-Cruz M, Kramer DM, Spetea C, Schroeder JI (2014) Plastidial transporters KEA1, -2, and -3 are essential for chloroplast osmoregulation, integrity, and pH regulation in Arabidopsis. Proc Natl Acad Sci U S A **111:** 7480-7485

Li M, Svoboda V, Davis G, Kramer D, Kunz HH, Kirchhoff H (2021) Impact of ion fluxes across thylakoid membranes on photosynthetic electron transport and photoprotection. Nat Plants **7:** 979-988

Li XP, Muller-Moule P, Gilmore AM, Niyogi KK (2002) PsbS-dependent enhancement of feedback de-excitation protects photosystem II from photoinhibition. Proc Natl Acad Sci U S A **99:** 15222-15227

Liu H, Su T, He W, Wang Q, Lin C (2020) The Universally Conserved Residues Are Not Universally Required for Stable Protein Expression or Functions of Cryptochromes. Mol Biol Evol **37:** 327-340

Mitchell P (1966) Chemiosmotic Coupling in Oxidative and Photosynthetic Phosphorylation. Biological Reviews of the Cambridge Philosophical Society **41:** 445-502

Muller M, Kunz HH, Schroeder JI, Kemp G, Young HS, Neuhaus HE (2014) Decreased capacity for sodium export out of Arabidopsis chloroplasts impairs salt tolerance, photosynthesis and plant performance. Plant J **78:** 646-658

Muller P, Li XP, Niyogi KK (2001) Non-photochemical quenching. A response to excess light energy. Plant Physiol **125:** 1558-1566

Mullineaux CW, Ruban AV, Horton P (1994) Prompt heat release associated with ΔpH-dependent quenching in spinach thylakoid membranes. Biochimica et Biophysica Acta (BBA) - Bioenergetics **1185:** 119-123

Pascal AA, Liu Z, Broess K, van Oort B, van Amerongen H, Wang C, Horton P, Robert B, Chang W, Ruban A (2005) Molecular basis of photoprotection and control of photosynthetic light-harvesting. Nature **436:** 134-137

Pearcy RW (1990) Sunflecks and Photosynthesis in Plant Canopies. Annual Review of Plant Physiology and Plant Molecular Biology **41:** 421-453

Peragine A, Yoshikawa M, Wu G, Albrecht HL, Poethig RS (2004) SGS3 and SGS2/SDE1/RDR6 are required for juvenile development and the production of trans-acting siRNAs in Arabidopsis. Genes Dev **18:** 2368-2379

Pinner E, Kotler Y, Padan E, Schuldiner S (1993) Physiological role of nhaB, a specific Na+/H+ antiporter in Escherichia coli. J Biol Chem **268:** 1729-1734

Pottosin I, Shabala S (2016) Transport Across Chloroplast Membranes: Optimizing Photosynthesis for Adverse Environmental Conditions. Mol Plant **9:** 356-370

Preston JC, Sandve SR (2013) Adaptation to seasonality and the winter freeze. Front Plant Sci **4:** 167

Reinhardt K, Smith WK, Carter GGA (2010) Clouds and cloud immersion alter photosynthetic light quality in a temperate mountain cloud forest. Botany **88:** 462-470

Robinson SP, Downton WJ (1984) Potassium, sodium, and chloride content of isolated intact chloroplasts in relation to ionic compartmentation in leaves. Arch Biochem Biophys **228:** 197-206

Ruiz-Lau N, Saez A, Lanza M, Benito B (2017) Genomic and Transcriptomic Compilation of Chloroplast Ionic Transporters of Physcomitrella patens. Study of NHAD Transporters in Na+ and K+ Homeostasis. Plant Cell Physiol **58:** 2166-2178

Sato Y, Nanatani K, Hamamoto S, Shimizu M, Takahashi M, Tabuchi-Kobayashi M, Mizutani A, Schroeder JI, Souma S, Uozumi N (2014) Defining membrane spanning domains and crucial membrane-localized acidic amino acid residues for K(+) transport of a Kup/HAK/KT-type Escherichia coli potassium transporter. J Biochem **155:** 315-323

Schleyer M, Bakker EP (1993) Nucleotide sequence and 3'-end deletion studies indicate that the K(+)-uptake protein kup from Escherichia coli is composed of a hydrophobic core linked to a large and partially essential hydrophilic C terminus. J Bacteriol **175:** 6925-6931

Schlosser A, Meldorf M, Stumpe S, Bakker EP, Epstein W (1995) TrkH and its homolog, TrkG, determine the specificity and kinetics of cation transport by the Trk system of Escherichia coli. J Bacteriol **177:** 1908-1910

Schneider D, Lopez LS, Li M, Crawford JD, Kirchhoff H, Kunz HH (2019) Fluctuating light experiments and semi-automated plant phenotyping enabled by self-built growth racks and simple upgrades to the IMAGING-PAM. Plant Methods **15:** 156

Schneider T, Bolger A, Zeier J, Preiskowski S, Benes V, Trenkamp S, Usadel B, Farré EM, Matsubara S (2019) Fluctuating Light Interacts with Time of Day and Leaf Development Stage to Reprogram Gene Expression. Plant Physiol **179:** 1632-1657

Schonknecht G, Hedrich R, Junge W, Raschke K (1988) A Voltage-Dependent Chloride Channel in the Photosynthetic Membrane of a Higher-Plant. Nature **336:** 589-592

Stahl T, Glockmann C, Soll J, Heins L (1999) Tic40, a new "old" subunit of the chloroplast protein import translocon. J Biol Chem **274:** 37467-37472

Sun Q, Zybailov B, Majeran W, Friso G, Olinares PD, van Wijk KJ (2009) PPDB, the Plant Proteomics Database at Cornell. Nucleic Acids Res **37:** D969-974

Taiz L, Zeiger E, Møller IM, Murphy AS (2015) Plant physiology and development, Ed Sixth edition. Sinauer Associates, Inc., Publishers, Sunderland, Massachusetts

Tang RJ, Zhao FG, Yang Y, Wang C, Li K, Kleist TJ, Lemaux PG, Luan S (2020) A calcium signalling network activates vacuolar K(+) remobilization to enable plant adaptation to low-K environments. Nat Plants **6:** 384-393

Tanudjaja E, Hoshi N, Su YH, Hamamoto S, Uozumi N (2017) Kup-mediated Cs(+) uptake and Kdp-driven K(+) uptake coordinate to promote cell growth during excess Cs(+) conditions in Escherichia coli. Sci Rep **7:** 2122

Tester M, Blatt MR (1989) Direct measurement of k channels in thylakoid membranes by incorporation of vesicles into planar lipid bilayers. Plant Physiol **91:** 249-252

Tomizioli M, Lazar C, Brugiere S, Burger T, Salvi D, Gatto L, Moyet L, Breckels LM, Hesse AM, Lilley KS, Seigneurin-Berny D, Finazzi G, Rolland N, Ferro M (2014) Deciphering thylakoid sub-compartments using a mass spectrometry-based approach. Mol Cell Proteomics **13:** 2147-2167

Tsujii M, Kera K, Hamamoto S, Kuromori T, Shikanai T, Uozumi N (2019) Evidence for potassium transport activity of Arabidopsis KEA1-KEA6. Sci Rep **9:** 10040

Uflewski M, Mielke S, Galvis VC, von Bismarck T, Chen X, Tietz E, Ruß J, Luzarowski M, Sokolowska E, Skirycz A, Eirich J, Finkemeier I, Schöttler MA, Armbruster U (2021) Functional characterization of proton antiport regulation in the thylakoid membrane. Plant Physiol

Vainonen JP, Sakuragi Y, Stael S, Tikkanen M, Allahverdiyeva Y, Paakkarinen V, Aro E, Suorsa M, Scheller HV, Vener AV, Aro EM (2008) Light regulation of CaS, a novel phosphoprotein in the thylakoid membrane of Arabidopsis thaliana. FEBS J **275:** 1767-1777

Voelker C, Schmidt D, Mueller-Roeber B, Czempinski K (2006) Members of the Arabidopsis AtTPK/KCO family form homomeric vacuolar channels in planta. Plant J **48:** 296-306

Voinnet O, Rivas S, Mestre P, Baulcombe D (2003) An enhanced transient expression system in plants based on suppression of gene silencing by the p19 protein of tomato bushy stunt virus. Plant J **33:** 949-956

Völkner C, Holzner LJ, Day PM, Ashok AD, Vries Jd, Bölter B, Kunz H-H (2021) Two plastid POLLUX ion channel-like proteins are required for stress-triggered stromal Ca2+ release. Plant Physiology

Waadt R, Schlucking K, Schroeder JI, Kudla J (2014) Protein fragment bimolecular fluorescence complementation analyses for the in vivo study of protein-protein interactions and cellular protein complex localizations. Methods Mol Biol **1062:** 629-658

Weinl S, Held K, Schlucking K, Steinhorst L, Kuhlgert S, Hippler M, Kudla J (2008) A plastid protein crucial for Ca2+-regulated stomatal responses. New Phytol **179:** 675-686

Wilson M, Haswell E (2012) A role for mechanosensitive channels in chloroplast and bacterial fission. Plant Signal Behav **7:** 157-160

Wu FH, Shen SC, Lee LY, Lee SH, Chan MT, Lin CS (2009) Tape-Arabidopsis Sandwich - a simpler Arabidopsis protoplast isolation method. Plant Methods **5:** 16

Zhu XG, Ort DR, Whitmarsh J, Long SP (2004) The slow reversibility of photosystem II thermal energy dissipation on transfer from high to low light may cause large losses in carbon gain by crop canopies: a theoretical analysis. Journal of Experimental Botany **55:** 1167-1175

CHAPTER FIVE: CONCLUSION

This dissertation investigates the roles and interplay of chloroplast ion transport proteins on the organelle's physiology. By characterizing novel proteins, uncovering functional interactions between previously characterized families, and revisiting the localization and role of another transport protein in plastids, we add significant knowledge to the plastid ion transportome. All protein candidates investigated in this dissertation share the common substrate K^+, yet we illustrate the different roles these seemingly similar proteins can play inside the plastid. All proteins seem to have in common that their functions are relevant for the plants' biotic and abiotic stress response, albeit under different predispositions.

Chapter Two characterized proteins capable of K^+-uptake into plastids. Nevertheless, the lack of specific phenotypic traits suggests that PEC1/2 are not primarily necessary for K^+-uptake. Instead, they are required for plastid Ca^{2+} signaling. In the Addendum to Chapter Two, we show that *PEC1* expression is controlled by the jasmonic acid (JA) receptor complex SCF^{COI1}. We attempt to provide context for stromal Ca^{2+} transients by proposing that PEC1 may function upstream of JA biosynthesis enzymes LOX2 and AOS, both co-expressed with *PEC1*, and impact their function through Ca^{2+} signaling. In *fou2* mutants, deregulated suborganellar cation fluxes lead to the over-accumulation of JA. Future work will investigate this possible link between PEC1 and over-accumulation of JA in *fou2* mutants. Chapter Three describes the interplay of two separate protein families in plastid osmoregulation. In the past, plastid KEA and MSL protein families have been investigated separately, yet a link has never been established. Both are critical for regulating the plastid water content, which is visibly disturbed in *kea1kea2* and *msl2msl3* double mutants. We provide initial evidence for the functional interaction between the two highest expressed family members, namely KEA1 and MSL2. In *kea1msl2* double

mutants, growth, pigment accumulation, and photosynthesis are strongly disturbed. This link was unknown before and showcases the interplay of different protein families with similar tasks in plant ion- and osmohomeostasis. Follow-up work will need to investigate the interaction of all four members of plastid envelope KEA and MSL proteins to decipher possible redundancies. This includes the additional generation and characterization of *kea1msl3*, *kea2msl2*, and *kea2msl3* double mutants. Doing so will further our understanding of the importance of ion transport proteins for organellar development and ion- and osmohomeostasis. Lastly, we revisited the localization and function of NHD1. We provide evidence for the thylakoid membrane localization of NHD1 and employ variable light conditions to showcase the need for the transporter in acclimation to fluctuating light. In nature, plants are subject to constantly changing growth regimes. Understanding proteins involved in partitioning of *pmf* was suggested to be critical for designing crops with higher productivity in the field. Future experiments will need to employ an additional loss-of-function line, either provided by the Arabidopsis Biological Resource Center (ABRC) or designed through CRISPR/Cas9-induced deletions, established recently in our laboratory. Additionally, creating a new antibody specific to NHD1 will give more insights into the localization and structure of the NHD1 carrier inside of thylakoid membranes.

In conclusion, work in this dissertation underscores the importance of plastid ion transport proteins in many aspects of plastid physiology and plant growth. We lay important groundwork for future studies in the realm of plastid Ca^{2+} signaling, osmohomeostasis, and fluctuating light acclimation in plants.